

Portable Analytical Platforms for Disease Diagnostics and Environmental Monitoring

by

Chen Zhao

Department of Mechanical Engineering McGill University

Montreal, Quebec, Canada

December 2017

A thesis submitted to McGill University in partial fulfillment of the requirements for a doctoral degree

© Chen Zhao, 2017

Dedication

To my parents who give me life and all the support to explore the world

Table of Contents

Ta	ble o	f Co	ntentsiv
Lis	st of]	Figu	resix
Lis	st of '	Tabl	esi
Ab	strac	et	ii
Ré	sume	ś	iv
Ac	knov	vledą	gement vi
Co	ntrik	outio	ons of Authorsvii
1	Ch	apte	er 1: Introduction1
	1.1	The	esis objectives
	1.2	The	esis organization
	1.3	Ref	ferences5
2	Ch	apte	er 2: Portable Analytical Platforms for Disease Diagnostics and Environmental
M	onito	ring	: A Review 8
	2.1	Intı	roduction
	2.2	Gu	idelines
	2.2	2.1	Affordability and easy accessibility
	2.2	2.2	Portability and low power consumption
	2.2	2.3	Rapid measurement with high performance
	2.2	2.4	User-friendliness 12
	2.3	Wo	orking principles
	2.3	.1	Optical sensors and analyzers
	2.3	3.2	Electrochemical sensors and analyzer
	2.4	Ap	plications

	2.4	l .1	Disease diagnosis	17
	2.4	1.2	Physiological monitoring	18
	2.4	1.3	Water quality monitoring	19
	2.4	1.4	Others	20
	2.5	Fut	ure trends	20
	2.6	Co	nclusion	22
	2.7	Ref	erence	23
Li	ink be	etwe	en Chapter 2 and Chapter 3	32
3	Ch	apte	er 3: A microfluidic paper-based electrochemical biosensor array for	
m	ultipl	exed	detection of metabolic biomarkers	34
	3.1	Intr	oduction	35
	3.2	Ma	terials and methods	36
	3.2	2.1	Materials	36
	3.2	2.2	Design and fabrication of the paper-based biosensor array	37
	3.2	2.3	Design of the potentiostat	38
	3.2	2.4	Detection principles	39
	3.3	Res	sults and Discussion	40
	3.3	3.1	Electrochemical characterization of the paper-based biosensor array	40
	3.3	3.2	Multiplexed detection of glucose, lactate, and uric acid	41
	3.4	Co	nclusion	45
	3.5	Acl	knowledgements	45
	3.6	Ref	erence	46
Li	ink be	etwe	en Chapter 3 and Chapter 4	48
4			r 4: A portable paper-based microfluidic platform for multiplexed	
		-	ical detection of HIV and HCV antibodies in serum	50

	4.1	Intr	roduction	51
	4.2	Exp	perimental design	52
	4.2	2.1	Design and Fabrication of the E-µPIA	52
	4.2	2.2	Design of the Potentiostat	53
	4.2	2.3	Biofunctionalization of the Reaction Zone and the WE	54
	4.2	2.4	Protocol of Electrochemical ELISA	56
	4.3	Res	sults	59
	4.3	3.1	Electrochemical Characterization of the E-µPIA	59
	4.3	3.2	Detection of HIV/HCV Antibodies in Serum	60
	4.4	Dis	scussion	62
	4.5	Coı	nclusions	62
	4.6	Acl	knowledgements	63
	4.7	Ref	ferences	63
L	ink be	etwe	en Chapter 4 and Chapter 5	66
5	Ch	ıapte	er 5: A thread-based wearable nanobiosensor	68
	5.1	Intı	roduction	69
	5.2	Exp	perimental methods	71
	5.2	2.1	Materials and reagents	71
	5.2	2.2	System design	72
	5.2	2.3	Design and fabrication of the biosensor patch	72
	5.2	2.4	Electrode fabrication	74
	5.2	2.5	Preparation of artificial sweat	77
	5.3	Res	sults and Discussion	77
	5.3	3.1	Pre-conditioning of the LS-WE	77
	5.3	3.2	Device calibration	78

	5.3	3.3	Off-body testing of real human sweat	80
4	5.4	Co	nclusion	81
4	5.5	Ref	erence	81
Liı	nk be	etwe	en Chapter 5 and Chapter 6	83
6	Ch	apte	er 6: A portable lab-on-a-chip system for gold-nanoparticle-based colorimet	ric
det	tectio	on of	metal ions in water	85
(5.1	Intr	oduction	86
(5.2	Exp	perimental methods	87
	6.2	2.1	Colorimetric detection of Pb ²⁺ and Al ³⁺	87
	6.2	2.2	Synthesis of colloidal AuNPs	89
	6.2	2.3	Design and fabrication of the portable system	90
	6.2	2.4	Assay protocols	92
(5.3	Res	sults and discussion	93
	6.3	3.1	Analysis of AuNP aggregation kinetics via the handheld reader	93
	6.3	3.2	Calibration results of Pb ²⁺ and Al ³⁺ assays	94
	6.3	3.3	Assay selectivity	96
(5.4	Coı	nclusions	96
(5.5	Acl	knowledgement	97
(5.6	Ref	erence	97
Liı	ık be	etwe	en Chapter 6 and Chapter 7	99
7	Ra	pid	on-site determination of total nitrogen in water using a portable analytical	
sys	tem.	•••••		101
-	7.1	Intı	oduction	102
-	7.2	Exp	periment design	103
	7 2) 1	Materials and reagents	103

	7.2	2.2	Reaction system design	104
	7.2	2.3	Assay protocol	107
	7.3	Res	sults and Discussions	109
	7.3	3.1	Oxidation optimization	109
	7.3	3.2	Colorimetric assay optimization	111
	7.4	Cor	nclusion	114
	7.5	Ref	erences	114
8	Ch	apte	er 8: Conclusion	118
	8.1	Sur	nmary of accomplishments and contributions	118
	8.2	Fut	ure work	120
	8.3	Pub	olications	121
	8.3	3.1	Refereed journal papers	121
	8.3	3.2	Journal papers in preparation (manuscripts available upon request)	122
	8.3	3.3	Conference papers (full paper)	123
	8.3	3.4	Book chapter	124
	8 3	2.5	Datent	124

List of Figures

Figure 2-1. Summary of the involved detection methods, applications and target molecules in
portable analytical platforms9
Figure 2-2. (A) Wireless mobile phone impedance sensing system for bacteria detection, which
is integrated with a smartphone sensing application and a wireless bacteria sensor [36]. (B)
Photograph of the pluggable microfluidic chip and a mobile phone for electrochemical detections
of PfHRP2, an important biomarker for malaria [28]
Figure 2-3. Cellphone analytical platform employing optical mechanisms (A) optical reader
installed on an Android-based smart-phone, illuminated by red (625 nm) and green (523 nm)
LEDs [42]. (B) Mercury detection application running on an Android phone [42]. (C)
Configuration of smartphone-based device for optical detection of glucose on μPAD [45]. (D)
Diagram of a phone-based mobile microscope for quantitative imaging on Wright stained blood
smear [26]
Figure 2-4. Three types of independent handheld electrochemical readers: (A) Glucometer
adaptable to an immune sensing platform for Aflatoxins [61]. (B) Custom-made potentiostat as a
universal platform for electrochemical detections for a variety of targets [29]. (C) Handheld
potentiostat for multiplexed detection of HIV and HCV co-infection [12]
Figure 2-5. (A) Photographs of a subject wearing a 'smart headband' and a 'smart wristband'
during stationary cycling [88]. (B) Schematic of the sensor array (including glucose, lactate,
sodium, potassium and temperature sensors) for multiplexed perspiration analysis [88]. (C)
Photograph of the mouth-guard biosensor integrated with wireless amperometric circuit board
[89]. (D) Photograph of the wireless amperometric circuit board: front side (left) and back side
(right) [89]
Figure 3-1. A microfluidic paper-based electrochemical biosensor array that interfaces with a
custom-made handheld potentiostat for multiplexed detection of metabolic biomarkers. (A) A
paper-based electrochemical biosensor array (1 \times 8). (B) A microcontroller-based multiplexing
potentiostat mounted with a paper-based biosensor array. The potentiostat has eight measurement
channels, and each channel is connected to a group of three sensing electrodes through metal
clamps. CE: counter electrode. WE: working electrode. RE: reference electrode. (C) Schematic

diagram of the potentiostat architecture with eight measurement channels. (D) A photograph of
the paper-based biosensor array inserted into the potentiostat
Figure 3-2. Electrochemical characterization of the paper-based biosensor array. (A) Typical
cyclic voltammograms of 10 mM $K_3[Fe(CN)_6]$ in 1M KCl solution in an electrochemical
biosensing module of the array device at various scan rates. (B) A plot of the cathodic peak
current vs. the square root of the scan rate, measured from the cyclic voltammograms (n=5) 41
Figure 3-3. (A) Chronoamperometric curves and (B) the calibration plot for measurement of
glucose in AU. The solid line in (B) represents a linear fit to experimental data with regression
equation: y=0.041x+0.054 (R ² =0.996, n=5)
Figure 3-4. (A) Chronoamperometric curves and (B) the calibration plot for measurement of
lactate in AU. The solid line in (B) represents a linear fit to experimental data with regression
equation: y=0.0076x+0.025 (R ² =0.995, n=5).
Figure 3-5 (A) Chronoamperometric curves and (B) the calibration plot for measurement of uric
acid in AU. The solid line represents a linear fit to experimental data with regression equation: y
$= 0.048x + 0.029 (R^2 = 0.994, n = 5).$ 45
Figure 4-1. A portable paper-based diagnostic platform integrating an $E-\mu PIA$ and a handheld
potentiostat. (A) The handheld potentiostat inserted with an E- μ PIA. (B) The E- μ PIA. (C)
Schematic architecture of the potentiostat circuit constructed based on a microcontroller unit
(MCU)
Figure 4-2. Wireless data transmission of the diagnostic platform, from the potentiostat, to a PC
or a smart phone, and finally to a remote site. The screens of the PC and the smart phone display
the graphical user interfaces of the PC software and the Android APP, respectively 54
Figure 4-3. Biofunctionalization process of the WE. (A) Molecular scheme of surface protein
functionalization on the surfaces of the WE through APDES and GA linkages. (B) Fluorescence
quantification of immobilized FITC-anti-IgG on reaction zones treated with GA at different
concentrations (n = 3)
Figure 4-4. Protocol of indirect electrochemical ELISA. (A) Scheme of the indirect ELISA for
detecting HIV/HCV antibodies. (B) Electrochemical reaction mechanism of pAPP and ALP-
antibody57
Figure 4-5. Electrochemical characterization of the reaction of pAPP and ALP-labelled anti-
mouse IgG (ALP-antibody). (A) Cyclic voltammetry on solutions of pAPP plus ALP-antibody

("pAPP + ALP") and pAPP along ("pAPP"). (B) Results of hydrodynamic linear sweeping on
the solutions of "pAPP + ALP" and "ALP". (C) The signal-to-background current ratio extracted
from the hydrodynamic sweeping results. (D) Chronoamperometry measurement results on the
solution of "pAPP" with ALP-antibody added subsequently. The CA potential of 0.12 V was
used
Figure 4-6. Electrochemical characterization of the E-µPIA. (A) Cyclic voltammetry (CV) of
individual immunosensors at the scanning rate from 10 mV/s to 50 mV/s. (B) Calibration results
of the peak current magnitude vs. the square root of the scan rate $(n = 5)$
Figure 4-7. Experimental results of device calibration and cross-reactivity testing for HIV/HCV
antibody detections. (A)(B) Calibration curves of (A) HIV and (B) HCV antibody detections (n =
8). (C) Output signals ($n = 5$) of HIV detection on serum samples with 10 ng/ml HIV antibody
only ("HIV 10 ng/ml") and with 10 ng/ml HIV antibody and 10 μ g/ml interference HCV
antibody ("HIV 10 ng/ml + HCV 10 μ g/ml"). (D) Output signals (n = 5) of HCV detection on
serum samples with 10 ng/ml HCV antibody only ("HCV 10 ng/ml") and with 10 ng/ml HCV
antibody and 10 $\mu g/ml$ interference HIV antibody ("HCV 10 $ng/ml + HIV$ 10 $\mu g/ml$ ")
Figure 5-1. (A) A volunteer wearing smart headband. (B) Design configuration on the wearable
device. (C) Electronic design principle. (D) Wireless smart headband
Figure 5-2. (A) Cross-section view of electrodes, and wearable device fabrication. (B) Packed
wearable devices on the wearer's head
Figure 5-3. (A) Bare carbon electrode surface. (B) ZnO-NW electrode surface. (C)(D)(E) SEM
photographs of ZnO-NW electrode at varied magnifications
Figure 5-4. (A) Cyclic voltammograms of the LS-WE. (B) Typical EMF potential curves
measured on artificial sweat spiked with lactate at different concentrations. (C) Calibration plot
of the lactate sensing EMF cell (n=5), which covers a linear range of 0-25 mM with the
regression equation: $y = 0.94x + 71$
Figure 5-5. (A) and (B): calibration results of the biosensor for sodium sensing (n=5). The
calibration curve covers 0.1-100 mM with a linear relationship of y=42.9x+59.2 80
Figure 5-6. Testing results of real human sweat and their comparison with those from standard
tests
Figure 6-1. Schematic mechanisms of Pb ²⁺ and Al ³⁺ detection using AuNPs: (A) A glutathione
(GSH) molecule binds with a label-free AuNP at its thiol group and simultaneously coordinates

with Pb2+ at its carboxylic groups, leading to aggregation of AuNPs and shift of absorbance
spectrum of the AuNP solution. (B) Citrate-capped AuNPs aggregate in the presence of Al3+,
inducing shift of absorbance spectrum of the AuNP solution. (C) Molecular structures of the
GSH and citrate cap. 87
Figure 6-2. The absorbance curve of AuNP solution with a peak at 520 nm. The insets include a
transmission electron microscopy (TEM) image of the gold nanoparticles and a photograph of
the AuNP aqueous solution
Figure 6-3. Schematic cross-section diagram of the portable analytical system which consists of
a four-microwell plate and a handheld colorimetric reader. The four-microwell plate is inserted
in the colorimetric reader for absorbance measurement
Figure 6-4. Photographs of the portable system. (A) A microwell plate filled with solutions of
AuNP and Al3+. (B) The colorimetric reader held by a hand, with a microwell plate inserted. (C)
Inside of the colorimetric reader with the LED array lighting up
Figure 6-5. Experimental results of the Pb ²⁺ assay. (A) The kinetic curve of AuNP aggregation
in Pb^{2+} solutions in terms of light absorbance at 610 nm. (B) Photographs of assay solutions at
different Pb2+ concentrations, which generated different levels of color change after 10-minute
reaction. (C) Calibration curves of the Pb2+ assay, obtained using the portable reader and UV-vis
spectrometer [25], with linear regression equations of $y = -0.00031x + 1.0$ and $y = 0.00050x + 1.0$
0.72, for data from the portable reader and UV-Vis spectrometer respectively94
Figure 6-6. Experimental results of the Al3+ assay. (A) The kinetic curve of AuNP aggregation
in Al^{3+} solutions in terms of light absorbance at 610 nm. (B) Photographs of assay solutions at
different Al3+ concentrations, which generated different levels of color change after 8-minute
reaction. (C) Calibration curves of the Al3+ assay, obtained using the portable reader and UV-Vis
spectrometer. The inset includes linear regression curves of the calibration data in the range of
100–400 ppb, with equations of $y = -0.00036x + 1.1$ (for data from the portable reader) and $y = -0.00036x + 1.1$
$0.0012x + 0.20 \ (for \ data \ from \ the \ UV-Vis \ spectrometer). \\ \\ 95$
Figure 7-1. Platform design schematic. (A) UVC-thermal digestion chamber. (B) Colorimetric
reaction step. (C) Colorimetric reader. (D) Interfaces of a smart phone application 105
Figure 7-2. (A) UVC-thermal reaction chamber. (B) Colorimetric reader. (C) The controlling
algorism of the application program

Figure 7-3. (A) Reaction mechanism of the colorimetric detection of nitrate detection. (B)
Absorbance spectrum of Azo product from UV-vis, with a max light absorption at $538 \text{ nm.} \dots 108$
Figure 7-4. Optimization of oxidation parameters reflected by absorbance (n=6). (A) Heating
temperature from 30 °C to 60 °C. (B) UV-thermal oxidation time from 10 min to 30 min. (C)
Substrate effect between water and borate buffer (pH=9)
Figure 7-5. Oxidation assay protocol optimization (n=6): (A) The NaOH volume effect (pH) on
the oxidation rate reflected by absorbance. (\mathbf{B}) The potassium persulfate (oxidizer) volume effect
on the oxidation rate reflected by absorbance
Figure 7-6. (A) Nitrate reduction efficiency over time, reflected by absorbance (n=6). (B)
Colorimetric assay efficiency over time, reflected by absorbance (n=6)
Figure 7-7. The testing results of reagents stability over time (n=6): (A) persulfate/NaOH
regents (one day at 4°C). (B) Reductant solution. (C) Colorimetric reagents over time (at 4°C
under dark environment)
Figure 7-8. Detection of TN by the colorimetric assay ($n=6$). The linear fitting equations are: $y =$
0.2565x - 0.0533 for our colorimetric reader; $y = 0.4283x - 0.025$ for the UV-vis reading 113

List of Tables

Table 3-1. Performance comparison of the paper-based biosensor array with commercial	al meters
[20] and μPAD [14]. *The dynamic linear ranges achieved in this work cover the α	clinically-
relevant ranges of the three biomarkers. LOD: Limit of detection.	45
Table 7-1 . The results of TN determination (mg N/L)	113

Abstract

High-performance analytical platforms have gained significant research interests recently and proved themselves as powerful tools for enabling low-cost, portable, and reliable analysis for a variety of practical applications. This thesis aims to develop novel portable analytical platforms for two important types of applications including disease diagnostics and environmental monitoring.

In one branch of this research, new types of cellulose-based microfluidic biosensors are developed for quantifying physiologically relevant biomarkers in human fluids, with target applications of point-of-care diagnosis and physiological condition monitoring. Specifically, an electrochemical microfluidic paper-based immunosensor array (E-µPIA) is proposed, featuring ultralow cost, high portability, high throughput, excellent user friendliness. To interface with the E-μPIA, a customized, handheld electrochemical reader (potentiostat) is designed for multiplexed readout of electrochemical signals from the E-µPIA with high resolution. Based on this platform, multiplexed detection of three metabolites (glucose, lactate, and uric acid) in urine samples is first demonstrated with comparable performance to existing standard tests. Then, the E-μPIA biosensing platform was further optimized for diagnosis of human immunodeficiency virus (HIV) and hepatitis C virus (HCV) co-infections in serum samples. Indirect ELISA of HIV/HCV antibodies is realized on the E-µPIA with LODs of 300 pg/ml and 750 pg/ml, respectively, both lower than that of standard HIV/HCV tests. Targeting wearable biosensing for physiological condition monitoring, a wearable microfluidic thread-based zinc-oxide-nanowire (ZnO-NW) biosensor is developed for continuous monitoring of lactate and sodium concentrations in sweat during perspiration. Based on this platform, multiplexed detection of lactate and sodium in human sweat is demonstrated with dynamic ranges of 0-25 mM and 0.1-100 mM, and LODs of 3.61 mM and 0.16 mM, respectively, both covering the clinical sweat levels. Accurate measurements on real sweat samples from a healthy donor are conducted, and the results (13.16 \pm 0.83 mM for lactate and 92.9 \pm 5mM for sodium) are in good agreement with standard test results.

Along the other branch of this research, novel portable chemical analyzers are developed for rapid, on-site detection of pollutants (metal ions and total nitrogen) in water. Heavy metal ions released into various water systems have severe impact on the environment, and excess exposure

to toxic metal ions through drinking water pose high risks to human health and cause lifethreatening diseases. To meet the urgent needs of on-site heavy metal ion detection, a portable analytical platform is developed for rapid and sensitive detection of aluminum (Al³⁺) and lead (Pb2+) ions in water. This platform involves a handheld colorimetric reader implementing gold nanoparticle based colorimetric assays for quantifying the concentrations of Al³⁺ and Pb²⁺. The LODs of 30 ppb for Pb²⁺ and 89 ppb for Al³⁺ are achieved, with comparable performance to that of a bench-top analytical spectrometer. Another important type of pollutant we target here is total nitrogen (TN), a nutrient pollutant in water that is primarily released from our sewage systems. The excess amount of TN present in water leads to algae bloom with a notable negative impact on the environment, the economy, and the human health. To face this situation, regular monitoring of TN levels in our water systems is required, for which portable TN analyzers represent an attractive solution. To this end, a novel analytical system is developed comprising a portable ultraviolet C reaction chamber (for digesting organic nitrogen) and a colorimetric reader (for final detection of total nitrite). With this system, rapid digestion and colorimetric determination of total nitrogen are achieved in 36 minutes, with a LOD of 1.20 mg/l, which is much lower than the required LOD of WHO standard (10 mg/l).

The portable platforms developed in this research hold significant potential for on-site analysis of disease markers and environmental pollutants, which will enable effective identification and control of pathological, physiological, and environmental threats to human health and our environment.

Résumé

L'intérêt scientifique porté aux plateformes analytiques hautes performances s'est accru considérablement ces dernières années. Cet outil puissant permet une analyse fiable, mobile et peu coûteuse pour une variété d'applications pratiques. L'objectif de cette thèse est de développer des nouvelles plateformes analytiques portables pour deux applications majeures à savoir le diagnostic des maladies et la surveillance de l'environnement.

Dans la première partie de cette recherche, de nouveaux types de bio-détecteurs microfluidiques à base de cellulose sont développés afin de quantifier les biomarqueurs pertinents dans les fluides humains, le but étant d'améliorer le diagnostic au point d'intervention et la surveillance de l'état physiologique du patient. Plus précisément, on propose un réseau électrochimique microfluidique d'immuno-sensibilité (E-µPIA) qui présente un coût très bas, une portabilité élevée, un débit élevé, le tout avec une grande facilité d'utilisation.

Pour interagir avec l'E-μPIA, un lecteur électrochimique portatif (potentiostat) personnalisé est conçu pour une lecture simultanée et haute résolution des signaux électrochimiques de l'E-μPIA. Cette plateforme est d'abord appliquée à la détection simultanée de trois métabolites (glucose, lactate et acide urique) dans des échantillons d'urine et les résultats sont comparés aux méthodes standard de détection existantes. Ensuite, la plateforme de bio-détection E-μPIA a été adaptée au diagnostic de la co-infection du Virus de l'Immunodéficience Humaine (VIH) et du Virus de l'Hépatite C (VHC) dans des échantillons de sérum. L'ELISA indirecte des anticorps anti-VIH/HCV est réalisée sur l'E-μPIA avec des LOD de 300 pg/mL et 750 pg/mL respectivement, doses inférieures à celles des tests standard de HIV/VHC.

Ciblant la bio-sensibilité portable pour la surveillance de l'état physiologique, un biocapteur microfluidique à base de nanofil (ZnO-NW) est développé pour la surveillance continue des concentrations de lactate et de sodium dans la sueur pendant la transpiration. Sur la base de cette plateforme, la détection simultanée de lactate et de sodium dans la sueur humaine est démontrée avec des plages dynamiques de 0 à 25 mM et de 0,1 à 100 mM, et des LOD de 0,6 mM respectivement, tous deux couvrant les niveaux de sueur cliniques. Des mesures précises de la sueur ont été effectuées à partir d'un donneur sain, et les résultats (10,16 ± 0,83 mM pour le lactate et 0,9 ± 5 mM pour le sodium) étaient en accord avec les résultats des tests standard.

Dans l'autre branche de cette recherche, de nouveaux analyseurs portables chimiques sont développés pour la détection rapide in situ de polluants dans l'eau (ions métalliques et azote). Les ions de métaux lourds libérés dans divers systèmes d'eau ont un impact important sur l'environnement et l'exposition excessive à des ions métalliques via l'absorption d'eau pose des risques élevés pour la santé humaine et peut causer des maladies mortelles. Pour répondre aux besoins urgents de détection d'ions de métaux lourds sur site, une plateforme analytique portable est développée pour la détection rapide et précise des ions aluminium (Al³⁺) et plomb (Pb²⁺) dans l'eau. Cette plateforme dispose d'un lecteur colorimétrique portatif dont l'analyse se base sur des nanoparticules d'or pour quantifier les concentrations d'Al³⁺ et de Pb²⁺. Les LOD de 30 ppb pour Pb²⁺ et de 89 ppb pour Al³⁺ sont atteints, avec des performances comparables à celles d'un spectromètre analytique de banc. Un autre type important de polluants que nous ciblons ici est l'azote total (TN), un polluant nutritif dans l'eau qui est principalement libérée par les égouts. L'excès de TN présent dans l'eau conduit à la floraison d'algues avec un impact négatif considérable sur l'environnement, l'économie et la santé humaine. Pour faire face à cette situation, une surveillance régulière des niveaux de TN dans nos réseaux d'eau est nécessaire et pour laquelle les analyseurs TN portables représentent une solution attrayante. À cet effet, on développe un nouveau système analytique comprenant une chambre de réaction ultraviolette C portative (pour « digérer » l'azote organique) et un lecteur colorimétrique (pour la détection finale du nitrate total). Grâce à ce système, la détermination colorimétrique de l'azote total est obtenue en 36 minutes, avec une LOD de 1,20 mg/L, ce qui est bien plus faible que la LOD requise par la norme de l'OMS (10 mg/L).

Les plateformes portables développées dans le cadre de cette recherche offrent un potentiel important d'analyse *in situ* des marqueurs de la maladie et des polluants environnementaux, ce qui permettra d'identifier et de contrôler efficacement les menaces pathologiques, physiologiques et environnementales pour la santé humaine et pour notre environnement.

Acknowledgement

Firstly, I would like to express my sincere gratitude to my advisor Prof. Xinyu Liu for the continuous support of my Ph.D. study and related researches, for his patience, motivation, and immense knowledge. His guidance helped me in the design of research projects and writing of this thesis. He remains my best role model to be a scientist, mentor, and teacher.

Besides my advisor, I would like to thank my thesis committee members Prof. Fiona Zhao and Prof. Srikar Vengallatore, for their insightful suggestions and encouragement for my Ph.D. study. My sincere thanks also go to Prof. Jinxia Liu and Prof. Martin M. Thuo for their support and advice in both collaborative research projects and my academia career. Without their generous support, it would be hard to pursue all my projects.

I appreciate the Faculty of Engineering at McGill University and the Natural Sciences and Engineering Research Council of Canada, for their financial supports to my study.

I would like to express my great appreciation to my colleagues in Biomedical Microsystem Laboratory and other friends who are always ready to help: Longyan Chen, Qiyang Wu, Guowei Zhong, Xiao Li, Hao Fu, Juntian Qu, Binbin Ying, Xianke Dong, Pengfei Song, Weize Zhang, Vicky Wang, Da-Eun Kim, Ayvi Islam and Corey Miles.

Last but not least, I would like to thank my parents, my brother, and my husband for supporting me spiritually all the time.

Contributions of Authors

This is a manuscript-based thesis consisting of three journal articles published and three journal articles to be published. The titles of the articles, names of the authors, and their contributions are listed below:

1. Portable Analytical Platforms for Disease Diagnostics and Environmental Monitoring: A Review

Chen Zhao and Xinyu Liu

Department of Mechanical Engineering, McGill University, Montreal, Quebec H3A 0C3, Canada.

To be submitted to *Biosensors and Bioelectronics*.

Author contributions:

Chen Zhao: Wrote the manuscript, organized the literature information, and prepared presentation items.

Xinyu Liu: Wrote the manuscript.

2. A microfluidic paper-based electrochemical biosensor array for multiplexed detection of metabolic biomarkers

Chen Zhao¹, Martin M. Thuo², and Xinyu Liu¹

Science and Technology of Advanced Materials, October 2013, 14, 054402.

DOI: https://doi.org/10.1088/1468-6996/14/5/054402

Author contributions:

Chen Zhao: Designed the platform, performed the experiments, analyzed the data, prepared the presentation items, and wrote the manuscript.

Martin M. Thuo: Contributed to the platform design, and analyzed the data.

Xinyu Liu: Proposed the idea, designed the experiments, analyzed the data, and wrote the manuscript.

¹ Department of Mechanical Engineering, McGill University, Montreal, Quebec H3A 0C3, Canada.

² Department of Chemistry, University of Massachusetts, Boston, Massachusetts 02125, USA.

3. A portable paper-based microfluidic platform for multiplexed electrochemical detection of HIV and HCV antibodies in serum

Chen Zhao and Xinyu Liu

Department of Mechanical Engineering, McGill University, Montreal, Quebec H3A 0C3, Canada.

Biomicrofluidics, April 2016, 10: 024119.

DOI: http://dx.doi.org/10.1063/1.4945311

Author contributions:

Chen Zhao: Designed the platform, performed the experiments, analyzed the data, prepared the presentation items and wrote the manuscript.

Xinyu Liu: Proposed the idea, designed the experiments, analyzed the data, and wrote the manuscript.

4. A thread-based wearable nanobiosensor

Chen Zhao¹, Xiao Li^{1,2}, Ted Li¹, Qiyang Wu¹, and Xinyu Liu¹

To be submitted to *Biosensors and Bioelectronics*.

Author contributions:

Chen Zhao: Designed the platform, performed the experiments, analyzed the data, prepared the presentation items, and wrote the manuscript.

Xiao Li: Designed the platform, and performed the experiments.

Ted Li: Performed the experiments.

Qiyang Wu: Performed the experiments.

X. Liu: Proposed the idea, designed the experiments, analyzed the data, and wrote the manuscript.

5. A portable lab-on-a-chip system for gold-nanoparticle-based colorimetric detection of metal ions in water

¹ Department of Mechanical Engineering, McGill University, Montreal, Quebec H3A 0C3, Canada.

² Department of Chemistry, Stanford University, Stanford, California 94305, USA.

Chen Zhao¹, Guowei Zhong², Da-Eun Kim¹, Jinxia Liu², and Xinyu Liu¹

Author contributions:

Chen Zhao: Designed the platform, performed the experiments, analyzed the data, prepared the presentation items and wrote the manuscript.

Guowei Zhong: Designed the platform, and performed the experiments.

Da-Eun Kim: Designed the platform.

Jinxia Liu: Proposed the idea, designed the experiments, and analyzed the data.

Xinyu Liu: Proposed the idea, designed the experiments, analyzed the data, and wrote the manuscript.

6. Rapid in-field determination of total nitrogen by a portable system

Chen Zhao^{#1}, Longyan Chen^{#1}, Guowei Zhong², Qiyang Wu¹, Jinxia Liu² and Xinyu Liu¹

To be submitted to *Analytical Chemistry*.

Author contributions:

Chen Zhao: Designed the platform, performed the experiments, analyzed the data, and wrote the manuscript.

Longyan Chen: Performed the experiments, analyzed the data, and wrote the manuscript.

Guowei Zhong: Designed the platform, performed the experiments, and analyzed the data.

Qiyang Wu: Designed the platform.

Jinxia Liu: Proposed the idea and designed the experiments.

Xinyu Liu: Proposed the idea, designed the experiments, analyzed the data, and wrote the manuscript.

¹ Department of Mechanical Engineering, McGill University, Montreal, Quebec H3A 0C3, Canada.

² Department of Civil Engineering and Applied Mechanics, McGill University, Montreal, Quebec H3A 0C3, Canada.

¹ Department of Mechanical Engineering, McGill University, Montreal, Quebec H3A 0C3, Canada.

² Department of Civil Engineering and Applied Mechanics, McGill University, Montreal, Quebec H3A 0C3, Canada.

^{*}Authors contributed equally to the work.

Chapter 1

Introduction

Chapter 1: Introduction

Recently, growing expectations have been shifted towards more accessible and responsive ways for delivering services in early detection of disease, health status supervision, food safety inspection, and environmental monitoring [1-3]. The monitoring of multiple vital variables requires specialized measurement instruments, but they are usually unavailable to be employed for *in-situ* purposes due to their expensive costs, bulky sizes, and operation complexity. High-performance portable analytical platforms involving miniature microfluidic devices have enabled more thorough assessment of a person's health status or environmental quality in compatibility with the point of test, low cost and high accessibility.

The commercialization of portable analytical platforms has already appeared for controlling of some specific issues, such as diabetes [4, 5], water turbidity [6], blood pressure [7] and pulse rate[8]. However, these products are hindered by their relative high price, limited numbers of targets, and inability to detect molecular biomarkers. Rapid advancement has been observed in various aspects of the development of portable analytical platforms. The evolution of miniaturized sensing techniques in the field of microfluidics, integrated with portable detection instruments, promotes the development of point-of-care disease diagnostics, telemedicine and *insitu* environmental monitoring. With these advancements, researchers established pioneer work in miniaturized sensing assays such as nano-sensor [9, 10], single cell biosensor [11], portable enzyme-linked immunoassays [12]; and analyzers such as cellphone-aided microscopes [13], photodiode-based optical detectors (for colorimetric assays) [14], and microcontroller-based handheld potentiostats (for electrochemical assays) [15].

Physiological biomarker diagnosis and *in-situ* water quality monitoring require accurate, instant, and regular monitoring at affordable costs in both home usage and industrial/medical surveillance. Smaller, faster, and cheaper analytical devices and platforms are highly desired for replacing time-consuming laboratory analyses, which will facilitate convenient and affordable inspections for increased patient survival rates and healthier life style. Timely biomarker detection is crucial for early disease diagnosis and physiological monitoring. High-performance analyzers are urgently needed for measuring biomarkers present at ultra-low levels for early stages of diseases. As another important issue, water quality monitoring plays a key role in environmental examination during everyday life. Toxic metal ions and organic compounds

released into the water systems contaminate the sources of rivers and lakes, and lead to a high risk to both human health and economics. *In-situ* monitoring of these two main pollutants are highly demanded to indicate water's suitability for drinking, farming, and ecosystem balance.

This thesis aims to provide effective engineering tools as solutions to the biochemical problems required for in-situ disease diagnostics and environmental monitoring. The common contribution remains in the design and instrumentation methodologies of those portable analytical systems for different types of (bio)analysis. In this research, we target at these two directions in measurements of physiological biomarkers and water quality factors by designing high-performance portable analytical platforms. Aiming at early-disease diagnosis, we first develop an electrochemical microfluidic paper-based immunosensor array (E-µPIA) and a customized handheld electrochemical reader. This platform enables multiplexed detection of metabolic and protein biomarkers with satisfactory results. Next, we design a non-invasave thread-based zinc-oxide-nanowire (ZnO-NW) biosensor and a wireless smart headband as a wearable platform for physiological condition monitoring. We conduct multiplexed detection of lactate and sodium in real sweat during human perspiration, which are vital signs revealing overexercising. On the front of environmental monitoring, we aim at water quality monitoring in the specific area of heavy metal ion and nutrient pollutant measurements. We develop a portable chemical analyzer for rapid on-site detection of aluminum and lead. Targeting total nitrogen detection, we develop an analytical system comprising an organic nitrogen digestion chamber and a colorimetric reader, and achieve rapid determination of total nitrogen.

1.1 Thesis objectives

The overall objective of this thesis is to develop portable analytical platforms to meet the requirements for on-site measurements of disease biomarkers and environmental pollutants. The platforms are designed to maintain superior sensing performance that is able to satisfy the criteria of ASSURED guideline of the World Health Organization (WHO): Affordable, Sensitive, Specific, User-friendly, Rapid and robust, Equipment free, and Deliverable to end-users [1, 16, 17]. The specific objectives of this thesis are:

To develop an electrochemical paper-based microfluidic biosensor array (E-μPIA) and a
handheld multiplexing potentiostat for the detection of metabolites (glucose, lactate and uric
acid) in urine samples.

- 2. To further optimize the E-μPIA biosensing platform for diagnosis of human immunodeficiency virus (HIV) and hepatitis C virus (HCV) co-infection in serum samples.
- 3. To design a wearable thread-based ZnO-NW nanobiosensor and its corresponding smart headband with signal readout electronics, for the real-time non-invasive monitoring of lactate and sodium concentrations in sweat.
- 4. To develop gold nanoparticle (AuNP) based colorimetric assays and a handheld colorimetric reader for on-site detection of lead and aluminum in water.
- 5. To develop a fast, reliable and accurate assay protocol, and a portable analytical platform for digestion and detection of total nitrogen in water.

1.2 Thesis organization

This is a manuscript-based thesis composed of eight chapters. The current chapter (Chapter 1) of this thesis briefly introduces the general concepts and challenges in the field of portable analytical platform, followed by the objectives and the structure of this thesis.

Chapter 2 presents a more detailed review of the research on developing portable analytical platforms. Requirements in the practical applications are summarized, and the design considerations to meet the requirements are discussed. The major working principles of current portable platforms regarding sensing mechanism and detection principles are introduced. Their design innovations for high performance and capabilities in practical uses are highlighted, covering the applications of disease diagnostics, physiological monitoring, food safety inspection, and environmental monitoring. In the end, a broadened view is proposed on the future trend of portable analytical platforms in point-of-test applications. In particular, chapter 2 points out two important applications to direct the future development of portable analytical platforms: (i) disease diagnostics at point of care and wearable non-invasive physiological monitoring; and (ii) *in-situ* water environmental monitoring. The two directions set the courses of the following chapters, as Chapters 3, 4 and 5 focus on physiological biomarker diagnosis using a paper-based electrochemical platform and a thread-based wearable sensing platform, and Chapter 5 and 6 introduce optical analytical platforms for detection of water pollutants including heavy metal ions and total nitrogen.

Chapter 3 introduces an electrochemical microfluidic paper-based immunosensor array (E-µPIA), featuring ultralow cost, high portability, high throughput, and excellent user friendliness. To interface

with the E-µPIA, a customized, handheld electrochemical reader (potentiostat) is designed for multiplexed readout of electrochemical signals from the E-µPIA with high resolution. Different from existing paper-based electrochemical devices, this device includes an array of eight electrochemical sensors and utilizes a handheld custom-made electrochemical reader (potentiostat) for signal readout. The biosensor array can detect multiple analytes in a sample solution and produce measurements for each analyte from a single run. Using the device, we demonstrate simultaneous detection of glucose, lactate, and uric acid in urine, with analytical performance comparable to that of the existing commercial and paper-based platforms. The paper-based biosensor array and its electrochemical reader enable the acquisition of high-density, statistically meaningful diagnostic information at the point of care in a rapid and cost-efficient way.

Chapter 4 further optimizes the E-µPIA and the potentiostat (presented in Chapter 3) as the first paper-based electrochemical immunosensing platform with multiplexing and telemedicine capabilities for diagnosing HIV/HCV co-infection. The optimized platform is capable of performing enzymelinked immunosorbent assays (ELISAs) simultaneously on eight samples within 20 minutes. The multiplexing feature of the platform allows it to produce multiple measurement data for HIV and HCV markers from a single run, and its wireless communication module can transmit the results to a remote site for telemedicine. The unique integration of paper-based microfluidics and mobile instrumentation renders our platform portable, low-cost, user-friendly, and high-throughput. Indirect ELISAs of HIV/HCV antibodies are realized on the E-µPIA with limits of detection (LODs) of 300 pg/ml and 750 pg/ml, respectively, both lower than those of standard HIV/HCV ELISAs.

Chapter 5 introduces a non-invasive wearable biosensing platform for monitoring physiological variables. A thread-based ZnO-NW biosensor is developed for continuous monitoring of lactate and sodium concentrations in sweat during perspiration. Based on this platform, multiplexed detections of lactate and sodium in human sweat are demonstrated with dynamic ranges of 0-25 mM and 0.1-100 mM, and LODs of 3.61 mM and 0.16 mM, respectively, both covering the clinical measurement ranges with satisfactory performance. Using the biosensor, the testing of real sweat samples from a healthy donor is demonstrated with results in good agreement with standard assays.

Chapter 6 reports a portable analytical system for colorimetric detection of lead (Pb²⁺) and aluminum (Al³⁺) ions in water based on gold nanoparticle probes and lab-on-a-chip instrumentation. The colorimetric detection of metal ions is conducted via single-step assays with low LODs and high selectivity. A custom-made micro-well plate and a handheld colorimetric reader are designed for

implementing the assays and quantifying the signal readout. The calibration experiments demonstrate that this portable system provides LODs of 30 ppb for Pb²⁺ and 89 ppb for Al³⁺, both comparable to bench-top analytical spectrometers. It promises an effective platform for metal ion analysis in a more economical and convenient way, particularly for use in water quality monitoring in field and resource-poor settings.

Chapter 7 introduces a novel analytical system comprising a portable ultraviolet C reaction chamber for digesting organic nitrogen and a colorimetric reader for final detection of total nitrite. With this system, rapid digestion and colorimetric determination of total nitrogen are achieved in 36 minutes, with a LOD of 1.20 mg/l, which is much lower than the required LOD of the World Health Organization standard (10 mg/l). Compared with existing laboratory instruments, the system requires much shorter incubation time and enables the digestion and measurement of TN in a portable and low-cost manner.

Finally, Chapter 8 highlights accomplishments and contributions of this research. At the end, an outlook into the future work is provided.

1.3 References

- [1] A. W. Martinez, S. T. Phillips, G. M. Whitesides, and E. Carrilho, "Diagnostics for the developing world: microfluidic paper-based analytical devices," ed: ACS Publications, 2009.
- [2] M. Urdea *et al.*, "Requirements for high impact diagnostics in the developing world," *Nature*, vol. 444, pp. 73-79, 2006.
- [3] C. D. Chin, V. Linder, and S. K. Sia, "Commercialization of microfluidic point-of-care diagnostic devices," *Lab on a Chip*, vol. 12, no. 12, pp. 2118-2134, 2012.
- [4] R. J. Smith, T. A. Stamp, D. D. Bouricius, and E. Lancaster, "Blood glucose meter," ed: Google Patents, 2009.
- [5] iHealth, "Glucose Meter, Blood Glucose Meters iHealth," 2017.
- [6] HACH, "High Performance Turbidity Meters Hach," 2017.
- [7] Omron, "Omron BP786CAN 10 Series Upper Arm Blood Pressure Monitor Plus Bluetooth Smart."
- [8] Zacurate, "Finger Heart Rate and Blood HbO2 Meter with silicon cover, batteries and lanyard (Blue)," 2017.
- [9] P. Rai, S. Oh, P. Shyamkumar, M. Ramasamy, R. E. Harbaugh, and V. K. Varadan, "Nano-bio-textile sensors with mobile wireless platform for wearable health monitoring of neurological and cardiovascular disorders," *Journal of The Electrochemical Society*, vol. 161, no. 2, pp. B3116-B3150, 2014.
- [10] C. Parolo and A. Merkoçi, "Paper-based nanobiosensors for diagnostics," *Chemical Society Reviews*, vol. 42, no. 2, pp. 450-457, 2013.

- [11] M. Roy, D. Seo, C.-H. Oh, M.-H. Nam, Y. J. Kim, and S. Seo, "Low-cost telemedicine device performing cell and particle size measurement based on lens-free shadow imaging technology," *Biosensors and Bioelectronics*, 2014.
- [12] C. M. McGeough and S. O'Driscoll, "Camera phone-based quantitative analysis of Creactive protein ELISA," *Biomedical Circuits and Systems, IEEE Transactions on*, vol. 7, no. 5, pp. 655-659, 2013.
- [13] A. Skandarajah, C. D. Reber, N. A. Switz, and D. A. Fletcher, "Quantitative Imaging with a Mobile Phone Microscope," *PloS one*, vol. 9, no. 5, p. e96906, 2014.
- [14] C. Zhao, G. Zhong, D.-E. Kim, J. Liu, and X. Liu, "A portable lab-on-a-chip system for gold-nanoparticle-based colorimetric detection of metal ions in water," *Biomicrofluidics*, vol. 8, no. 5, p. 052107, 2014.
- [15] A. Nemiroski *et al.*, "Universal mobile electrochemical detector designed for use in resource-limited applications," *Proceedings of the National Academy of Sciences*, vol. 111, no. 33, pp. 11984-11989, 2014.
- [16] D. Mabey, R. W. Peeling, A. Ustianowski, and M. D. Perkins, "Tropical infectious diseases: diagnostics for the developing world," *Nature Reviews Microbiology*, vol. 2, no. 3, pp. 231-240, 2004.
- [17] R. Peeling and D. Mabey, "Point of care tests for diagnosing infections in the developing world," *Clinical microbiology and infection*, vol. 16, no. 8, pp. 1062-1069, 2010.

Chapter 2

Portable Analytical Platforms for Disease Diagnostics and Environmental Monitoring: A Review

Chapter 2: Portable Analytical Platforms for Disease Diagnostics

and Environmental Monitoring: A Review

Chen Zhao and Xinyu Liu*

Department of Mechanical Engineering, McGill University, 817 Sherbrooke Street West,

Montreal, Quebec H3A 0C3, Canada

*Corresponding author: xinyu.liu@mcgill.ca.

To be submitted to Biosensors and Bioelectronics.

High-performance analytical platforms have emerged as promising technology for many on-site

applications in healthcare, environmental monitoring, food safety inspection, and so forth,

because they maintain prominent attributes of rapid reaction, reliable performance, high

sensitivity, and low cost. In this paper, we review the research on developing portable analytical

platforms for rapid, reliable, and inexpensive on-site measurements of biochemical parameters

related to healthcare, healthy lifestyle, and environmental safety. The major working principles

are introduced as the electrochemical methods and optical methods, and their corresponding

detector designs as the custom-made detectors and the cellphone-based detectors. Specially, the

achievements are summarized towards disease diagnostics and water pollutant detections with

focus on the involved biomarkers including metabolites, immunoassays, electrolytes, metal ions,

and nutrients. Regarding the challenges and opportunities, insights are given over the aspects of

performance improvement and real-sample trial.

Keywords: portable analytical platform, electrochemical detection, optical detection, disease

diagnostics, environmental monitoring

2.1 Introduction

High-performance analytical platforms have gained significant research interests recently and

proved themselves as powerful tools for enabling low-cost, portable, and reliable analysis for a

variety of practical applications. The designs of *in-situ* measurement devices such as the water

quality analyzer, household medical care equipment, food safety analyzer, and non-invasive

8

physiological monitor largely rely on the techniques of portable analytical platforms, which have been considered as the most prospective alternative to conventional bench-top analytical instruments [1-5]. Combining with miniature microfluidic devices, these platforms bring the laboratory technologies to the point of test for disease diagnosis and environmental monitoring with high compatibility, low cost and high accessibility.

Commercial applications of portable analytical platforms appear in the control of some specific issues, such as diabetes [6, 7], water turbidity [8], blood pressure [9] and pulse rate [10]. However, these products are hindered by their relative high prices, limited numbers of targets, and inability to detect certain biomarkers. The evolution of miniaturized sensing techniques, in particular, microfluidic technologies, with portable detection instruments, promoted the development of telemedicine and *in-situ* environmental monitoring. These portable analytical platforms have found important applications in personal healthcare [11, 12], food safety inspection [13], and environmental monitoring including water [14, 15], air [16], and soil [17].

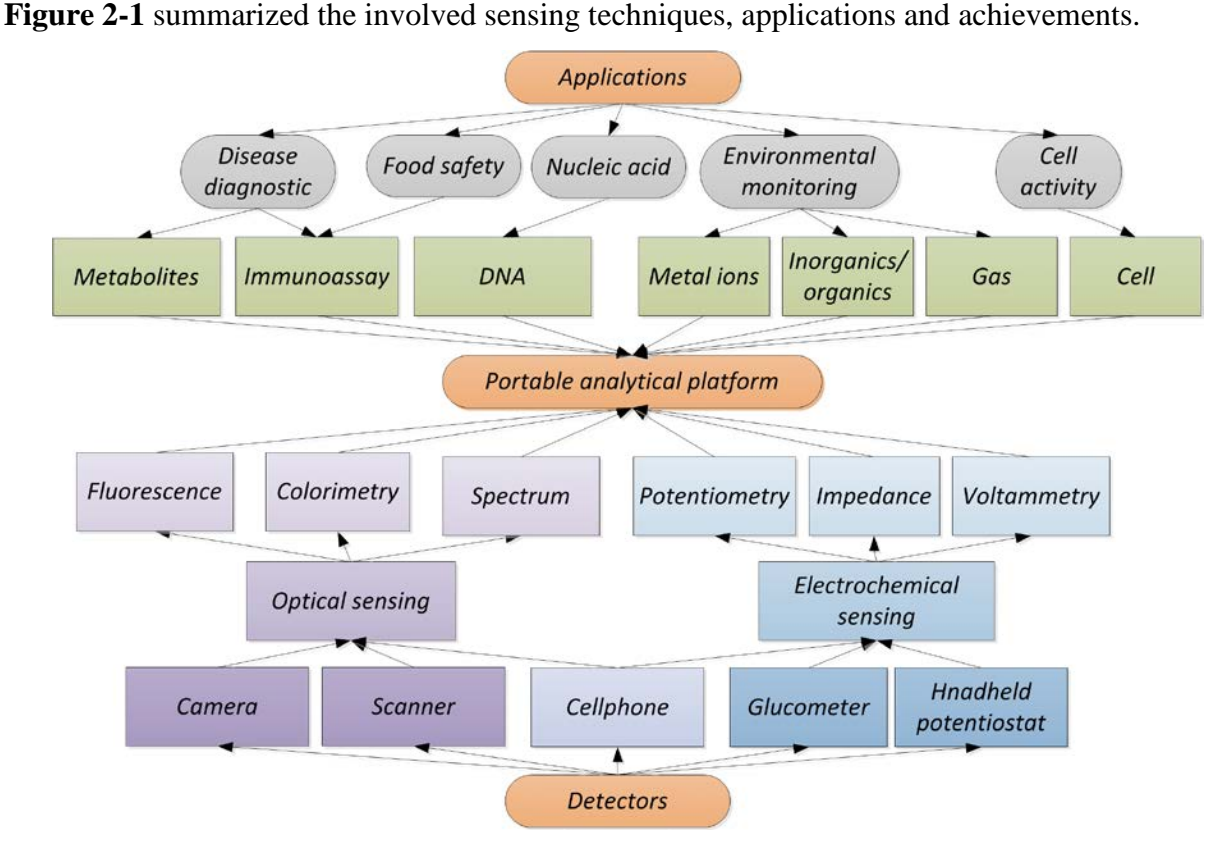


Figure 2-1. Summary of the involved detection methods, applications and target molecules in portable analytical platforms.

2.2 Guidelines

The well-accepted criteria for rapid diagnostics are the ASSURED guideline of the World Health Organization (WHO): Affordable, Sensitive, Specific, User-friendly, Rapid and robust, Equipment free, and Deliverable to end-users [18-20]. Although these criteria were first proposed for evaluating rapid diagnostic tests [18], they are also applicable to designs of other portable analytical tools targeting *in-situ* applications involving both disease diagnostics and environmental monitoring. Many existing platforms have been tailored to meet these criteria to guarantee their advantageous features such as low costs of material and manufacturing, ease of operation, low dependence on equipment, excellent portability, and good compatibility with mass production.

2.2.1 Affordability and easy accessibility

Cost efficiency is one of the major considerations in the design of these platforms. There arise many inexpensive sensor fabrication techniques and detection methods, especially the microfluidic devices and its integration with portable detectors. The fabrication processes of microfluidic devices are easy to access without requiring high-end instruments and technologies. Commonly used materials include polydimethylsiloxane (PDMS), poly(methyl methacrylate) (PMMA), cellulose, and commercial test strips. Zhao et al. reported a customized potentiostat integrating with paper-based microfluidic analytical devices for the detection of metabolites and human immunodeficiency virus (HIV)/ hepatitis C virus (HCV) co-infection. The cost of manufacturing a paper-based device are calculated to be \$0.02 and the potentiostat as \$90 featuring ultralow-cost sensor and affordable detector [11]. Traditional microfluidic materials such as PDMS and PMMA maintain excellent transparency, and ensure promising optical sensing performance using mature digital imaging methods. Besides, the opaqueness, high contrast and uniform surface allow paper-based microfluidic devices (µPADs) to be excellent substrate for colorimetric reactions. For those microfluidic devices, many platforms employ commercial consumer electronics as detectors including but not limited to cameras [21], scanners [22], webcam [23], and cellphones [24]. All these instruments require much lower prices than those of the bench-top facilities, and promise the high affordability and easy accessibility for insitu uses.

2.2.2 Portability and low power consumption

All existing portable analytical platforms are designed to maintain low weight with less power consumption. The sensors and detectors are usually powered by portable batteries or onchip power supplies, and these power sources can also provide electrical excitations for certain type of reactions such as electrochemical tests. Recently, cellphone-based analytical platforms have been widely reported due to its merits of self-satisfying capability to provide illumination [25], digital imaging [26], electrochemical signals [27], on-chip data analysis [28], and wireless signal transmissions [29]. Lillehoj *et al.* reported a pluggable electrochemical platform for Plasmodium falciparum histidine-rich protein 2 (PfHRP2) protein measurement, while the phone processor provides power and electrochemical potentials to external printed circuit boards (PCBs) [28] (Figure 2-2 (B)). In the view of the computational integration of a telephone, cellphone-based analytical devices can also serve as a central platform for data analysis and information database in the remote sensing systems [30-35]. Figure 2-2 (A) shows a smartphone-based portable bacteria pre-concentrating microfluidic sensor and impedance sensing system, which use Bluetooth for wireless connectivity and a customized cellphone application for data transmissions [36].

2.2.3 Rapid measurement with high performance

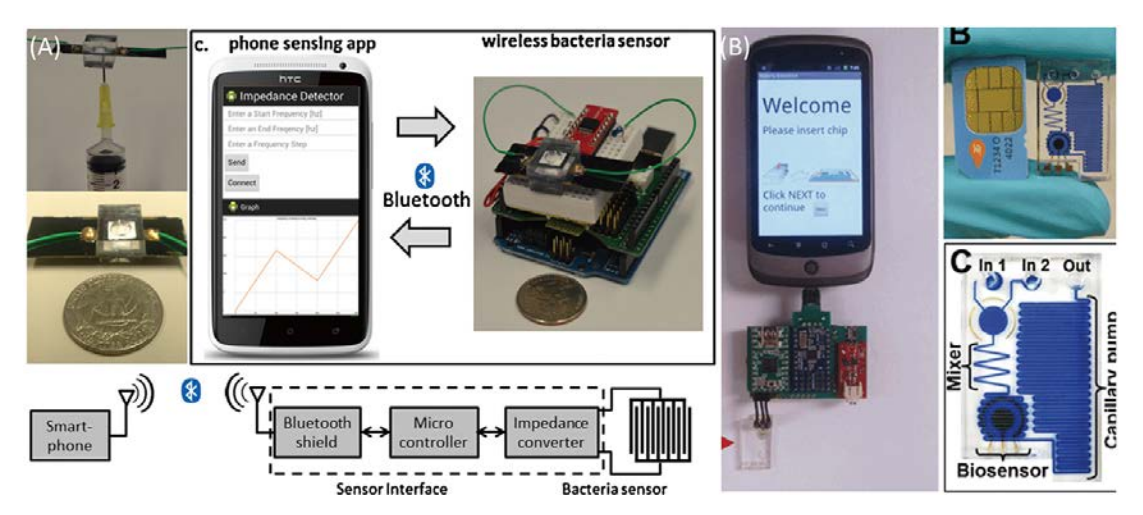


Figure 2-2. (**A**) Wireless mobile phone impedance sensing system for bacteria detection, which is integrated with a smartphone sensing application and a wireless bacteria sensor [36]. (**B**) Photograph of the pluggable microfluidic chip and a mobile phone for electrochemical detections of *Pf*HRP2, an important biomarker for malaria [28].

These platforms leverage advantages of miniaturized sensors to achieve less reagent consumption, fewer experimental procedures, and more rapid measurements. Cellulose-based microfluidic devices, i.e. paper-based sensors, provide high surface-to-volume ratios and abundant reaction sites, which promise higher efficiency during fluid manipulation and reagent reaction. Their assay protocols are usually modified to have small sample volumes, fewer reagent volumes, and less incubation time [37]. In the measurement level, many portable instruments are designed to intimately contact with those assays, perform testing, obtain results, and analyze data in a short period of time. It reduces the turnaround time compared with regular assays requiring liquid transferring, instrument preheating, and data processing. To further improve the performance, designs of multiplexing and multi-layer configurations can be easily implemented into the devices, enabled by detectors with multiplexing capabilities. Besides, nanomaterials are also introduced to those assays for higher sensitivity and lower limits of detection, such as gold nanoparticles [21, 38], silver nanoparticles [39, 40], and graphene oxide [41].

2.2.4 User-friendliness

On those analytical platforms, there're many user-friendly design considerations, including simplified procedures for less training requirements, custom-made detectors for fewer manipulations, and mobile applications for easier data analysis. Figure 2-3 (A) and (B) show a customized application interface for fluorescence detection and spatial mapping of mercury contamination in water samples using a smart phone and disposable test tubes for solution samples [42]. Besides that, various communication methods have been proposed rendering it an easy way of delivering the results to both end-users and health centers, including text message [43], USB [28], Bluetooth [36] and Wi-Fi [44]. Those tools can be used for receiving instructions and transferring data from local devices to central processing unit through mobile network and internet, even in rural area and developing countries lacking necessary hardware facilities. G. M. Whitesides' group highlighted such a cellphone-based electrochemical device using charging cable and audio port for data collection and transmission from a local custom-made potentiostat to mobile network [29].

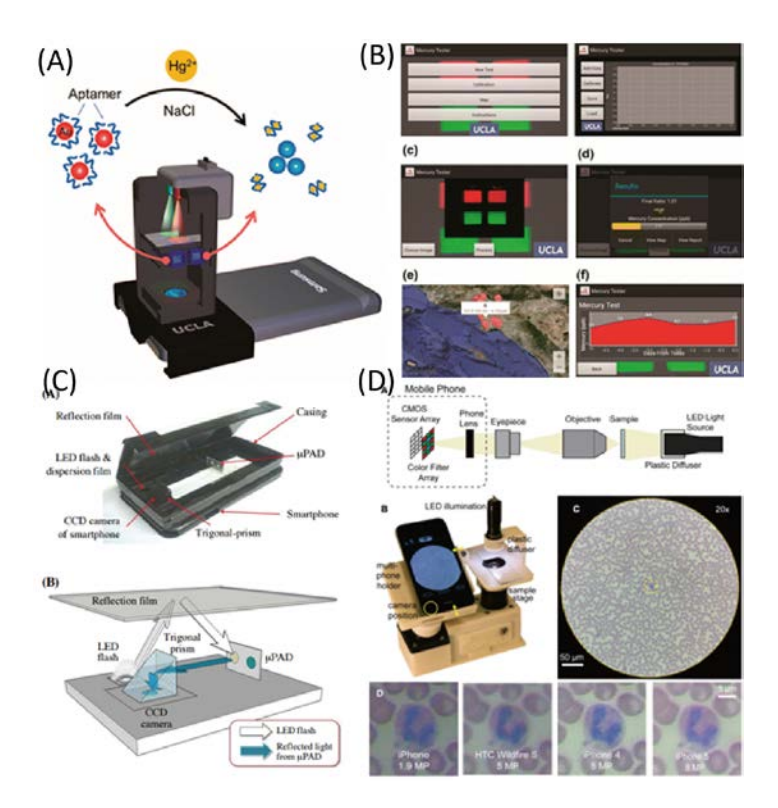


Figure 2-3. Cellphone analytical platform employing optical mechanisms (**A**) optical reader installed on an Android-based smart-phone, illuminated by red (625 nm) and green (523 nm) LEDs [42]. (**B**) Mercury detection application running on an Android phone [42]. (**C**) Configuration of smartphone-based device for optical detection of glucose on μPAD [45]. (**D**) Diagram of a phone-based mobile microscope for quantitative imaging on Wright stained blood smear [26].

2.3 Working principles

Based on the measurement mechanisms, the design principles of miniature analytical platforms can be classified as optical detections and electrochemical detections. Optical sensors utilize an optical element as signal output, such as the color change in the format of RGB, wavelength shifting, and illumination intensity. To interface these assays, optical analyzers utilize illumination sources and compact cameras/photodiodes for lighting and imaging. On the other hand, electrochemical sensors usually involve the value changes in current, potential, impedance, and capacitance. In virtue of that, electrical analyzers employ external power and processor units for electrochemical signal generation and data collection. **Figure 2-1** shows the classifications of portable sensing platforms and categories to each sub-section.

2.3.1 Optical sensors and analyzers

Optical sensors are constructed on various optical mechanisms, including fluorescence detections [46-48], colorimetric reactions [49-51], and plasmonic resonance based detections [42, 52]. *In-situ* optical detections can be achieved using portable microscopes [53, 54], spectrometers [55, 56], quantitative scanners [57], and cellphones cameras [56]. **Figure 2-3** shows three cellphone-based optical sensing systems. Besides, many optical sensor systems are integrated with customized detectors built from compact cameras, scanners, cellphones, and high-performance photodiodes. Within optical sensors, some takes the mechanism of the relationship between light transmission rate and analyte reactions. The substrates of those sensors are usually built on materials with excellent transparency such as PDMS [36, 56, 58], PMMA [59] and disposable tubes [42]. Another type of devices relies on digital imaging to distinguish the concentration information after analyte reaction. Those sensors are built based on superior light reflection on substrates with good opaqueness such as paper test strips [50], paper-based microfluidic devices [45, 60, 61], and textile-based microfluidic devices [62].

Paper-based sensors maintain merits of light weight, low cost, high porosity, and clean white background. They promote the development of optical portable systems, and enable flexible integration, portability, miniaturization, and mass production. Their specific porous structures ensure abundant binding sites for biomolecule immobilization. Apart from that, paper-based devices are biocompatible and chemical inert, making them excellent microfluidic platforms to adopt mature assay protocols. Since 2009, paper-based microfluidics have expanded their applications to different tests such as nucleic acid detection [63], immunoassay [64, 65], blood type test [66], human metabolite assay [67-69], and environmental analyses of pollutants like mercury [38, 70], ammonia [71], and lead [72]. Moreover, paper maintains the distinguished features of flexibility in shape and fabrication. It is easy to incorporate with multiplexing and multi-layer structures for high throughput, and nanomaterials for high analytical performance such as gold nanoparticles [38, 72], silver nanoparticles [39, 70], and silica nanoparticles [73].

In terms of portable optical detectors, many platforms are designed as integrated systems containing signal generation, image capturing, data collection and analysis. Cellphone-based biosensing has been considered as one of the most prospective platforms for mobile point-of-care (POC) diagnosis, as it has easy accessibility and powerful capabilities. Phone cameras can be used for image capturing in an optical biosensing system, with successful demonstrations on

iPhones [46, 74-76] and Android phones [77-79]. Their wide range of optical capabilities enables sensing mechanisms in fluorescence [46-48], colorimetry [49-51], plasmonic resonance [42], microscopy [53, 54], and spectrometry [55, 56]. **Figure 2-3 (C)** shows an integrated platform including a μPAD for running optical glucose bioassay and a cellphone for quantitative colorimetric measurement, which provides an alternative to quantitative scientific imaging [45]. **Figure 2-3 (D)** shows the diagram of a phone-based mobile microscope for quantitative imaging on Wright stained blood smear [26].

For cellphone-based sensors, some designs utilize the light source from a phone and regard the light transmission rate as the output signal [25]. Others utilize an external illumination source for lighting while the phone camera for image capturing [26, 42]. For instance, Greenbaum *et al.* presented a lens-free, cost-effective and field-portable super-resolution color microscope, which transforms the color component of RGB image into YUV colorspace and separate color information from brightness. It weighs less than 145 grams with dimensions smaller than $17 \times 6 \times 5$ cm, which is suitable for field settings and POC uses [53]. Those studies reveal a promising imaging alternative to traditional RGB tools relying on bench-top instrumentations.

2.3.2 Electrochemical sensors and analyzer

Different from optical sensing, electrochemical sensing relies on the electrical output from a chemical reaction and automatic data collection by a potentiostatic controller from electrochemical cells. There are three types of portable electrochemical analyzers, involving glucometer [80, 81], cellphone-aided tools [28, 29], and custom-made potentiostat (*e.g.*, "cheapstat") [82]. The glucometer, as the first commercialized portable analytical platform for POC glucose test, has been further investigated for the feasibility of diagnosing other diseases such as cancer [83], HIV [84], mycotoxins [61], and the analysis for metal ion of copper [80]. Using this platform, glucometer acts as the original potentiostat without modification. Instead, specific assay protocol is created and modified to generate glucose in an acceptable range as the final product to accommodate the glucometer. Through calibrating the generated glucose concentration, it can trace back the original analytes such as telomerase activity in cancer cells [83], copper ion concentrations for water quality control [80], and HIV relevant DNA sequences for HIV screening [84]. **Figure 2-4 (A)** illustrates a glucometer-based analytical platform adaptable to an immune sensing platform for Aflatoxins detection [61].

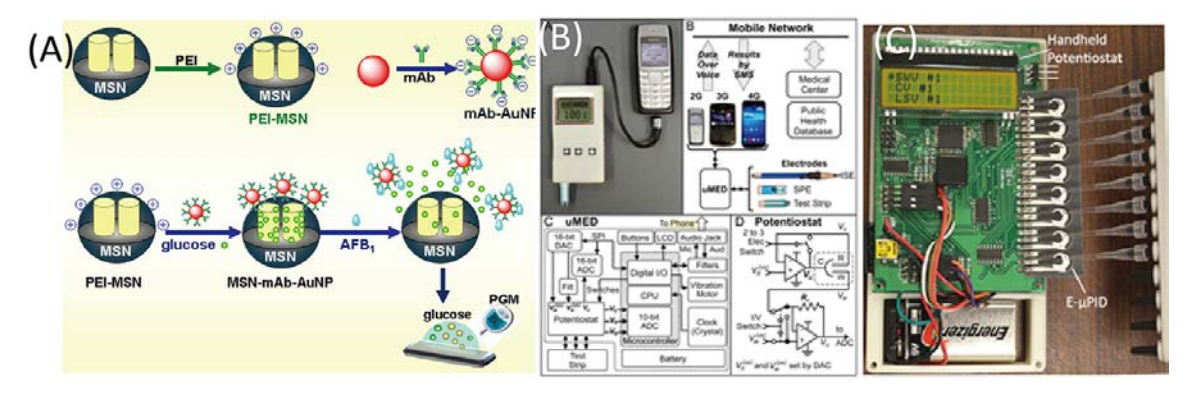


Figure 2-4. Three types of independent handheld electrochemical readers: **(A)** Glucometer adaptable to an immune sensing platform for Aflatoxins [61]. **(B)** Custom-made potentiostat as a universal platform for electrochemical detections for a variety of targets [29]. **(C)** Handheld potentiostat for multiplexed detection of HIV and HCV co-infection [12].

As another popular electrical platform, custom-made handheld potentiostat has arisen as a professional and powerful state-of-art tool for *in-situ* electrochemical tests abiding by the WHO's ASSURED criteria. It is developed on a microcontroller-based electronic circuit programmed with specific electrochemical waveforms, and collects the resulting current automatically. It is capable of carrying out various electrochemical protocols (e.g., cyclic voltammetry, square-wave voltammetry, and anodic stripping voltammetry) and providing sufficient performance in chemical and biomarker detections. The custom-made potentiostat is easy to integrate with many advantageous features such as multiplexing, wireless data transmission, on-chip calculation, analysis and display. With that, multiple types of measurements can be conducted on the custom-made potentiostat, including but not limited to, metabolites [11, 29], immunoassay [12, 29], and heavy metal ions [29], making it a powerful alternative to bench-top potentiostat. **Figure 2-4** (**C**) shows a fully integrated multiplexing handheld potentiostat capable of carrying out electrochemical detections with telemedicine capability.

Cellphone-based electrochemical analyzers also attract growing interests due to the fact that they can be programmed to collect the data, make plots, and send data to mobile network and health center. Pluggable printed circuit board (PCB) is a popular method designed to interface with cellphone for electrochemical measurements [28, 85]. A phone acts as the central controller and sends orders to the PCB, and the PCB will load the parameters of an electrochemical test to the samples, and send the data back to the phone for analysis. Besides that, cellphone can also act

as a communication center which works with a handheld potentiostat [29]. **Figure 2-4 (B)** illustrates a custom-made potentiostat connected with a regular cellphone aiming at electrochemical detections for a variety of targets. The cellphone connects the potentiostat through its audio port, and acts as a communication center for remote data transmission. Such a design structure enables the affordable electrochemical monitoring of diseases in developing countries and rural areas lacking high-end measuring/communication equipment.

2.4 Applications

Through miniaturization of sensing materials and electronics, studies have demonstrated the integration of multiple functions into analytical platforms. Various portable tools have contributed to on-site analysis for applications such as disease diagnostics [28, 60, 85-87], physiological healthcare monitoring [88-94], water environmental monitoring [15, 42, 61], and many others like nucleic acid testing [63, 95-97] and food safety inspection [4, 98, 99].

2.4.1 Disease diagnosis

Diagnostic analytes in human body fluids can be classified into metabolites, immune reactive proteins, nucleic acids, bacteria, virus, and cells. Human metabolism is a series of complex biophysical and biochemical reactions, and the metabolites are the fundamental biochemical components for regulating and balancing the life-sustaining chemical transformations within the cells of living organisms [100]. Metabolites are direct indicators for disease control in daily routine; for instance, the blood glucose level is a major parameter to control in treating diabetes. Many metabolic measurements in human fluids have been achieved based on colorimetric or electrochemical enzymatic reactions on portable platforms, including uric acid [11] and albumin in urine [101], glucose in blood [102], and nitrite in saliva [103]. Another important group of biomarkers for disease diagnosis are the immunological proteins. The detection of these protein markers have been realized on many portable analytical platforms, and many tests are based on the mature enzyme-linked immunosorbent assays (ELISAs). ELISA is for detection of immunoreactive proteins such as antigen and antibody, and is the most effective method for diagnosis of many diseases such as cancer [104], tuberculosis (TB) [79], and sexually transmitted infections [12]. On portable analytical platforms, there have been successful demonstrations of detecting HIV, TB, and malaria in whole blood [79], PfHRP2 antigens for malaria in human serum [28], H1N1from aerosol samples [87], and prostate specific antigen

(PSA) in serum [59]. For instance, Ahmed *et al.* reported a power-free, portable "Chip EIA" ELISA, which is more suitable for point-of-care testing and eliminates the need for pumps and valves through a simple permanent magnet and magnetic nanoparticles [59]. Quantitative signal readout was obtained through the use of cellphone camera imaging and the analysis of the images, and the platform was employed for testing PSA in 19 serum samples.

2.4.2 Physiological monitoring

Recently, there have been multiple research platforms for physiological monitoring based on wearable devices made from textiles [105], polymers [88], and flexible substrates like tattoos [106] and artificial teeth [89]. Efforts have been spent on the development of wearable biosensors for monitoring of biochemical markers like metabolites [88-90], electrolytes [88, 91] and pH [92] in body fluid from saliva [89], sweat [88, 93], and tear [90, 94]. Wang et al. proposed the integration of a miniaturized circuit chip inside an artificial teeth for the monitoring of uric acid in saliva, and the chip transmits radio frequency signals to an independent receiver in real time [89] (Figure 2-5 (C) and (D)). Considering the easy availability and abundant amount of sweat and the non-invasiveness of perspiration, many wearable platforms focus on the monitoring of biomarkers in sweat, which can reveal the information of important metabolites and electrolyte such as lactate, glucose, uric acid, sodium, potassium and chloride. Pioneering work on wearable sweat biosensors was demonstrated by the Diamond Group, which measured sweat pH and sweating rate during exercise paired with emitter-detector LEDs [107, 108]. They also proposed an elasticated belt with electrochemical detection for sweat sodium, which involves the polyvinyl chloride tubed ion selective electrode coupled with a commercial digital multimeter [109].

As the uniqueness of wearable real-time devices, their detectors must be either independent or capable of wireless communication in the scenario of long time continuous working with biosensors. A recent work was reported by the group of Ali Javey in 2016 (**Figure 2-5** (**A**) and (**B**)). They developed a wearable, fully integrated sensor arrays for multiplexed detection of glucose, lactate, sodium, potassium and temperature during perspiration [88]. Through continuous monitoring of body fluid, these wearable analytical platforms possess a significant potential to the practical controlling of fitness, electrolyte imbalance, physical well-being, and personal healthcare.

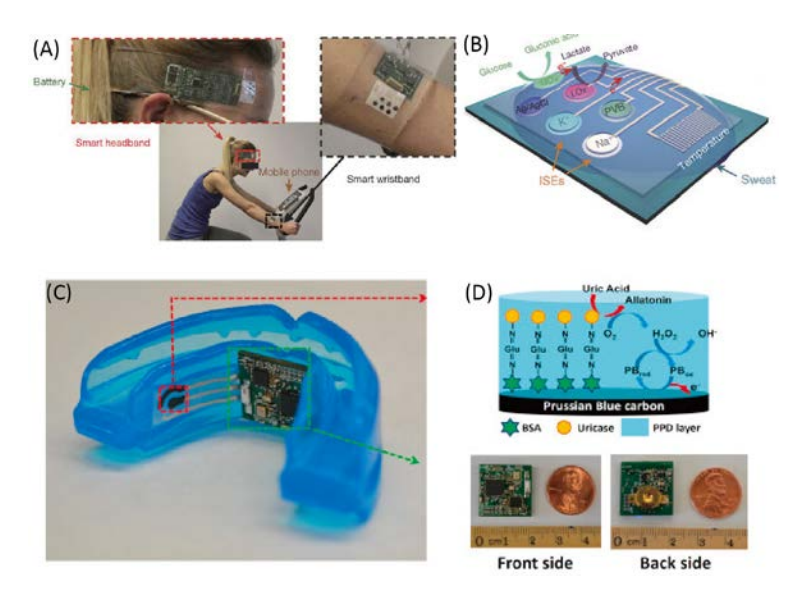


Figure 2-5. **(A)** Photographs of a subject wearing a 'smart headband' and a 'smart wristband' during stationary cycling [88]. **(B)** Schematic of the sensor array (including glucose, lactate, sodium, potassium and temperature sensors) for multiplexed perspiration analysis [88]. **(C)** Photograph of the mouth-guard biosensor integrated with wireless amperometric circuit board [89]. **(D)** Photograph of the wireless amperometric circuit board: front side (left) and back side (right) [89].

2.4.3 Water quality monitoring

Water is the essential element in human life for both drinking and everyday use. Water contamination poses harm to the massive biosphere, human being and economics, and urges quick and reliable real-time water quality monitoring. Major contaminants in water include nutrients (nitrogen and phosphorus compounds), metals ions (copper, zinc, cadmium, lead and mercury), and many other chemical toxins. By measuring those common targets regularly, one can achieve responsive monitoring and effective control of the water quality.

Heavy metal ions released into various water systems have severe impact on the environment and human beings, and excess exposure to toxic metal ions through drinking water pose high risks to human health and cause life-threatening diseases [15]. Thus, it is highly demanded to develop rapid, low-cost and sensitive analytical methods for detection of metal ions in water. Based on portable analytical platforms, there have been many studies for metal ions released in water such as inorganic salts of Co(NO₃)₂, K₂Cr₂O₇, K₂CrO₄, Ni(NO₃)₂, Cu(NO₃)₂, KMnO₄

[110], mercury (III) [42], lead and aluminum [15], and iron [61]. Those platforms promise convenient solutions for monitoring metal ions released into the environment.

Besides heavy metal ions, monitoring of nutrient wastes also has important implications in environment protection. They have direct sources from human-related activities such as industrial waste water, domestic sewage, organic fertilizers and manures from agricultural activities, and human and animal excreta. Excess amounts of these wastes readily move with the water bodies, and causes significant water contamination and health issues on a global scale [111]. Common inorganics and organics contain phosphorus, nitrogen, and sulfate. Recent studies have demonstrated *in-situ* detection of phosphorous [112], nitrate/nitrite/ammonium [113] on various portable platforms such as cellphone-based and customized optical analyzers. As a representative, Diamond *et al.* proposed a portable centrifugal microfluidic CD reactor for detection of total inorganic nitrogen (nitrate/nitrite/ammonium) [113]. The *in-situ* monitoring of these inorganics and organics will play a great role in many fields including chemical industries, agriculture, pharmaceuticals, and water treatment industries.

2.4.4 Others

There are several studies on nucleic acid measurements on mobile devices, including rough determination of target DNA segmentation based on fluorescence [96], mutation detection based on tag coated magnetic microbeads for deafness-related mutations [95], single DNA molecule imaging and sizing on a phone based microscope [97], and extraction and detection of Salmonella genomic nucleic acids on a paper-based microfluidic device [63]. Nevertheless, portable biosensing also provides an accessible, low-cost, portable and accurate tool for food contamination and spoilage detections. There have been successful demonstrations in the ripeness tester from spectral analysis in banana [4], and health supplementary of vitamin D [76]. More importantly, it can help reveal the detection of foodborne bacterial pathogens of salmonella [60], E.coli [86], and rbST biomarker analysis in milk [99].

2.5 Future trends

High-performance analytical platforms are attracting increasing interest from researchers and industries due to their capability of providing low-cost and reliable tools in many applications. Rapid developments have been observed in miniaturized microfluidic devices, flexible handheld detectors, and advanced peripheral supports. Considering the current state of the art in those

devices and the future demands, five technological trends are expected: (i) improvement of assay protocols for fully integrated detections; (ii) hybridization of miniaturized microfluidic devices, made from different materials such as paper, PDMS, glass, and PMMA, to achieve more flexible functions for practical in-field testing involving complex fluid operations such as species separation and automated fluidic control; (iii) addition of battery and flexible electronics to achieve self-powered platforms; (iv) real sample trials; (v) smart and convenient personal healthcare.

- 1. Many of the existing portable analytical platforms are demonstrated using spiked samples, such as serum, clean waters, and artificial buffers. The analytical tests in real world usually require extra procedures for separation from whole blood and polluted water before running a test. Additional assay protocols should be developed to meet the needs of fluid filtration or extraction with low volumes of samples. Paper with micrometer-sized pores can be easily modified for blood separation, which could be integrated in paper-based diagnostic platforms for fully integrated diagnostic tests at POC [114-117]. In addition, chromatography paper was widely used in thin-layer chromatography [118-121], and could possibly enrich the separation functions of paper-based biosensors, i.e. for amino acid separation and determination in food.
- 2. The hybridization of microfluidics based on paper, PDMS, glass, and PMMA also show significant promise in the future research [41, 122, 123]. Such hybrids can take advantages from different types of substrates to achieve better performance than that of single type of substrate. For example, the integration of paper and traditional polymer-based microfluidic devices inherits the advantages of protein immobilization in cellulose paper and controlled fluidic flow in polymer chips. Automatic fluidic and timing control [124-126] could also be integrated for automatic manipulation of multi-step procedures in both disease diagnosis and environmental measurement.
- 3. As portable analytical devices are usually small-sized and light-weight, they require lower volumes of samples and reagents, and less reaction time. It could save much electrical energy required to power the reaction than that of traditional optical/electrochemical sensors. For electrochemical detections, they can be triggered at millivolt levels lower than 3.3 V, a battery could be a perfect energy provider [127, 128]. Besides that, flexible electronics built from paper [129-131], polymers [132], and fabrics [133] possesses increasing importance in the field of capacitors, transistors, piezoresistors and other complex circuits. Combining the platforms with

battery-powered flexible electronics can be an attractive revolution for the future diagnosis and everyday life. It can serve as a self-powered, low-cost, and environmental-friendly tool.

- 4. Diagnosis in the real world involves more practical problems rather than clean lab-based experiments. There will be more systematical studies on applying the portable analytical platforms to clinical sample trials. Challenges lie in the complexity of real samples. The sensor performance should be verified and enhanced by introducing interfering biomarkers in the calibration sample. The selectivity test should be carried out to verify sensor's capability in a variety of compounds with similar chemical characteristics. Those tests should be conducted within the normal range of markers, and also abnormal concentrations.
- 5. Personal healthcare will be largely improved in terms of convenience, cost, and accuracy. Non-invasive wireless sensors and screening services will be developed for mobile health surveillance, monitoring and data mining for diseases like tumor, cancer, and intracorporal bleeding. Emergency information database should be constructed based on the regular monitoring and analysis of biomedical variables related to personal healthcare for prevention of fatal diseases. Intelligent applications will be developed for the prediction of dangerous movement for patients, nutrition analysis from food intake, and chronic disease diagnostic.

2.6 Conclusion

The development of portable analytical platforms has enabled the improvement of human healthcare and environmental monitoring in a rapid, reliable and low-cost manner without barriers from the requirements of expertized technicians or sophisticated equipment. This paper reviews the development and state of the art of portable analytical platforms, with the design considerations, sensing techniques, and progresses regarding the in-field applications of disease diagnostics, water environmental monitoring, and food safety inspection. The major sensing mechanisms and detection principles have been discovered through optical sensing and electrochemical sensing. Optical sensors rely on the chemical reactions with optical outputs such as fluorescence, colorimetry, wavelength shift, and plasmonic resonance. They usually depend on portable detectors built from cameras, scanners or customized photodiode devices to serve as an image observation part. Electrochemical sensors are based on the electrons transferred in a chemical reaction through electrodes, which are built on chemically inert substrates such as cellulose, PDMS, glass and silicon. They usually take advantage of the computational processor

of a microcontroller or cellphone for electrical signal generation and collection. Cellphone-based sensing techniques are highlighted as they are capable of both sensing techniques with easy access. They can serve as multiple roles in imaging, illumination, electricity, data processing, and tele-transmission. The achievements of portable analytical platforms are summarized towards disease diagnostics, water pollution, and food safety applications, with the focus on the involved markers including metabolites, immunoassays, heavy metal ions, nutrient pollutions, and nucleic acids. For the future trends, we propose some possible concepts and ideas from the view of (i) improvement of assay protocols, (ii) hybridization of microfluidic devices made from different materials, (iii) integration of self-powered flexible electronics, (iv) real sample trials, and (v) smart personal healthcare with challenges, critical considerations and possible approaches.

2.7 Reference

- [1] A. Jang, Z. Zou, K. K. Lee, C. H. Ahn, and P. L. Bishop, "State-of-the-art lab chip sensors for environmental water monitoring," *Measurement Science and Technology*, vol. 22, no. 3, p. 032001, 2011.
- [2] Z. Iqbal and R. B. Bjorklund, "Colorimetric analysis of water and sand samples performed on a mobile phone," (in English), *Talanta*, vol. 84, no. 4, pp. 1118-1123, May 30 2011.
- [3] A. Pantelopoulos and N. G. Bourbakis, "A survey on wearable sensor-based systems for health monitoring and prognosis," *IEEE Transactions on Systems, Man, and Cybernetics, Part C (Applications and Reviews)*, vol. 40, no. 1, pp. 1-12, 2010.
- [4] Y. Intaravanne, S. Sumriddetchkajorn, and J. Nukeaw, "Cell phone-based two-dimensional spectral analysis for banana ripeness estimation," *Sensors and Actuators B: Chemical*, vol. 168, no. 0, pp. 390-394, 6/20/2012.
- [5] A. J. Bandodkar and J. Wang, "Non-invasive wearable electrochemical sensors: a review," *Trends in biotechnology*, vol. 32, no. 7, pp. 363-371, 2014.
- [6] R. J. Smith, T. A. Stamp, D. D. Bouricius, and E. Lancaster, "Blood glucose meter," ed: Google Patents, 2009.
- [7] iHealth, "Glucose Meter, Blood Glucose Meters iHealth," 2017.
- [8] HACH, "High Performance Turbidity Meters Hach," 2017.
- [9] Omron, "Omron BP786CAN 10 Series Upper Arm Blood Pressure Monitor Plus Bluetooth Smart."
- [10] Zacurate, "Finger Heart Rate and Blood HbO2 Meter with silicon cover, batteries and lanyard (Blue)," 2017.
- [11] C. Zhao, M. M. Thuo, and X. Liu, "A microfluidic paper-based electrochemical biosensor array for multiplexed detection of metabolic biomarkers," *Science and Technology of Advanced Materials*, vol. 14, no. 5, p. 054402, 2013.

- [12] C. Zhao and X. Liu, "A portable paper-based microfluidic platform for multiplexed electrochemical detection of human immunodeficiency virus and hepatitis C virus antibodies in serum," *Biomicrofluidics*, vol. 10, no. 2, p. 024119, 2016.
- [13] K. Narsaiah, S. N. Jha, R. Bhardwaj, R. Sharma, and R. Kumar, "Optical biosensors for food quality and safety assurance—a review," *Journal of food science and technology*, vol. 49, no. 4, pp. 383-406, 2012.
- [14] S. Herranz, M. Marazuela, and M. Moreno-Bondi, "Automated portable array biosensor for multisample microcystin analysis in freshwater samples," *Biosensors and Bioelectronics*, vol. 33, no. 1, pp. 50-55, 2012.
- [15] C. Zhao, G. Zhong, D.-E. Kim, J. Liu, and X. Liu, "A portable lab-on-a-chip system for gold-nanoparticle-based colorimetric detection of metal ions in water," *Biomicrofluidics*, vol. 8, no. 5, p. 052107, 2014.
- [16] J. L. Fu and F. Ayazi, "Dual-mode piezo-on-silicon resonant temperature and humidity sensor for portable air quality monitoring systems," in *Sensors*, 2010 IEEE, 2010, pp. 2131-2135: IEEE.
- [17] T. L. Rowlandson *et al.*, "Evaluation of several calibration procedures for a portable soil moisture sensor," *Journal of hydrology*, vol. 498, pp. 335-344, 2013.
- [18] D. Mabey, R. W. Peeling, A. Ustianowski, and M. D. Perkins, "Tropical infectious diseases: diagnostics for the developing world," *Nature Reviews Microbiology*, vol. 2, no. 3, pp. 231-240, 2004.
- [19] R. Peeling and D. Mabey, "Point of care tests for diagnosing infections in the developing world," *Clinical microbiology and infection*, vol. 16, no. 8, pp. 1062-1069, 2010.
- [20] A. W. Martinez, S. T. Phillips, G. M. Whitesides, and E. Carrilho, "Diagnostics for the developing world: microfluidic paper-based analytical devices," ed: ACS Publications, 2009.
- [21] W.-Y. Wu, Z.-P. Bian, W. Wang, and J.-J. Zhu, "PDMS gold nanoparticle composite film-based silver enhanced colorimetric detection of cardiac troponin I," *Sensors and Actuators B: Chemical*, vol. 147, no. 1, pp. 298-303, 2010.
- [22] C. M. Cheng *et al.*, "paper based elisa," *Angewandte Chemie International Edition*, vol. 49, no. 28, pp. 4771-4774, 2010.
- [23] J. Balsam, H. A. Bruck, Y. Kostov, and A. Rasooly, "Image stacking approach to increase sensitivity of fluorescence detection using a low cost complementary metal-oxide-semiconductor (CMOS) webcam," *Sensors and Actuators B: Chemical*, vol. 171, pp. 141-147, 2012.
- [24] A. W. Martinez, S. T. Phillips, E. Carrilho, S. W. Thomas III, H. Sindi, and G. M. Whitesides, "Simple telemedicine for developing regions: camera phones and paper-based microfluidic devices for real-time, off-site diagnosis," *Analytical chemistry*, vol. 80, no. 10, pp. 3699-3707, 2008.
- [25] Z. Iqbal and M. Eriksson, "Classification and quantitative optical analysis of liquid and solid samples using a mobile phone as illumination source and detector," *Sensors and Actuators B: Chemical*, vol. 185, pp. 354-362, 2013.
- [26] A. Skandarajah, C. D. Reber, N. A. Switz, and D. A. Fletcher, "Quantitative Imaging with a Mobile Phone Microscope," *PloS one*, vol. 9, no. 5, p. e96906, 2014.

- [27] J. L. Delaney, C. F. Hogan, J. Tian, and W. Shen, "Electrogenerated chemiluminescence detection in paper-based microfluidic sensors," *Analytical chemistry*, vol. 83, no. 4, pp. 1300-1306, 2011.
- [28] P. B. Lillehoj, M.-C. Huang, N. Truong, and C.-M. Ho, "Rapid electrochemical detection on a mobile phone," *Lab on a Chip*, vol. 13, no. 15, pp. 2950-2955, 2013.
- [29] A. Nemiroski *et al.*, "Universal mobile electrochemical detector designed for use in resource-limited applications," *Proceedings of the National Academy of Sciences*, vol. 111, no. 33, pp. 11984-11989, 2014.
- [30] K. Malzahn, J. R. Windmiller, G. Valdes-Ramirez, M. J. Schoning, and J. Wang, "Wearable electrochemical sensors for in situ analysis in marine environments," (in English), *Analyst*, vol. 136, no. 14, pp. 2912-2917, 2011.
- [31] J. R. Windmiller and J. Wang, "Wearable Electrochemical Sensors and Biosensors: A Review," (in English), *Electroanalysis*, vol. 25, no. 1, pp. 29-46, Jan 2013.
- [32] S. S. Bhadoria and H. Gupta, "A Wearable Personal Healthcare and Emergency Information Based On Mobile Application," 2013.
- [33] K. J. Fraser *et al.*, "Wearable electrochemical sensors for monitoring performance athletes," in *SPIE Photonic Devices+ Applications*, 2011, pp. 81180C-81180C-12: International Society for Optics and Photonics.
- [34] N. D. Lane, E. Miluzzo, H. Lu, D. Peebles, T. Choudhury, and A. T. Campbell, "A survey of mobile phone sensing," *IEEE Communications magazine*, vol. 48, no. 9, 2010.
- [35] T. Das, P. Mohan, V. N. Padmanabhan, R. Ramjee, and A. Sharma, "PRISM: platform for remote sensing using smartphones," in *Proceedings of the 8th international conference on Mobile systems, applications, and services*, 2010, pp. 63-76: ACM.
- [36] J. Jiang *et al.*, "Smartphone based portable bacteria pre-concentrating microfluidic sensor and impedance sensing system," *Sensors and Actuators B: Chemical*, vol. 193, pp. 653-659, 2014.
- [37] S. Byrnes, G. Thiessen, and E. Fu, "Progress in the development of paper-based diagnostics for low-resource point-of-care settings," *Bioanalysis*, vol. 5, no. 22, pp. 2821-2836, 2013.
- [38] G.-H. Chen, W.-Y. Chen, Y.-C. Yen, C.-W. Wang, H.-T. Chang, and C.-F. Chen, "Detection of mercury (II) ions using colorimetric gold nanoparticles on paper-based analytical devices," *Analytical chemistry*, vol. 86, no. 14, pp. 6843-6849, 2014.
- [39] N. Ratnarathorn, O. Chailapakul, C. S. Henry, and W. Dungchai, "Simple silver nanoparticle colorimetric sensing for copper by paper-based devices," *Talanta*, vol. 99, pp. 552-557, 2012.
- [40] F. Liu *et al.*, "Aptamer based test stripe for ultrasensitive detection of mercury (II) using a phenylene-ethynylene reagent on nanoporous silver as a chemiluminescence reagent," *Microchimica Acta*, vol. 181, no. 5-6, pp. 663-670, 2014.
- [41] P. Zuo, X. Li, D. C. Dominguez, and B.-C. Ye, "A PDMS/paper/glass hybrid microfluidic biochip integrated with aptamer-functionalized graphene oxide nanobiosensors for one-step multiplexed pathogen detection," *Lab on a Chip*, 10.1039/C3LC50654A vol. 13, no. 19, pp. 3921-3928, 2013.
- [42] Q. Wei *et al.*, "Detection and Spatial Mapping of Mercury Contamination in Water Samples Using a Smart-Phone," *ACS Nano*, vol. 8, no. 2, pp. 1121-1129, 2014/02/25 2014.

- [43] C. D. Chin *et al.*, "Mobile device for disease diagnosis and data tracking in resource-limited settings," *Clinical chemistry*, vol. 59, no. 4, pp. 629-640, 2013.
- [44] M. Roy, D. Seo, C.-H. Oh, M.-H. Nam, Y. J. Kim, and S. Seo, "Low-cost telemedicine device performing cell and particle size measurement based on lens-free shadow imaging technology," *Biosensors and Bioelectronics*, 2014.
- [45] H. J. Chun, Y. M. Park, Y. D. Han, Y. H. Jang, and H. C. Yoon, "Paper-based glucose biosensing system utilizing a smartphone as a signal reader," *BioChip Journal*, vol. 8, no. 3, pp. 218-226, 2014.
- [46] B. Awqatty, S. Samaddar, K. J. Cash, H. A. Clark, and J. M. Dubach, "Fluorescent sensors for the basic metabolic panel enable measurement with a smart phone device over the physiological range," *Analyst*, vol. 139, no. 20, pp. 5230-5238, 2014.
- [47] J. Balsam, H. A. Bruck, and A. Rasooly, "Capillary array waveguide amplified fluorescence detector for mHealth," *Sensors and Actuators B: Chemical*, vol. 186, pp. 711-717, 2013.
- [48] H. C. Koydemir *et al.*, "Rapid imaging, detection and quantification of Giardia lamblia cysts using mobile-phone based fluorescent microscopy and machine learning," *Lab on a Chip*, 2014.
- [49] L. Shen, J. A. Hagen, and I. Papautsky, "Point-of-care colorimetric detection with a smartphone," *Lab on a Chip*, vol. 12, no. 21, pp. 4240-4243, 2012.
- [50] J. I. Hong and B.-Y. Chang, "Development of the smartphone-based colorimetry for multi-analyte sensing arrays," *Lab on a Chip*, vol. 14, no. 10, pp. 1725-1732, 2014.
- [51] V. Oncescu, M. Mancuso, and D. Erickson, "Cholesterol testing on a smartphone," *Lab Chip*, 10.1039/C3LC51194D vol. 14, no. 4, pp. 759-63, Feb 21 2014.
- [52] X. Zeng *et al.*, "On-chip Plasmonic Interferometer Array for Portable Multiplexed Biosensing System," in *CLEO: QELS_Fundamental Science*, 2014, p. FM3K. 3: Optical Society of America.
- [53] A. Greenbaum, N. Akbari, A. Feizi, W. Luo, and A. Ozcan, "Field-portable pixel superresolution colour microscope," *PloS one*, vol. 8, no. 9, p. e76475, 2013.
- [54] D. Shin, M. C. Pierce, A. M. Gillenwater, M. D. Williams, and R. R. Richards-Kortum, "A fiber-optic fluorescence microscope using a consumer-grade digital camera for in vivo cellular imaging," *PLoS One*, vol. 5, no. 6, p. e11218, 2010.
- [55] D. Gallegos *et al.*, "Label-free biodetection using a smartphone," *Lab on a Chip*, 10.1039/C3LC40991K 2013.
- [56] R. Gupta, R. G. Reifenberger, and G. U. Kulkarni, "Cellphone Camera Imaging of a Periodically Patterned Chip as a Potential Method for Point-of-Care Diagnostics," *ACS Applied Materials & Interfaces*, vol. 6, no. 6, pp. 3923-3929, 2014/03/26 2014.
- [57] J. X. Wong, F. S. Liu, and H.-Z. Yu, "Mobile app-based quantitative scanometric analysis," *Analytical chemistry*, 2014.
- [58] P. Preechaburana, M. C. Gonzalez, A. Suska, and D. Filippini, "Surface plasmon resonance chemical sensing on cell phones," *Angewandte Chemie*, vol. 124, no. 46, pp. 11753-11756, 2012.
- [59] H. Adel Ahmed and H. M. Azzazy, "Power-free chip enzyme immunoassay for detection of prostate specific antigen (PSA) in serum," *Biosensors and Bioelectronics*, vol. 49, pp. 478-484, 2013.
- [60] T. S. Park, W. Li, K. E. McCracken, and J. Y. Yoon, "Smartphone quantifies Salmonella from paper microfluidics," *Lab Chip*, vol. 13, no. 24, pp. 4832-40, Dec 21 2013.

- [61] D. Tang *et al.*, "Low-cost and highly sensitive immunosensing platform for aflatoxins using one-step competitive displacement reaction mode and portable glucometer-based detection," *Analytical chemistry*, vol. 86, no. 22, pp. 11451-11458, 2014.
- [62] X. Li, J. Tian, and W. Shen, "Thread as a versatile material for low-cost microfluidic diagnostics," *ACS applied materials & interfaces*, vol. 2, no. 1, pp. 1-6, 2009.
- [63] C. F. Fronczek, T. San Park, D. K. Harshman, A. M. Nicolini, and J.-Y. Yoon, "Paper microfluidic extraction and direct smartphone-based identification of pathogenic nucleic acids from field and clinical samples," *RSC Advances*, vol. 4, no. 22, pp. 11103-11110, 2014.
- [64] X. Liu et al., "A portable microfluidic paper-based device for ELISA," in Micro Electro Mechanical Systems (MEMS), 2011 IEEE 24th International Conference on, 2011, pp. 75-78: IEEE.
- [65] E. Fu, T. Liang, P. Spicar-Mihalic, J. Houghtaling, S. Ramachandran, and P. Yager, "Two-dimensional paper network format that enables simple multistep assays for use in low-resource settings in the context of malaria antigen detection," *Analytical chemistry*, vol. 84, no. 10, pp. 4574-4579, 2012.
- [66] M. Li, J. Tian, M. Al-Tamimi, and W. Shen, "Paper-Based Blood Typing Device That Reports Patient's Blood Type "in Writing"," *Angewandte Chemie International Edition*, vol. 51, no. 22, pp. 5497-5501, 2012.
- [67] J. Nie, Y. Liang, Y. Zhang, S. Le, D. Li, and S. Zhang, "One-step patterning of hollow microstructures in paper by laser cutting to create microfluidic analytical devices," *Analyst*, 10.1039/C2AN36219H vol. 138, no. 2, pp. 671-676, 2013.
- [68] E. M. Fenton, M. R. Mascarenas, G. P. Lopez, and S. S. Sibbett, "Multiplex lateral-flow test strips fabricated by two-dimensional shaping," (in eng), *ACS applied materials & interfaces*, Research Support, U.S. Gov't, Non-P.H.S. vol. 1, no. 1, pp. 124-9, Jan 2009.
- [69] W. Dungchai, O. Chailapakul, and C. S. Henry, "Use of multiple colorimetric indicators for paper-based microfluidic devices," *Analytica Chimica Acta*, vol. 674, no. 2, pp. 227-233, 2010.
- [70] A. Apilux, W. Siangproh, N. Praphairaksit, and O. Chailapakul, "Simple and rapid colorimetric detection of Hg (II) by a paper-based device using silver nanoplates," *Talanta*, vol. 97, pp. 388-394, 2012.
- [71] B. M. Jayawardane, I. D. McKelvie, and S. D. Kolev, "Development of a gas-diffusion microfluidic paper-based analytical device (μPAD) for the determination of ammonia in wastewater samples," *Analytical chemistry*, vol. 87, no. 9, pp. 4621-4626, 2015.
- [72] M. Zhang *et al.*, "Three-dimensional paper-based electrochemiluminescence device for simultaneous detection of Pb 2+ and Hg 2+ based on potential-control technique," *Biosensors and Bioelectronics*, vol. 41, pp. 544-550, 2013.
- [73] E. Evans, E. F. M. Gabriel, T. E. Benavidez, W. K. T. Coltro, and C. D. Garcia, "Modification of microfluidic paper-based devices with silica nanoparticles," *Analyst*, vol. 139, no. 21, pp. 5560-5567, 2014.
- [74] M. W. Kadlec, D. You, J. C. Liao, and P. K. Wong, "A Cell Phone–Based Microphotometric System for Rapid Antimicrobial Susceptibility Testing," *Journal of Laboratory Automation*, vol. 19, no. 3, pp. 258-266, June 1, 2014 2014.
- [75] S. A. Khan, G. T. Smith, F. Seo, and A. K. Ellerbee, "Label-free and non-contact optical biosensing of glucose with quantum dots," *Biosensors and Bioelectronics*, vol. 64, pp. 30-35, 2015.

- [76] S. Lee, V. Oncescu, M. Mancuso, S. Mehta, and D. Erickson, "A smartphone platform for the quantification of vitamin D levels," *Lab Chip*, vol. 14, no. 8, pp. 1437-42, Apr 21 2014.
- [77] H.-C. Wu, C.-J. Chang, C.-C. Lin, M.-C. Tsai, C.-C. Chang, and M.-H. Tseng, "Developing Screening Services for Colorectal Cancer on Android Smartphones," *Telemedicine and e-Health*, 2014.
- [78] A. F. Coskun, R. Nagi, K. Sadeghi, S. Phillips, and A. Ozcan, "Albumin testing in urine using a smart-phone," *Lab on a Chip*, 10.1039/C3LC50785H 2013.
- [79] O. Mudanyali, S. Dimitrov, U. Sikora, S. Padmanabhan, I. Navruz, and A. Ozcan, "Integrated rapid-diagnostic-test reader platform on a cellphone," *Lab on a Chip*, 10.1039/C2LC40235A vol. 12, no. 15, pp. 2678-2686, 2012.
- [80] J. Su, J. Xu, Y. Chen, Y. Xiang, R. Yuan, and Y. Chai, "Sensitive detection of copper (II) by a commercial glucometer using click chemistry," *Biosensors and Bioelectronics*, vol. 45, pp. 219-222, 2013.
- [81] L. Yan *et al.*, "Target-responsive "sweet" hydrogel with glucometer readout for portable and quantitative detection of non-glucose targets," *Journal of the American Chemical Society*, vol. 135, no. 10, pp. 3748-3751, 2013.
- [82] A. A. Rowe *et al.*, "CheapStat: An open-source, "do-it-yourself" potentiostat for analytical and educational applications," *PloS one*, vol. 6, no. 9, p. e23783, 2011.
- [83] W. Wang, S. Huang, J. Li, K. Rui, J.-R. Zhang, and J.-J. Zhu, "Coupling a DNA-Based Machine with Glucometer Readouts for Amplified Detection of Telomerase Activity in Cancer Cells," *Scientific reports*, vol. 6, 2016.
- [84] J. Xu, B. Jiang, J. Xie, Y. Xiang, R. Yuan, and Y. Chai, "Sensitive point-of-care monitoring of HIV related DNA sequences with a personal glucometer," *Chemical Communications*, vol. 48, no. 87, pp. 10733-10735, 2012.
- [85] P. Lillehoj, M.-C. Huang, and C.-M. Ho, "A handheld, cell phone-based electrochemical biodetector," in *Micro Electro Mechanical Systems (MEMS)*, 2013 IEEE 26th International Conference on, 2013, pp. 53-56: IEEE.
- [86] V. K. Rajendran, P. Bakthavathsalam, and B. M. J. Ali, "Smartphone based bacterial detection using biofunctionalized fluorescent nanoparticles," *Microchimica Acta*, pp. 1-7, 2014.
- [87] H.-J. Kwon, C. F. Fronczek, S. V. Angus, A. M. Nicolini, and J.-Y. Yoon, "Rapid and Sensitive Detection of H1N1/2009 Virus from Aerosol Samples with a Microfluidic Immunosensor," *Journal of laboratory automation*, p. 2211068213504205, 2013.
- [88] W. Gao *et al.*, "Fully integrated wearable sensor arrays for multiplexed in situ perspiration analysis," *Nature*, vol. 529, no. 7587, pp. 509-514, 2016.
- [89] J. Kim *et al.*, "Wearable salivary uric acid mouthguard biosensor with integrated wireless electronics," *Biosensors and Bioelectronics*, vol. 74, pp. 1061-1068, 2015.
- [90] H. Yao *et al.*, "A contact lens with integrated telecommunication circuit and sensors for wireless and continuous tear glucose monitoring," *Journal of Micromechanics and Microengineering*, vol. 22, no. 7, p. 075007, 2012.
- [91] A. J. Bandodkar *et al.*, "Epidermal tattoo potentiometric sodium sensors with wireless signal transduction for continuous non-invasive sweat monitoring," *Biosensors and bioelectronics*, vol. 54, pp. 603-609, 2014.

- [92] V. F. Curto *et al.*, "Real-time sweat pH monitoring based on a wearable chemical barcode micro-fluidic platform incorporating ionic liquids," *Sensors and Actuators B: Chemical*, vol. 171, pp. 1327-1334, 2012.
- [93] M. Gamella *et al.*, "A novel non-invasive electrochemical biosensing device for in situ determination of the alcohol content in blood by monitoring ethanol in sweat," *Analytica chimica acta*, vol. 806, pp. 1-7, 2014.
- [94] S. Iguchi *et al.*, "A flexible and wearable biosensor for tear glucose measurement," *Biomedical microdevices*, vol. 9, no. 4, pp. 603-609, 2007.
- [95] G. Zhang *et al.*, "Validation of a mobile phone-assisted microarray decoding platform for signal-enhanced mutation detection," *Biosens Bioelectron*, vol. 26, no. 12, pp. 4708-14, Aug 15 2011.
- [96] D. Lee, W. P. Chou, S. H. Yeh, P. J. Chen, and P. H. Chen, "DNA detection using commercial mobile phones," *Biosensors and Bioelectronics*, vol. 26, no. 11, pp. 4349-4354, 7/15/2011.
- [97] Q. Wei *et al.*, "Imaging and Sizing of Single DNA Molecules on a Mobile-Phone," *ACS nano*, 2014.
- [98] D. J. You, K. J. Geshell, and J. Y. Yoon, "Direct and sensitive detection of foodborne pathogens within fresh produce samples using a field-deployable handheld device," (in English), *Biosensors & Bioelectronics*, vol. 28, no. 1, pp. 399-406, Oct 15 2011.
- [99] S. K. Ludwig *et al.*, "Cellphone-based detection platform for rbST biomarker analysis in milk extracts using a microsphere fluorescence immunoassay," *Analytical and bioanalytical chemistry*, vol. 406, no. 27, pp. 6857-6866, 2014.
- [100] S. Schuster, D. A. Fell, and T. Dandekar, "A general definition of metabolic pathways useful for systematic organization and analysis of complex metabolic networks," *Nature biotechnology*, vol. 18, no. 3, p. 326, 2000.
- [101] A. F. Coskun, R. Nagi, K. Sadeghi, S. Phillips, and A. Ozcan, "Albumin testing in urine using a smart-phone," *Lab on a Chip*, vol. 13, no. 21, pp. 4231-4238, 2013.
- [102] Z. Nie, F. Deiss, X. Liu, O. Akbulut, and G. M. Whitesides, "Integration of paper-based microfluidic devices with commercial electrochemical readers," *Lab on a Chip*, vol. 10, no. 22, pp. 3163-3169, 2010.
- [103] S. A. Klasner, A. K. Price, K. W. Hoeman, R. S. Wilson, K. J. Bell, and C. T. Culbertson, "Paper-based microfluidic devices for analysis of clinically relevant analytes present in urine and saliva," *Analytical and bioanalytical chemistry*, vol. 397, no. 5, pp. 1821-1829, 2010.
- [104] Y.-H. Lin, C.-C. Wang, and K. F. Lei, "Bubble-driven mixer integrated with a microfluidic bead-based ELISA for rapid bladder cancer biomarker detection," *Biomedical microdevices*, vol. 16, no. 2, pp. 199-207, 2014.
- [105] P. Rai, S. Oh, P. Shyamkumar, M. Ramasamy, R. E. Harbaugh, and V. K. Varadan, "Nano-bio-textile sensors with mobile wireless platform for wearable health monitoring of neurological and cardiovascular disorders," *Journal of The Electrochemical Society*, vol. 161, no. 2, pp. B3116-B3150, 2014.
- [106] W. Jia *et al.*, "Electrochemical tattoo biosensors for real-time noninvasive lactate monitoring in human perspiration," *Analytical chemistry*, vol. 85, no. 14, pp. 6553-6560, 2013.

- [107] S. Coyle *et al.*, "Textile sensors to measure sweat pH and sweat-rate during exercise," in *Pervasive Computing Technologies for Healthcare*, 2009. *PervasiveHealth 2009. 3rd International Conference on*, 2009, pp. 1-6: IEEE.
- [108] D. Morris, S. Coyle, Y. Wu, K. T. Lau, G. Wallace, and D. Diamond, "Bio-sensing textile based patch with integrated optical detection system for sweat monitoring," *Sensors and Actuators B: Chemical*, vol. 139, no. 1, pp. 231-236, 2009.
- [109] B. Schazmann *et al.*, "A wearable electrochemical sensor for the real-time measurement of sweat sodium concentration," *Analytical Methods*, vol. 2, no. 4, pp. 342-348, 2010.
- [110] L. L. Zamora, A. Mellado Romero, and J. M. Calatayud, "Quantitative colorimetric analysis of some inorganic salts using digital photography," *Analytical Letters*, vol. 44, no. 9, pp. 1674-1682, 2011.
- [111] B. De Borba, R. F. Jack, and J. Rohrer, "Determination of Total Nitrogen and Phosphorus in Wastewaters by Alkaline Persulfate Digestion Followed by IC."
- [112] G. Duffy, I. Maguire, B. Heery, C. Nwankire, J. Ducrée, and F. Regan, "PhosphaSense: A fully integrated, portable lab-on-a-disc device for phosphate determination in water," *Sensors and Actuators B: Chemical*, 2016.
- [113] M. Czugala *et al.*, "CMAS: fully integrated portable centrifugal microfluidic analysis system for on-site colorimetric analysis," *RSC Advances*, vol. 3, no. 36, pp. 15928-15938, 2013.
- [114] T. Songjaroen, W. Dungchai, O. Chailapakul, C. S. Henry, and W. Laiwattanapaisal, "Blood separation on microfluidic paper-based analytical devices," *Lab on a Chip*, vol. 12, no. 18, pp. 3392-3398, 2012.
- [115] A. Nilghaz and W. Shen, "Low-cost blood plasma separation method using salt functionalized paper," *RSC Advances*, vol. 5, no. 66, pp. 53172-53179, 2015.
- [116] J.-H. Kim, T. Woenker, J. Adamec, and F. E. Regnier, "Simple, miniaturized blood plasma extraction method," *Analytical chemistry*, vol. 85, no. 23, pp. 11501-11508, 2013.
- [117] P. Jarujamrus, J. Tian, X. Li, A. Siripinyanond, J. Shiowatana, and W. Shen, "Mechanisms of red blood cells agglutination in antibody-treated paper," *Analyst*, vol. 137, no. 9, pp. 2205-2210, 2012.
- [118] L. OuYang, C. Wang, F. Du, T. Zheng, and H. Liang, "Electrochromatographic separations of multi-component metal complexes on a microfluidic paper-based device with a simplified photolithography," *RSC Advances*, vol. 4, no. 3, pp. 1093-1101, 2014.
- [119] L. Y. Shiroma, M. Santhiago, A. L. Gobbi, and L. T. Kubota, "Separation and electrochemical detection of paracetamol and 4-aminophenol in a paper-based microfluidic device," *Analytica chimica acta*, vol. 725, pp. 44-50, 2012.
- [120] R. F. Carvalhal, M. Simão Kfouri, M. H. de Oliveira Piazetta, A. L. Gobbi, and L. T. Kubota, "Electrochemical detection in a paper-based separation device," *Analytical chemistry*, vol. 82, no. 3, pp. 1162-1165, 2010.
- [121] W. Liu, J. Kou, H. Xing, and B. Li, "Paper-based chromatographic chemiluminescence chip for the detection of dichlorvos in vegetables," *Biosensors and Bioelectronics*, vol. 52, pp. 76-81, 2014.
- [122] M. Dou, D. C. Dominguez, X. Li, J. Sanchez, and G. Scott, "A versatile PDMS/paper hybrid microfluidic platform for sensitive infectious disease diagnosis," *Analytical chemistry*, vol. 86, no. 15, pp. 7978-7986, 2014.

- [123] N. Godino, R. Gorkin, K. Bourke, and J. Ducrée, "Fabricating electrodes for amperometric detection in hybrid paper/polymer lab-on-a-chip devices," *Lab on a Chip*, vol. 12, no. 18, pp. 3281-3284, 2012.
- [124] B. J. Toley, B. McKenzie, T. Liang, J. R. Buser, P. Yager, and E. Fu, "Tunable-Delay Shunts for Paper Microfluidic Devices," *Analytical Chemistry*, vol. 85, no. 23, pp. 11545-11552, 2013/12/03 2013.
- [125] A. C. Glavan *et al.*, "Rapid fabrication of pressure-driven open-channel microfluidic devices in omniphobic RF paper," *Lab on a Chip*, 10.1039/C3LC50371B 2013.
- [126] X. Li, P. Zwanenburg, and X. Liu, "Magnetic timing valves for fluid control in paper-based microfluidics," *Lab on a chip*, vol. 13, no. 13, pp. 2609-2614, 2013.
- [127] S. Wang *et al.*, "Rechargeable battery-triggered electrochemiluminescence detection on microfluidic origami immunodevice based on two electrodes," *Chemical Communications*, vol. 48, no. 80, pp. 9971-9973, 2012.
- [128] S. Wang *et al.*, "Battery-triggered microfluidic paper-based multiplex electrochemiluminescence immunodevice based on potential-resolution strategy," *Lab on a Chip*, vol. 12, no. 21, pp. 4489-4498, 2012.
- [129] B. Epstein and H. Brooks, "The theory of extreme values and its implications in the study of the dielectric strength of paper capacitors," *Journal of applied physics*, vol. 19, no. 6, pp. 544-550, 2004.
- [130] H. Church, "Factors affecting the life of impregnated-paper capacitors," *Proceedings of the IEE-Part III: Radio and Communication Engineering*, vol. 98, no. 52, pp. 113-122, 1951.
- [131] L. Egerton and D. McLean, "Paper Capacitors Containing Chlorinated Impregnants. Mechanism of Stablization," *Industrial & Engineering Chemistry*, vol. 38, no. 5, pp. 512-517, 1946.
- [132] Y. J. Jung *et al.*, "Aligned carbon nanotube—polymer hybrid architectures for diverse flexible electronic applications," *Nano letters*, vol. 6, no. 3, pp. 413-418, 2006.
- [133] T. Linz, C. Kallmayer, R. Aschenbrenner, and H. Reichl, "Embroidering electrical interconnects with conductive yarn for the integration of flexible electronic modules into fabric," in *Wearable Computers*, 2005. *Proceedings. Ninth IEEE International Symposium on*, 2005, pp. 86-89: IEEE.

Link between Chapter 2 and Chapter 3

In the previous chapter, the advances of portable analytical platforms were reviewed for fast, reliable, and low-cost on-site measurements of biochemical variables regarding disease diagnostics, healthcare monitoring, and environmental safety. The major working principles were introduced, including the electrochemical method and optical methods, and their corresponding detector designs such as the custom-made detectors (photodiode devices and handheld potentiostats) and the commercial portable detectors (cameras, scanners, glucometers and cellphones). The major achievements were summarized towards disease diagnostics, water pollution applications, and food safety inspection, with focus on the involved targets including metabolites, immunoassays, heavy metal ions, and nutrients. Among them, two major applications were highlighted: (i) disease diagnostic at point of care (Chapter 3 and 4) and noninvasive wearable physiological monitoring (Chapter 5); and (ii) water pollutants monitoring (Chapter 6 and 7). The following five chapters are dedicated to the two directions accordingly. In the next chapter, a novel multiplexing paper-based electrochemical microfluidic device integrated with a handheld potentiostat is introduced. This platform is applied in the diagnostic of three metabolites (glucose, lactate, and uric acid) in urine samples, and achieves comparable performance to existing standard tests.

Chapter 3

A microfluidic paper-based electrochemical biosensor array for multiplexed detection of metabolic biomarkers

Chapter 3: A microfluidic paper-based electrochemical biosensor array for multiplexed detection of metabolic biomarkers

Chen Zhao¹, Martin M. Thuo², and Xinyu Liu¹*

*Corresponding author: <u>xinyu.liu@mcgill.ca</u>.

Science and Technology of Advanced Materials, Vol. 14, No. 5, 054402 (7pp), 2013.

DOI: https://doi.org/10.1088/1468-6996/14/5/054402.

Reproduced and adapted with permissions from Science and Technology of Advanced Materials

Paper-based microfluidic devices have emerged as simple yet powerful platforms for performing low-cost analytical tests. This paper reports a microfluidic paper-based electrochemical biosensor array for multiplexed detection of physiologically relevant metabolic biomarkers. Different from existing paper-based electrochemical devices, our device includes an array of eight electrochemical sensors and utilizes a handheld custom-made electrochemical reader (potentiostat) for signal readout. The biosensor array can detect several analytes in a sample solution and produce multiple measurements for each analyte from a single run. Using the device, simultaneous detection of glucose, lactate and uric acid in urine is demonstrate, with analytical performance comparable to that of the existing commercial and paper-based platforms. The paper-based biosensor array and its electrochemical reader will enable the acquisition of high-density, statistically meaningful diagnostic information at the point of care in a rapid and cost-efficient way.

Keywords: Paper-based microfluidics, biosensors, electrochemical detection, multiplexing, metabolic markers, disease diagnostics

¹ Department of Mechanical Engineering, McGill University, 817 Sherbrooke Street West, Montreal, QC H3A 0C3, Canada.

² Department of Chemistry, University of Massachusetts, 100 Morrissey Building, Boston, MA 02125, USA.

3.1 Introduction

Accurate detection of disease-relevant biomarkers plays a central role in control and treatment of diseases. However, existing advanced diagnostic technologies usually cannot meet various needs of medical care in developing countries, in the field, and in home healthcare settings, due to their dependence on sophisticated clinical infrastructure, long turnaround time, and relatively high costs. To invent new technologies suitable for use at the point of care and/or in resource limited settings, microfluidic paper-based analytical devices (μPADs) have emerged as powerful diagnostic tools by virtue of their low cost, portability and ease of operate [1-5]. MicroPADs comprise single or multiple layers of paper substrates with hydrophilic paper channels patterned by hydrophobic materials, and can transport fluids autonomously for performing single- or multi-step analytical assays and quantifying concentrations of various analytes in human fluids (e.g., urine, serum, and blood) [6-10].

In terms of detection method, colorimetric detection has been widely employed in many μ PAD designs because of its simplicity and compatibility with camera-phone-based telemedicine [6, 11-13]; it is suitable for both qualitative and (semi-)quantitative tests. Electrochemical detection has also been popular in μ PAD designs, and is more appealing due to its high accuracy and sensitivity [14-19]. Many electrochemical μ PADs have been demonstrated with much lower limit of detection (LOD) than colorimetric assays. In addition, electrochemical detection is insensitive to ambient illumination conditions and impurities in the samples (e.g., dust and insoluble particulate), making it particularly suitable for use in field and/or dirty environments.

Existing electrochemical µPADs often work with a benchtop potentiostat for signal readout, and this bulky and expensive equipment makes it unfavorable to carry out electrochemical tests at the point of care and/or in resource-poor environments. Although portable potentiostats are also commercially available, their costs are still relatively high (>\$1,000) and thus less affordable in the developing world. To further reduce the equipment cost of electrochemical detection, both commercially available and custom-made solutions have been explored. An experimental strategy was proposed to integrate electrochemical µPADs with a glucose meter, which is a highly mature and inexpensive commercial electrochemical reader, to detect different types of analytes other than glucose [20]. An inexpensive, open-source potentiostat, so called 'CheapStat', was also developed based on a microcontroller-based electronic circuit [21]. This device is capable of carrying out various electrochemical protocols (e.g., cyclic voltammetry

(CV), square-wave voltammetry and anodic stripping voltammetry) and providing sufficient performance in chemical and biomarker detections. Further research is needed to develop new types of μ PADs to fully utilize this customizable platform and demonstrate portable paper-based electrochemical biosensing.

Both the glucose meter and the CheapStat represent fairly inexpensive and highly promising platforms for electrochemical detection on μ PADs. However, these electrochemical readers only accommodate one paper sensor at a time, and repeated human operations (pipetting, signal reading and device exchanging) are needed while performing a large number of tests. This poses a practical hurdle in diagnoses involving large-volume tests of multiple biomarkers, for instance, clinical identification of unknown origin of a fever which may attribute to several possible diseases such as tuberculosis, human immunodeficiency virus and mononucleosis. In response to the requirement for large-volume diagnostic tests using μ PADs, a paper-based electrochemical biosensor array and a multiplexing electrochemical reader is presented, both of which can work together to perform eight analytical tests automatically within a single run. Using the biosensor array, the simultaneous detection of three metabolic biomarkers is demonstrated with analytical performance comparable to existing commercial meters and paper-based platforms.

3.2 Materials and methods

3.2.1 Materials

Potassium ferricyanide, D-(+)-glucose, sodium L-lactate, uric acid, glucose oxidase (from *Aspergillus niger*, 147.9 U/mg), lactate oxidase (from *Pediococcus sp.*, ~39 U/mg), uricase (from *Candida sp.*, >2 U/mg), and chromatography paper (*Whatman* 1 Chr) were purchased from *Sigma-Aldrich*, Canada. All chemicals were used as received without further purification. An artificial urine (AU) solution was made according to a previously reported recipe [15], which contained 1.1 mM lactic acid, 2.0 mM citric acid, 25 mM sodium bicarbonate, 170 mM urea, 2.5 mM calcium chloride, 90 mM sodium chloride, 2.0 mM magnesium sulfate, 10 mM sodium sulfate, 7.0 mM potassium dihydrogen phosphate, 7.0 mM dipotassium hydrogen phosphate, and 25 mM ammonium chloride. All the chemicals were mixed in deionized (DI) water and the pH of this solution was adjusted to 6.0 with hydrochloric acid and sodium hydrate. Carbon ink (E3456) and silver ink (E1660) were purchased from *Ercon* (Wareham, MA). All electronic components for constructing the electrochemical reader were purchased from *Mouser*

Electronics (Mansfield, TX), and printed circuit boards (PCBs) were fabricated through *RushPCB Inc.* (San Jose, CA).

3.2.2 Design and fabrication of the paper-based biosensor array

Figure 3-1 (A) and (B) illustrate a microfluidic paper-based biosensor array and a handheld potentiostat for electrochemical signal readout. The paper-based device includes eight biosensing modules, which are used to quantify three metabolic biomarkers (i.e., glucose, lactate, and uric acid) in AU. As shown in Figure 3-1 (B), each module includes a paper channel patterned with hydrophobic wax and three carbon electrodes (WE: working electrode; CE: counter electrode; and RE: reference electrode) screen-printed on the test zone of the paper channel. For the detection of glucose, lactate, and uric acid, enzyme-catalyzed reactions were employed and corresponding enzymes and electron-transfer mediators were stored in the test zones to react with the analytes and produce electrical signals. The three electrodes are connected with screen-printed silver strips (Figure 3-1 (B)), and these silver strips serve as contact pads for electrically interfacing with metal clips on the PCB board of the potentiostat.

Paper channels were fabricated on chromatographic paper using solid wax printing [22], and carbon electrodes and silver strips on the surface of the paper device through screen printing [20]. The patterns of microfluidic channels and electrodes were first laid out using AutoCAD. Base on the channel design, wax patterns were printed to define paper channels (un-printed areas) on chromatography paper (*Whatman* 1 Chr) using a commercial solid wax printer (ColorQube 8570, *Xerox*), and baked the printed paper on a hot plate at 150°C for 1 minutes to allow the melted wax to vertically penetrate the paper substrate and form complete hydrophobic barriers of the channels. According to the designed patterns of electrodes and silver strips, screen-printing stencils were cut into vinyl stencil film (*Grafix Frisket*® film) with a laser cutter (VersaLASER VLS2.30, *Universal Laser Systems*). Then, the stencil was taped on top of the wax paper, filled the laser-cut openings of the stencil with carbon or silver ink, and baked the paper device on a hot plate at 65 °C for 20 minutes until the ink dried. The whole fabrication process took an hour, and five 1×8 devices were typically fabricated from a single batch. **Figure 3-1** (A) shows a photograph of the paper-based biosensor array. The total material cost of the device is \$0.02 (calculated based on commercial prices in small quantities).

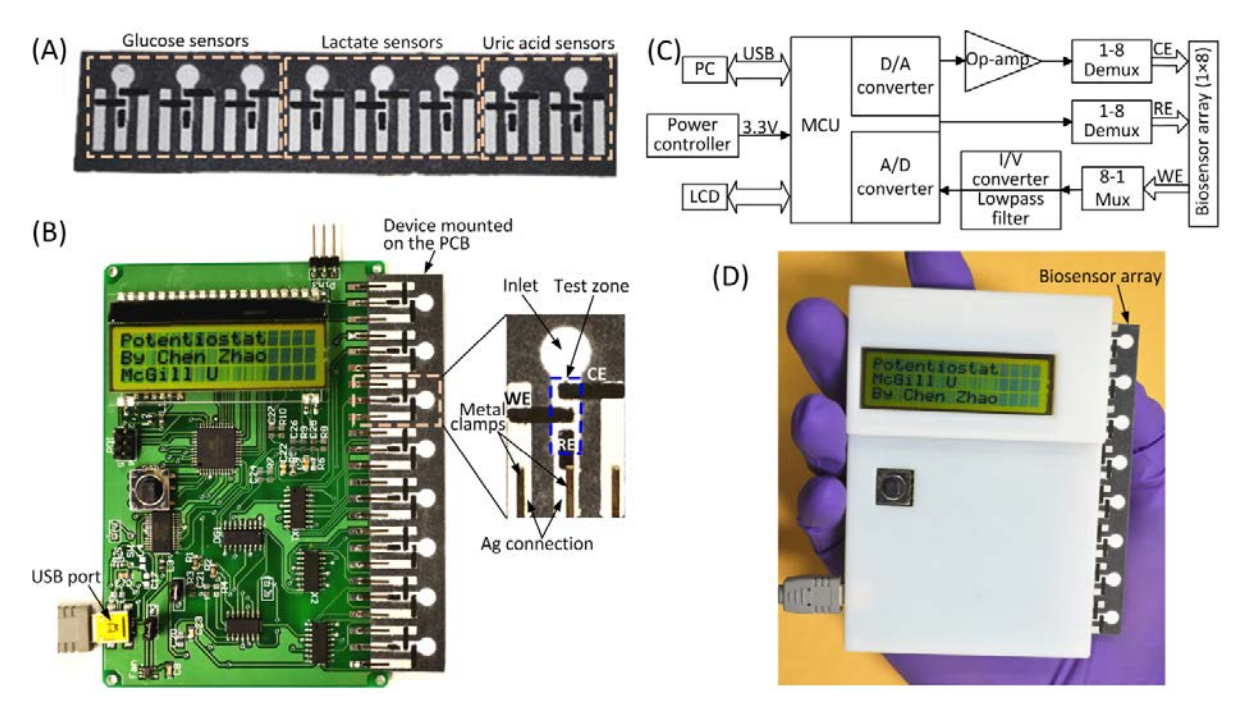


Figure 3-1. A microfluidic paper-based electrochemical biosensor array that interfaces with a custom-made handheld potentiostat for multiplexed detection of metabolic biomarkers. (**A**) A paper-based electrochemical biosensor array (1×8). (**B**) A microcontroller-based multiplexing potentiostat mounted with a paper-based biosensor array. The potentiostat has eight measurement channels, and each channel is connected to a group of three sensing electrodes through metal clamps. CE: counter electrode. WE: working electrode. RE: reference electrode. (**C**) Schematic diagram of the potentiostat architecture with eight measurement channels. (**D**) A photograph of the paper-based biosensor array inserted into the potentiostat.

3.2.3 Design of the potentiostat

A handheld inexpensive potentiostat that can interface with μPADs and carry out different electrochemical protocols will extend the electrochemical μPADs to on-site use. In this work, an eight-channel potentiostat was developed based on a similar circuit architecture to the CheapStat [21]. **Figure 3-1 (B)** and **Figure 3-1 (C)** show a photograph and a schematic diagram of the potentiostat circuit respectively, where a low-power microcontroller (ATMEGA32, *Atmel*; with 12-bit A/D converters) serves as the core for generation of voltammetric excitations and acquisition of electrochemical signals. In contrast to the single-channel CheapStat [21], a multiplexing mechanism was integrated into the circuit to allow automatic scanning of the eight electrochemical sensing components. We designed an insertable slot, which can electrically

connect the 24 electrodes of a 1×8 biosensor array device upon insertion, making the device connection fairly easy. Six measurement ranges of electrochemical currents ($\pm10~\mu A$, $\pm60~\mu A$, $\pm100~\mu A$, $\pm400~\mu A$, $\pm600~\mu A$, and $\pm1~mA$) can be adjusted via on-board jumpers, for accommodating various reactions that produce different levels of electrochemical currents. The smallest current measurement resolution is 35 nA with the measurement range of $\pm10~\mu A$. In our current design, the microcontroller circuit is powered by a USB cable connected to a computer (**Figure 3-1 (B)**), through which the potentiostat can transmit acquired data to the computer for analysis. It is completely feasible to directly display the results on the LCD screen by implementing simple data analysis algorithms in the firmware of the microcontroller. In addition, a 3 V button battery can be integrated on the PCB to power the circuit, thus eliminate the USB connection and make the potentiostat completely portable. **Figure 3-1 (D)** shows a photograph of the handheld potentiostat with a paper-based device inserted on the right side. The total cost of electronic components used to construct the potentiostat is ~\$90 (calculated based on commercial prices in small quantities).

3.2.4 Detection principles

As a proof-of-concept demonstration, we measured concentrations of D-glucose, L-lactate, and uric acid in AU using chronoamperometry performed by the potentiostat on the biosensor array. Corresponding enzymes (i.e., glucose oxidase, lactate oxidase, and uricase) and an electron-transfer mediator (potassium ferricyanide – $K_3[Fe(CN)_6]$) were stored in the test zones (**Figure 3-1 (B)**) of the eight biosensing modules in a dry form. To perform a test, a 4 μ L drop of spiked AU sample was added to the inlet of each biosensing module, then wicked to the test zone and reacted with the stored reagents. During the reaction, the enzymes GOx (glucose oxidase), LOx (lactate oxidase), and UOx (uricase) catalyzed the oxidation of corresponding analyte into different species (glucose to gluconic acid, lactate to pyruvate, and uric acid to allantoin), with a concomitant reduction of $Fe(CN)_6^{3-}$ into $Fe(CN)_6^{4-}$ (**Equations 3-1** to **3-3**). The generated $Fe(CN)_6^{4-}$ ions were quantified using chronoamperometry.

Glucose +
$$2K_3[Fe(CN)_6] + H_2O \xrightarrow{GOx}$$
 Gluconic Acid + $2K_4[Fe(CN)_6]$ (3-1)

Lactate +
$$2K_3[Fe(CN)_6] + H_2O \xrightarrow{LOx} Pyruvate + 2K_4[Fe(CN)_6]$$
 (3-2)

Uric Acid +
$$2K_3[Fe(CN)_6] + H_2O \xrightarrow{UOx} Allantoin + CO_2 + 2K_4[Fe(CN)_6]$$
(3-3)

After device fabrication, test zones of the device were washed with 10 μL of alcohol to remove potential contaminants introduced during fabrication, and dried at room temperature. Before experiments, reagent mixtures of enzymes and the electron-transfer mediator (K₃[Fe(CN)₆]) were freshly prepared at the following concentrations: (i) 250 U/mL glucose oxidase in 600 mM K₃[Fe(CN)₆] and 1 M KCl; (ii) 50 U/mL lactate oxidase in 200 mM K₃[Fe(CN)₆] and 1 M KCl; and (iii) 27 U/mL uricase in 100 mM K₃[Fe(CN)₆] and 1 M KCl. Four microliter drops of particular reagent mixtures were added to the eight test zones of the device for detection of the three analytes. After being dried in a light-resistant incubator at 4 °C for 20 minutes, the device was ready for electrochemical detections.

3.3 Results and Discussion

3.3.1 Electrochemical characterization of the paper-based biosensor array

Before applying the paper-based biosensor array to detection of the three analytes in AU, the electrochemical behavior of each biosensing module on the array device was experimentally characterized through cyclic voltammetry (CV) using 10 mM $K_3[Fe(CN)_6]$ in 1M KCl as a model electroactive compound. In the experiments, a 6 μ L drop of 10 mM $K_3[Fe(CN)_6]$ in 1M KCl was first added to the inlet of a biosensing module and reached the test zone by wicking. Upon the application of a CV wave, the $Fe(CN)_6^{3-}$ was reduced at the cathodic electrode and the resultant $Fe(CN)_6^{4-}$ was oxidized at the anodic electrode. We programmed the potentiostat to apply CV waves with six scan rates (50 mV/s, 100 mV/s, 200 mV/s, 300 mV/s, 400 mV/s, and 500 mV/s) to the working electrode (vs. the graphite pseudo-reference electrode), and measured the generated currents in the measurement range of $\pm 10~\mu$ A.

We acquired and analyzed the current-potential data on a computer connected with the potentiostat through the USB interface. **Figure 3-2** (**A**) shows a group of typical cyclic voltammograms at different scan rates, of which the ratio of cathodic peak current (i_{pc}) and anodic peak current (i_{pa}) is close to the unity ($i_{pa}/i_{pc}=1.0$) for all the scan rates between 50 mV/s and 500 mV/s. The peak shape of the cyclic voltammograms reveals a typical reversible (Nernstian) electrochemical reaction [23].

Theoretically, the polarization overpotential (the difference between potentials at i_{pc} and i_{pa}) is $|E_{pc} - E_{pa}| = 57 \text{ mV/}n$ for a n-electron-transfer process. For the redox-active couple of $\text{Fe}(\text{CN})_6^{3-}/\text{Fe}(\text{CN})_6^{4-}$, the number of transferred electrons n = 1, giving an overpotential value of

57 mV. However, the polarization overpotential values measured from our devices ranged from 80 mV to 250 mV with shifts at the reduction and oxidation peaks. The shifting was attributed to the relative instability of the graphite pseudo-reference electrode in multiple CV scans. However, it was observed that, when used at the first time, different biosensing modules in the same device and from different devices revealed fairly small variations in overpotential. The experimental data of measuring glucose, lactate, and uric acid in AU (as presented in **Section 3.3.2**), performed using fresh devices, also demonstrate reproducible analytical performance. Therefore, our paper-based biosensor arrays possess reliable biosensing capabilities for single-use diagnostic applications.

3.3.2 Multiplexed detection of glucose, lactate, and uric acid

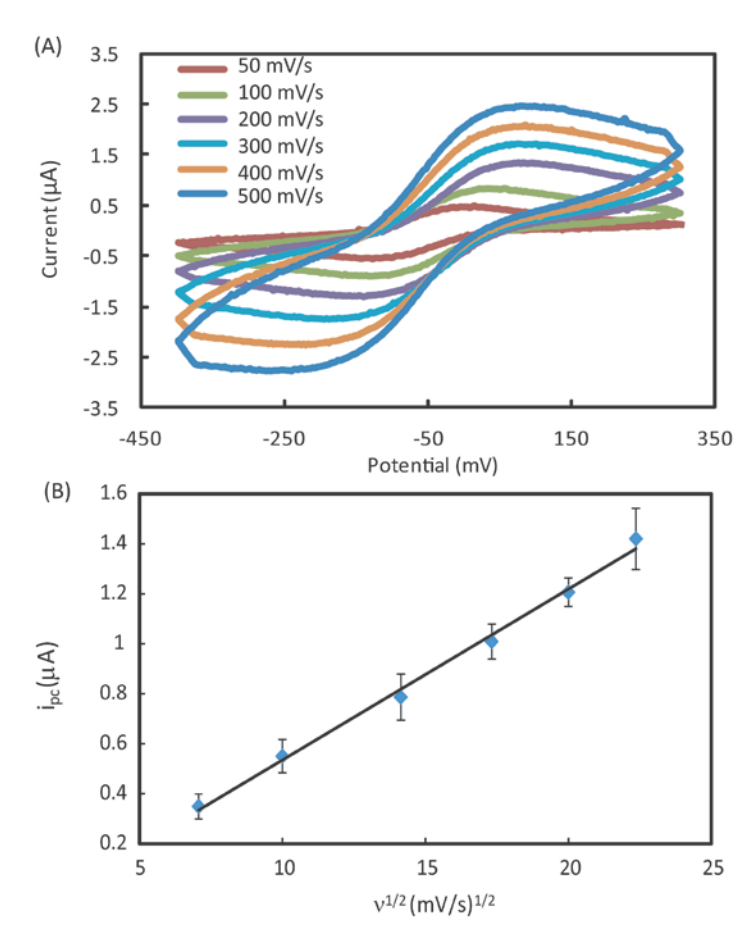


Figure 3-2. Electrochemical characterization of the paper-based biosensor array. (**A**) Typical cyclic voltammograms of 10 mM $K_3[Fe(CN)_6]$ in 1M KCl solution in an electrochemical biosensing module of the array device at various scan rates. (**B**) A plot of the cathodic peak current vs. the square root of the scan rate, measured from the cyclic voltammograms (n=5).

We used the biosensor array device and the handheld potentiostat for multiplexed quantification of three clinically-relevant metabolic markers (glucose, lactate and uric acid) in AU using chronoamperometry. High levels of glucose in blood indicate diabetes, while low blood sugar, so called hypoglycemia, could mean metabolic disorders or complications of diabetes treatment. Altered concentrations of lactate in blood may result from liver diseases, sepsis, or metabolic disorders, and lactate concentrations above 5 mM with severe metabolic acidosis predicts high morality [24]. Excess accumulations of uric acid in the blood are linked to dyslipidemia, obesity, and an increased risk for cardiovascular diseases[25, 26].

On a biosensor array, the eight biosensing modules were spilt into three groups for detecting the three markers. For instance, three biosensing modules could be used for glucose detection, three modules for lactate detection, and two modules for uric acid detection (**Figure 3-1 (A)**). Chronoamperometry was chosen for analyte detection because it offers better accuracy and sensitivity and is easier to implement than other electrochemical techniques [14, 15]. A 500 mV step potential was applied to the working electrode (vs. the graphite pseudo-reference electrode), and monitored the resulting current as a function of time. It was found that, for the current device design, the initial high charging current decayed to a steady state within 90 s after applying the step potential. Thus, the steady-state Faradaic current was measured by taking the average of currents measured in 90–100 s post-step-potential for all the three markers. The measured Faradaic current is proportional to the concentration of target analyte, which can be described by the Cottrell equation [1].

In the experiments, all the channels of the potentiostat were set with a measurement range of ±10 μA. We prepared AU samples spiked with glucose (0–20 mM), lactate (0–25 mM), and uric acid (0–10 mM) to generate the calibration data, and these concentration ranges covered the possible levels of the three markers in urine. To start a test on a 1×8 biosensor array, we first inserted the device into the device slot of the potentiostat, then added 4 μL drops of spiked AU to the eight inlets on the biosensor array, waited for 2 minutes to allow the sample to thoroughly react with the pre-loaded reagents, and finally applied the 500 mV step potential and measured the chronoamperometric curves of current vs. time. **Figure 3-3**, **Figure 3-4**, and **Figure 3-5** illustrate (**A**) groups of typical chronoamperometric curves and (**B**) calibration plots for measurement of glucose, lactate, and uric acid in AU, demonstrating a linear relationship between the measured current and the analyte concentration for all the three markers. **Table 3-1**

summarizes the analytical performance of the biosensor array device. The LOD values of our device for glucose (0.12 mM), lactate (0.59 mM), and uric acid (0.18 mM) were found to be comparable to and even superior than these of commercial meters (glucose: 0.83 mM, lactate:1.1 mM) and paper-based platforms (glucose: 0.21 mM, lactate: 0.36 mM, and uric acid: 1.38 mM). The linear dynamic ranges of our device cover the possible clinically-relevant levels of all the three markers in urine. These results prove the sufficient biosensing capability of our device for quantitative detection of the three metabolits. We believe that this paper-based device and its portable potentiostat will also be useful for performing electrochemical detection of other biomarkers in human fluids (e.g., antigens/antibodies, virus, and DNA segments), and chemicals/pollutants in environmental samples (e.g., heavy metal ions, bacteria, and toxins).

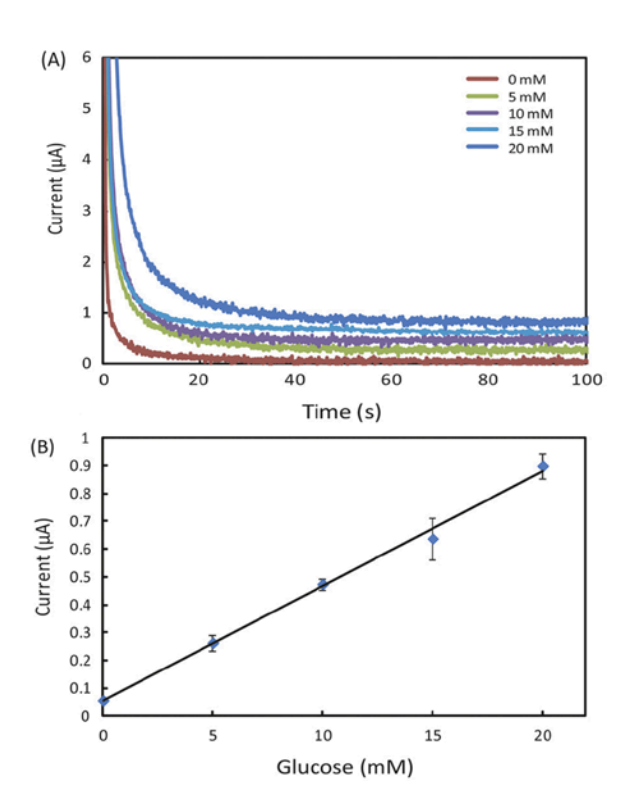


Figure 3-3. **(A)** Chronoamperometric curves and **(B)** the calibration plot for measurement of glucose in AU. The solid line in **(B)** represents a linear fit to experimental data with regression equation: y=0.041x+0.054 ($R^2=0.996$, n=5).

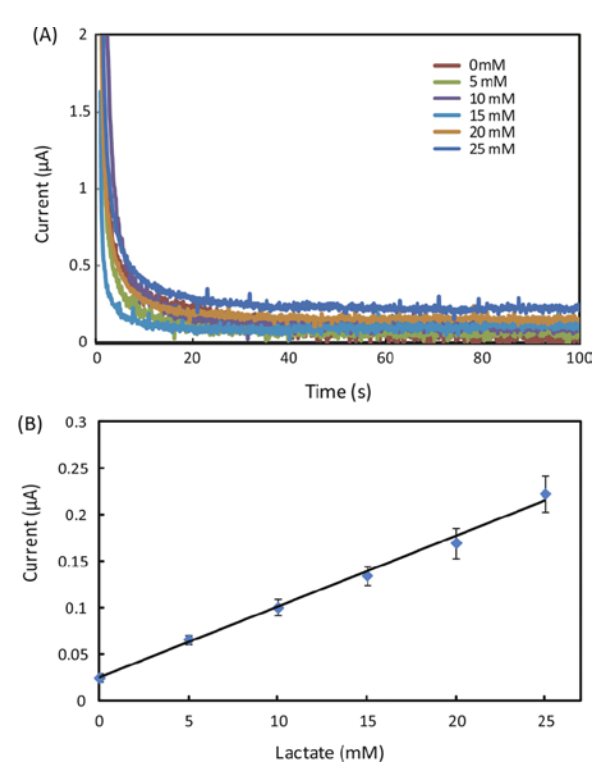


Figure 3-4. (**A**) Chronoamperometric curves and (**B**) the calibration plot for measurement of lactate in AU. The solid line in (**B**) represents a linear fit to experimental data with regression equation: y=0.0076x+0.025 ($R^2=0.995$, n=5).

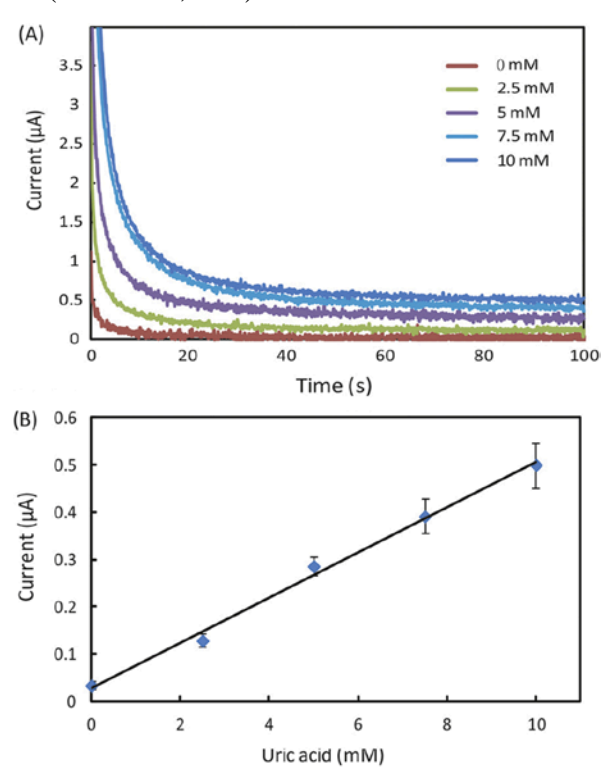


Figure 3-5 (A) Chronoamperometric curves and **(B)** the calibration plot for measurement of uric acid in AU. The solid line represents a linear fit to experimental data with regression equation: y = 0.048x + 0.029 ($R^2 = 0.994$, n = 5).

Table 3-1. Performance comparison of the paper-based biosensor array with commercial meters [20] and μPAD [14]. *The dynamic linear ranges achieved in this work cover the clinically-relevant ranges of the three biomarkers. LOD: Limit of detection.

Analyte	Analytical performance (mM)				
	Dynamic	Clinically	LOD	LOD	LOD
	linear range*	relevant ranges	(this	(commercial	(ref.[14])
	(this work)	[14]	work)	meters [20])	
Glucose	0-20	0.1-0.8	0.35	0.83	0.21
Lactate	0-25	5.5-22	1.76	1.1	0.36
Uric acid	0-10	1.5-4.4	0.52	N/A	1.38

3.4 Conclusion

In this work, a microfluidic paper-based electrochemical biosensor array (1×8) was developed, capable of performing diagnostic tests of multiple biomarkers in a multiplexing and high-throughput fashion. An inexpensive, compact potentiostat was designed and constructed to interface with the paper-based biosensor array for electrochemical signal readout. The paper-based device and the potentiostat formed a portable, self-contained, easy-to-operate electrochemical biosensing platform, which is particularly useful for low-cost, point-of-care diagnostic applications. As a proof of concept, the biosensor array was used for multiplexed detection of three metabolic biomarkers (glucose, lactate, and uric acid). The experimental results demonstrated that our device provides analytical performance (LOD and dynamic linear range) sufficient for clinical assays of all the three markers. This paper-based biosensing platform will find important applications in point-of-care diagnosis and on-site environmental testing.

3.5 Acknowledgements

This work was supported by Grand Challenge Canada (through a Star in Global Health Award), Natural Sciences and Engineering Research Council of Canada, and Canadian Foundation for Innovation, Canadian Research Chairs Program, and McGill University.

3.6 Reference

- [1] A. W. Martinez, S. T. Phillips, G. M. Whitesides, and E. Carrilho, "Diagnostics for the developing world: microfluidic paper-based analytical devices," (in eng), *Analytical chemistry*, vol. 82, no. 1, pp. 3-10, Jan 1 2010.
- [2] C. Parolo and A. Merkoci, "Paper-based nanobiosensors for diagnostics," (in eng), *Chemical Society reviews*, Research Support, Non-U.S. Gov't vol. 42, no. 2, pp. 450-7, Jan 21 2013.
- [3] X. Li, D. R. Ballerini, and W. Shen, "A perspective on paper-based microfluidics: Current status and future trends," *Biomicrofluidics*, vol. 6, no. 1, p. 011301, 2012.
- [4] K. Abe, K. Suzuki, and D. Citterio, "Inkjet-printed microfluidic multianalyte chemical sensing paper," (in eng), *Analytical chemistry*, vol. 80, no. 18, pp. 6928-34, Sep 15 2008.
- [5] P. Zuo, X. Li, D. C. Dominguez, and B.-C. Ye, "A PDMS/paper/glass hybrid microfluidic biochip integrated with aptamer-functionalized graphene oxide nanobiosensors for one-step multiplexed pathogen detection," *Lab on a Chip*, 10.1039/C3LC50654A vol. 13, no. 19, pp. 3921-3928, 2013.
- [6] A. W. Martinez, S. T. Phillips, M. J. Butte, and G. M. Whitesides, "Patterned Paper as a Platform for Inexpensive, Low-Volume, Portable Bioassays," *Angewandte Chemie International Edition*, vol. 46, no. 8, pp. 1318-1320, 2007.
- [7] A. W. Martinez, S. T. Phillips, and G. M. Whitesides, "Three-dimensional microfluidic devices fabricated in layered paper and tape," (in eng), *Proceedings of the National Academy of Sciences of the United States of America*, Research Support, Non-U.S. Gov't vol. 105, no. 50, pp. 19606-11, Dec 16 2008.
- [8] X. Li, J. Tian, T. Nguyen, and W. Shen, "Paper-Based Microfluidic Devices by Plasma Treatment," *Analytical chemistry*, vol. 80, no. 23, pp. 9131-9134, 2008/12/01 2008.
- [9] L. Ge *et al.*, "Photoelectrochemical Lab-on-Paper Device Based on an Integrated Paper Supercapacitor and Internal Light Source," *Analytical chemistry*, vol. 85, no. 8, pp. 3961-3970, 2013/04/16 2013.
- [10] X. Y. Liu *et al.*, "A portable microfluidic paper-based device for ELISA," in *Micro Electro Mechanical Systems (MEMS)*, 2011 IEEE 24th International Conference on, 2011, pp. 75-78.
- [11] A. W. Martinez, S. T. Phillips, E. Carrilho, S. W. Thomas, 3rd, H. Sindi, and G. M. Whitesides, "Simple telemedicine for developing regions: camera phones and paper-based microfluidic devices for real-time, off-site diagnosis," (in eng), *Analytical chemistry*, vol. 80, no. 10, pp. 3699-707, May 15 2008.
- [12] W. Dungchai, O. Chailapakul, and C. S. Henry, "Use of multiple colorimetric indicators for paper-based microfluidic devices," *Analytica Chimica Acta*, vol. 674, no. 2, pp. 227-233, 2010.
- [13] X. Li, P. Zwanenburg, and X. Liu, "Magnetic timing valves for fluid control in paper-based microfluidics," *Lab on a chip*, vol. 13, no. 13, pp. 2609-2614, 2013.
- [14] W. Dungchai, O. Chailapakul, and C. S. Henry, "Electrochemical Detection for Paper-Based Microfluidics," (in English), *Analytical chemistry*, vol. 81, no. 14, pp. 5821-5826, Jul 15 2009.
- [15] Z. H. Nie *et al.*, "Electrochemical sensing in paper-based microfluidic devices," (in English), *Lab on a Chip*, vol. 10, no. 4, pp. 477-483, 2010.

- [16] D. J. Zang, L. Ge, M. Yan, X. R. Song, and J. H. Yu, "Electrochemical immunoassay on a 3D microfluidic paper-based device," (in English), *Chemical Communications*, vol. 48, no. 39, pp. 4683-4685, 2012.
- [17] X. J. Li, Z. H. Nie, C.-M. Cheng, A. B. Goodale, and G. M. Whitesides, "Paper-based electrochemical ELISA," in *International Conference on Miniaturized Systems for Chemistry and Life Sciences*, Groningen, The Netherlands, 2010, pp. 1487-1489.
- [18] S. Ge, L. Ge, M. Yan, X. Song, J. Yu, and J. Huang, "A disposable paper-based electrochemical sensor with an addressable electrode array for cancer screening," *Chemical Communications*, 10.1039/C2CC34887J vol. 48, no. 75, pp. 9397-9399, 2012.
- [19] D. Zang, M. Yan, S. Ge, L. Ge, and J. Yu, "A disposable simultaneous electrochemical sensor array based on a molecularly imprinted film at a NH2-graphene modified screen-printed electrode for determination of psychotropic drugs," *Analyst*, 10.1039/C3AN00109A vol. 138, no. 9, pp. 2704-2711, 2013.
- [20] Z. Nie, F. Deiss, X. Y. Liu, O. Akbulut, and G. M. Whitesides, "Integration of paper-based microfluidic devices with commercial electrochemical readers," (in eng), *Lab on a Chip*, Research Support, Non-U.S. Gov't vol. 10, no. 22, pp. 3163-9, Nov 21 2010.
- [21] A. A. Rowe *et al.*, "CheapStat: An Open-Source, "Do-It-Yourself" Potentiostat for Analytical and Educational Applications," *PLoS ONE*, vol. 6, no. 9, p. e23783, 2011.
- [22] E. Carrilho, A. W. Martinez, and G. M. Whitesides, "Understanding wax printing: a simple micropatterning process for paper-based microfluidics," (in eng), *Analytical chemistry*, vol. 81, no. 16, pp. 7091-5, Aug 15 2009.
- [23] A. J. Bard and L. R. Faulkner, *Electrochemical Methods: Fundamentals and Applications*. New York: Wiley, 2000.
- [24] B. Phypers and J. T. Pierce, "Lactate physiology in health and disease," *Continuing Education in Anaesthesia, Critical Care & Pain*, vol. 6, no. 3, pp. 128-132, 2006.
- [25] M. K. Kutzing and B. L. Firestein, "Altered Uric Acid Levels and Disease States," *Journal of Pharmacology and Experimental Therapeutics*, vol. 324, no. 1, pp. 1-7, January 1, 2008 2008.
- [26] J. Fang and M. H. Alderman, "Serum uric acid and cardiovascular mortality," *JAMA: the journal of the American Medical Association*, vol. 283, no. 18, pp. 2404-2410, 2000.

Link between Chapter 3 and Chapter 4

In the previous chapter, we introduced the technique to fabricate a multiplexing paper-based electrochemical microfluidic device array and its integration with a handheld potentiostat. A major part of the efforts was devoted to the design of paper-based electrochemical multiplexing device and the portable electrochemical potentiostat. As a proof-of-concept, this platform was first applied for the detection of single-step enzymatic reactions of metabolites in artificial urine. This chapter continued to improve the design of the electrochemical microfluidic paper-based immunosensor array (E-μPIA) and the portable potentiostat for diagnosis of human immunodeficiency virus (HIV) and hepatitis C virus (HCV) co-infections in serum samples. The E-μPIA was modified with protein linkers to provide covalent bonding for antigen/antibody immobilization in the multi-step immunoassay protocol; the potentiostat was also optimized with wireless modules to enable remote diagnostics. On this platform, indirect enzyme-linked immunosorbent assays of HIV/HCV antibodies were realized with LODs of 300 pg/ml and 750 pg/ml, respectively, both lower than that of standard HIV/HCV tests.

Chapter 4

A portable paper-based microfluidic platform for multiplexed electrochemical detection of HIV and HCV antibodies in serum

Chapter 4: A portable paper-based microfluidic platform for multiplexed electrochemical detection of HIV and HCV antibodies in serum

Chen Zhao and Xinyu Liu*

Department of Mechanical Engineering, McGill University, 817 Sherbrooke Street West,

Montreal, QC H3A 0C3, Canada.

817 Sherbrooke Street West, Montreal, QC H3A 0C3, Canada.

Corresponding author: <u>xinyu.liu@mcgill.ca</u>.

Biomicrofluidics 10, 024119 (2016).

doi: http://dx.doi.org/10.1063/1.4945311.

Reproduced and adapted with permission from *Biomicrofluidics*.

This paper presents a portable paper-based microfluidic platform for multiplexed electrochemical detection of antibody markers of human immunodeficiency virus (HIV) and hepatitis C virus (HCV) in serum samples. To our best knowledge, this is the first paper-based electrochemical immunosensing platform, with multiplexing and telemedicine capabilities, for diagnosing HIV/HCV co-infection. The platform consists of an electrochemical microfluidic paper-based immunosensor array (E-µPIA) and a handheld multi-channel potentiostat, and is capable of performing enzyme-linked immunesorbent assays (ELISAs) simultaneously on eight samples within 20 minutes (using a prepared E-µPIA). The multiplexing feature of the platform allows it to produce multiple measurement data for HIV and HCV markers from a single run, and its wireless communication module can transmit the results to a remote site for telemedicine. The unique integration of paper-based microfluidics and mobile instrumentation renders our platform portable, low-cost, user-friendly, and high-throughput.

Keywords: HIV/HCV co-infection, paper-based microfluidics, electrochemical sensing, handheld potentiostat, telemedicine

4.1 Introduction

Human immunodeficiency virus (HIV) and hepatitis C virus (HCV) infections have been among the leading causes of morbidity and mortality worldwide in recently years. Due to their common routes of transmission, co-infection of HIV and HCV exists in an estimated one-third of HIV positive patients [1-4], which is a severe health problem in the world, especially in developing countries. Infection with HIV, when present in either HCV transmitting or HCV exposed patients, can cause an increase on the risk of transmission of HCV [5]; apart from that, when exposed to HCV, HIV-infected patients are less likely to clear the acute infection [5, 6].

Point-of-care (POC) tests for sexually transmitted infections (STIs) are commercially available, but not often affordable or accessible to many patients in the developing world, where the burden of STIs is the greatest. Besides the affordability issue, the existing POC tests are usually designed to indicate a binary status (positive or negative), and cannot accurately quantify concentrations of the disease markers in a sample, which has a great meaning in determination of the infection stage. Thus, low-cost, quantitative POC tests with satisfactory performance are of urgent need for STI diagnosis.

Microfluidic paper-based analytical devices (μPADs), as an emerging tool for low-cost diagnostics, have recently gained significant research interests [7, 8]. Electrochemical μPADs (E-μPADs) represent a popular choice for developing POC tests because of their diverse sensing capabilities, high accuracy and sensitivity [9-12]. With advancement of portable electrochemical instrumentation, the integration of E-μPADs with portable, low-cost electrochemical readers (i.e., potentiostat) makes it possible for paper-based tests to be carried out remotely at the POC and/or in the field with enhanced analytical performance [13-15].

Aiming at POC diagnosis of HIV/HCV co-infection, a paper-based, integrated diagnostic platform is developed, capable of multiplexed electrochemical enzyme-linked immunesorbant assays (ELISAs) of HIV/HCV antibody markers and remote transmission of diagnostic results for telemedicine. There exist E-µPADs for carrying out ELISAs of cancer and tumor markers [16, 17]. However, to our best knowledge, no paper-based platform is reported previously for diagnosis of the HIV/HCV co-infection. The platform integrates an electrochemical microfluidic paper-based immunosensor array (E-µPIA) and a custom-made, handheld potentiostat; it can carry out ELISAs on eight serum samples in parallel, generate assay results in 20 minutes, and transmit the data to a host computer or smart phone via wireless transmission. Based on the

developed platform, the ELISA protocol is optimized and improved for the assay sensitivity via surface biofunctionalization of sensing electrodes. Accurate quantification of antibodies against HIV p24 core antigen and HCV core antigen is demonstrated in mouse serum with limits of detection (LOD) of 300 pg/ml and 750 pg/ml, respectively. We also show negligible cross-reactivity of the HIV and HCV assays, proving the feasibility of diagnosing HIV/HCV co-infection in protein-rich serum samples.

4.2 Experimental design

4.2.1 Design and Fabrication of the E-µPIA

Error! Reference source not found. (A) shows the internal structure of the custom-made potentiostat with an E- μ PIA inserted in its electrical connection slot. **Figure 4-1** (B) shows the E- μ PIA that has eight electrochemical immunosensors for detecting HIV and HCV antibodies (four immunosensors for each marker). Each immunosensor consists of a circular paper reaction zone and a group of three screen-printed electrodes (working electrode – WE, counter electrode – CE, and reference electrode – RE). The center spacing of adjacent reaction zones is 9 mm, which is compatible with the tip spacing of a standard multi-channel pipette and thus allows a user to add samples to the eight immunosensors simultaneously (**Figure 4-1 (A)**).

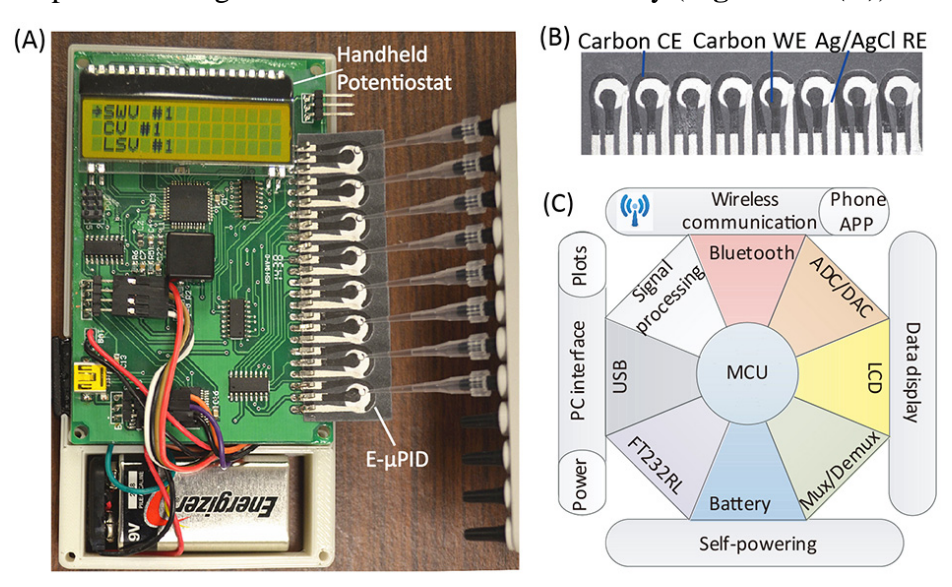


Figure 4-1. A portable paper-based diagnostic platform integrating an E- μ PIA and a handheld potentiostat. (**A**) The handheld potentiostat inserted with an E- μ PIA. (**B**) The E- μ PIA. (**C**) Schematic architecture of the potentiostat circuit constructed based on a microcontroller unit (MCU).

The WE and CE were made from carbon ink, and the RE was made from Ag/AgCl ink. The Ag/AgCl RE provides stable reference potential during electrochemical measurement, and is widely used in screen-printed electrochemical cells [18-20]. The RE is placed close to the WE and the CE to reduce the uncompensated resistance of the electrochemical cell between the WE and the RE [11, 21]. To fabricate an E-μPIA, we firstly patterned the eight reaction zones on a piece of cellulose chromatography paper (Whatman® CHR #1, GE Healthcare) via wax printing, and then formed the electrodes on top of the reaction zones via stencil printing. Details of the device fabrication process can be found in a previous report [15].

4.2.2 Design of the Potentiostat

To improve the throughput of HIV and HCV detection, we designed a handheld, eight-channel potentiostat for signal readout from the E-μPIA. Figure 4-1 (A) shows the printed circuit board (PCB) of the potentiostat. The circuit architecture of the potentiostat is illustrated in Figure 4-1 (C), which primarily includes a microcontroller unit (MCU; ATxmega32A4, Atmel) with a 12-bit analog-to-digital converter (ADC) and a 12-bit digital-to-analog converter (DAC), a signal multiplexing/demultiplexing unit (74HC4051D, NXP Semiconductors), a signal processing circuit (for converting an electrochemical current into a voltage), a liquid crystal display (LCD; EADOGM163EA, Electronic Assembly), a universal serial bus (USB) to universal asynchronous receiver/transmitter (UART) interface circuit (FT232RL, FTDI), a Bluetooth wireless communication unit, and a 9V battery. The total material cost of the potentiostat is CAD \$60 (calculated based on prices in small quantities). Through user programming, the potentiostat can perform different types of electrochemical measurements on the E-μPIA, including cyclic voltammetry (CV), linear sweeping voltammetry (LSV), chronoamperometry (CA), and square wave voltammetry (SWV).

The basic design and working principle of the multiplexing potentiostat has been reported previously [15]. In this work, we constructed an updated version of our previous potentiostat design and integrated a few additional features useful for POC diagnosis, including on-board battery, Bluetooth communication, and custom-made personal computer (PC) software and smart-phone Android application – APP (for data receiving and processing). **Figure 4-2** illustrates the wireless communication architecture of our diagnostic platform, from the handheld potentiostat, to a PC or a smart phone, and finally to a remote cite. The PC software and smart-

phone APP both can open the Bluetooth port of the potentiostat, trigger the electrochemical measurement, and receive data via wireless communication. The assay data can be also transmitted from the potentiostat to a PC through the USB interface. The data can be further transmitted to a remote site (e.g., centralized laboratory or public health database) via the internet (by a PC or a smart phone) or the mobile network (by a smart phone), for tele-diagnosis or healthcare data collection.

4.2.3 Biofunctionalization of the Reaction Zone and the WE

After 4–8 weeks of exposure to the HIV virus, a human body will produce a detectable level of antibodies due to the immune response against HIV [22]. Tests detecting the presence of serum antibody against the HIV p24 core antigen have been commonly used for clinical HIV diagnosis [23]. For HCV diagnosis, the antibody against HCV core antigen is a commonly used marker and provides accurate test results [24]. We used indirect ELISA to quantify concentrations of HIV and HCV antibodies in serum samples, which is based on the sequential affinity bindings of the viral antigen, viral antibody, and secondary antibody.

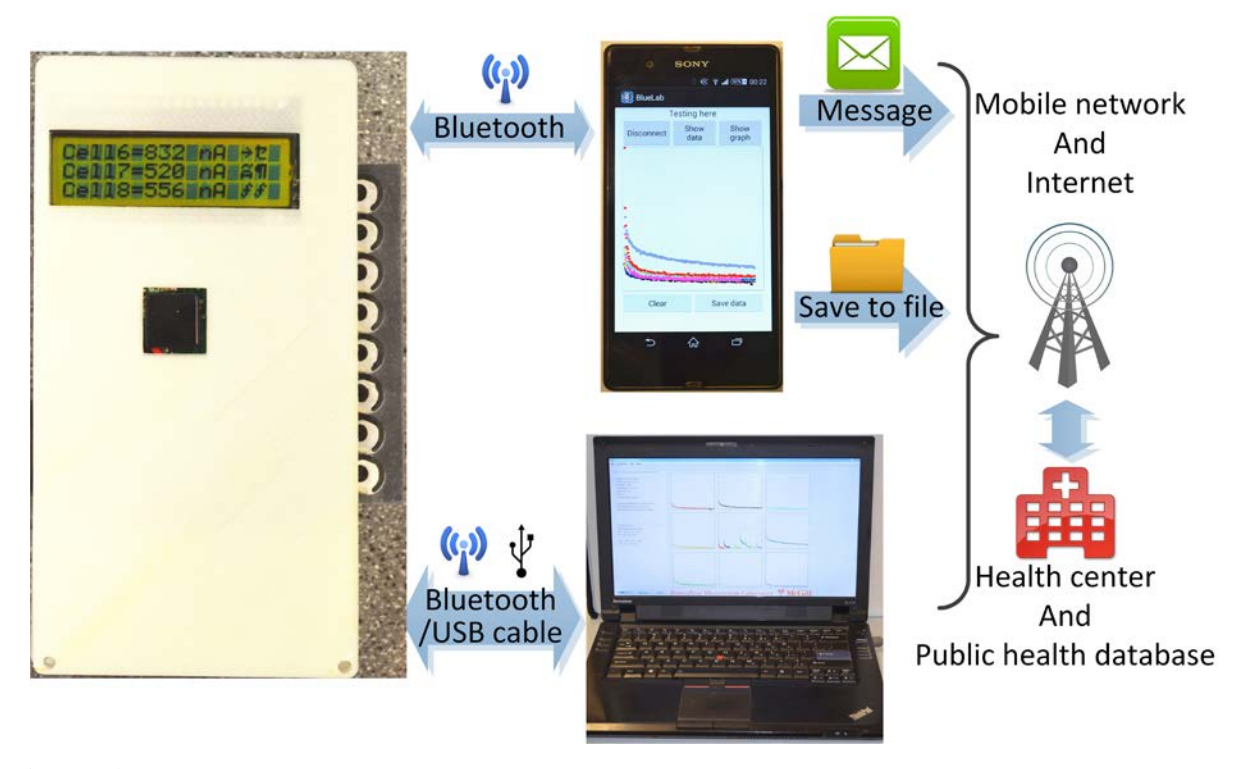


Figure 4-2. Wireless data transmission of the diagnostic platform, from the potentiostat, to a PC or a smart phone, and finally to a remote site. The screens of the PC and the smart phone display the graphical user interfaces of the PC software and the Android APP, respectively.

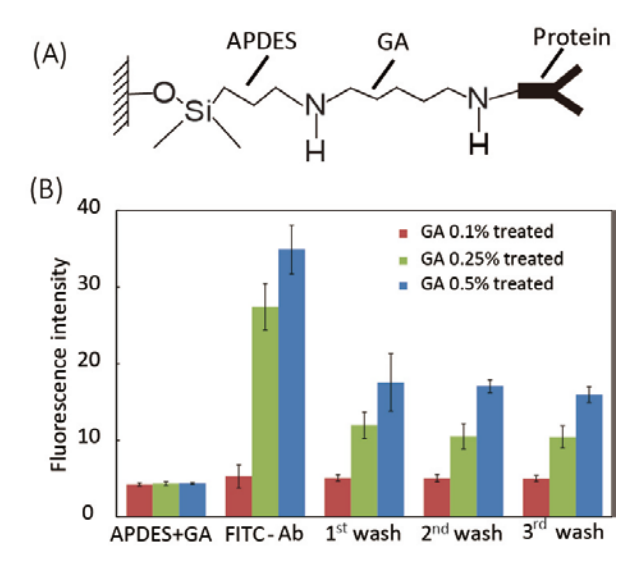


Figure 4-3. Biofunctionalization process of the WE. (**A**) Molecular scheme of surface protein functionalization on the surfaces of the WE through APDES and GA linkages. (**B**) Fluorescence quantification of immobilized FITC-anti-IgG on reaction zones treated with GA at different concentrations (n = 3).

To capture the target antibodies in serum, the viral antigens need to be first immobilized on the WE and the reaction zones. We modified the paper reaction zone and the WE with 3-amino-propyldimethylethoxysilane (APDES) and glutaraldehyde (GA). APDES treatment improves the hydrophilicity of the carbon WE and the paper reaction zone [12, 25], and the APDES molecule also bonds with the hydroxyl (-OH) groups on the surfaces of paper and WE, and thus provide amine (-NH2) groups for subsequent GA bonding (**Figure 4-3 (A)**). The GA, as an effective protein crosslinking reagent, was added onto the reaction zone to bond with -NH2 groups from APDES, providing aldehyde (CHO-) groups for protein immobilization (**Figure 4-3 (A)**).

We first treated the working electrode with 2 µL of 2% (v/v) APDES for three times, and waited for 10 minutes after each treatment. 2% of APDES is high enough to make the carbon WE more hydrophilic, but does not obviously attack the wax barrier of the reaction zone (we observed that treating the electrodes with >2% APDES made the wax barrier of the zone less hydrophobic and thus unable to confine fluids effectively). We then added 2 µL of GA onto the working electrode and waited for 30 minutes. We explored the effect of GA concentration on the protein immobilization efficiency. We found that GA solution at ≥0.5% became relatively viscous and made the reaction zone hydrophobic after treatment. Thus, we used 2 µL of GA at three different concentrations—0.1%, 0.25% and 0.5% (v/v)—to treat the working electrode, and

investigated the hydrophilicity and protein immobilization efficiency of the electrode after the GA treatment. To quantify the protein immobilization efficiency, we applied 4 μ L of 20 μ g/ml FITC-labelled IgG antibody (FITC-anti-IgG) to each working electrode, waited for 3 min, washed it with 30 μ L of PBS for three times, and finally quantified the fluorescence intensity of the zone.

Figure 4-3 (B) shows the fluorescence intensities of the working electrodes right after APDES and GA treatments ("APDES+GA"), after the addition of FITC-anti-IgG ("FITC-Ab"), and after three repeated washes ("1st wash" to "3rd wash"). We found that the treatment with 0.1% GA did not obviously decrease the hydrophilicity of the reaction zone and the WE; however, electrodes treated with 0.1% GA only captured a limited amount of FITC-anti-IgG after three washes (fluorescence intensity increases by 24.9%). When treated with 0.25% GA, the reaction zone and the WE became less hydrophilic but still wicked fluids efficiently, and their protein immobilization efficiency increased significantly (fluorescence intensity increased by 140% after 3 washes). When the GA concentration was further increased to 0.5%, an even larger amount of FITC-anti-IgG was captured by the WE (fluorescence intensity increased by 300% after 3 washes). However, the working electrodes treated with 0.5% GA became more hydrophobic, and thus did not allow fluids wick through the reaction zone effectively for carrying out the assay. Therefore, 0.25% GA was chosen in the finalized biofunctionalization protocol. One can also observe that, after protein immobilization on working electrode (treated with 0.25% GA), excess un-bound FITC-anti-IgG can be efficiently washed off via three washes.

4.2.4 Protocol of Electrochemical ELISA

We employed indirect ELISAs (**Figure 4-4 (A)**) for detection of both HIV and HCV antibodies. To start a test, we first added 3 µL of 50 µg/ml viral core antigen (HIV p24 or HCV core antigen) to the APDES-GA-treated reaction zones of an E-µPIA (four zones for HIV tests and four zones for HCV tests), and incubated the device at ambient conditions for 10 minutes. We then spotted 6 µL of blocking buffer (Roche Blocking Reagent, cat. #: 13906900) to the reaction zones and allowed them to dry at ambient conditions for 25 minutes (to prevent non-specific absorptions). After that, we added 3 µl of commercial mouse serum, spiked with different concentrations of HIV or HCV antibody, and waited for three minutes, during which the HIV or HCV antibody in the serum conjugated, as the primary antibody of the indirect

ELISA, with the immobilized HIV or HCV antigen. We washed the reaction zone with 20 μ l of 1× PBS for three times to remove the unbound species of the serum. We next added 4 μ L of 40 μ g/ml alkaline phosphatase (ALP) labeled goat anti-mouse IgG to the reaction zone, which served as the secondary antibody and bound with the primary HIV or HCV antibody. After three-minute incubation, we washed the reaction zone with 20 μ L of 1× PBS for three times. At this point, the amount of ALP bound to the reaction zone surface is proportional to the amount of HIV or HCV antibody bound to the same surface. Finally, we added 6 μ L of an electrochemical substrate for ALP, p-aminophenyl phosphate or pAPP (5 mg/ml), to the reaction zone, which was catalyzed by the ALP and produced an amperometric current output. After 3-minute incubation, we performed CA measurement to quantify the produced current signal. The entire ELISA process took 55 minutes, including a 35-minute device preparation time for immobilizing the capture antigens and blocking the void sites on the substrate. Thus, with a prepared E- μ PIA, a user can complete the assay of eight samples in 20 minutes.

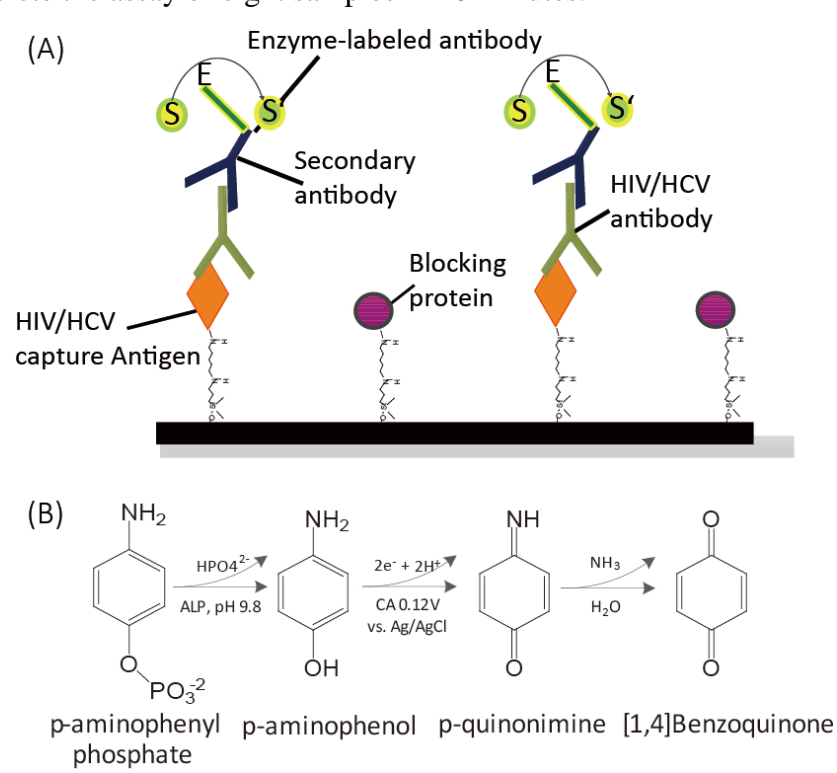


Figure 4-4. Protocol of indirect electrochemical ELISA. (**A**) Scheme of the indirect ELISA for detecting HIV/HCV antibodies. (**B**) Electrochemical reaction mechanism of pAPP and ALP-antibody.

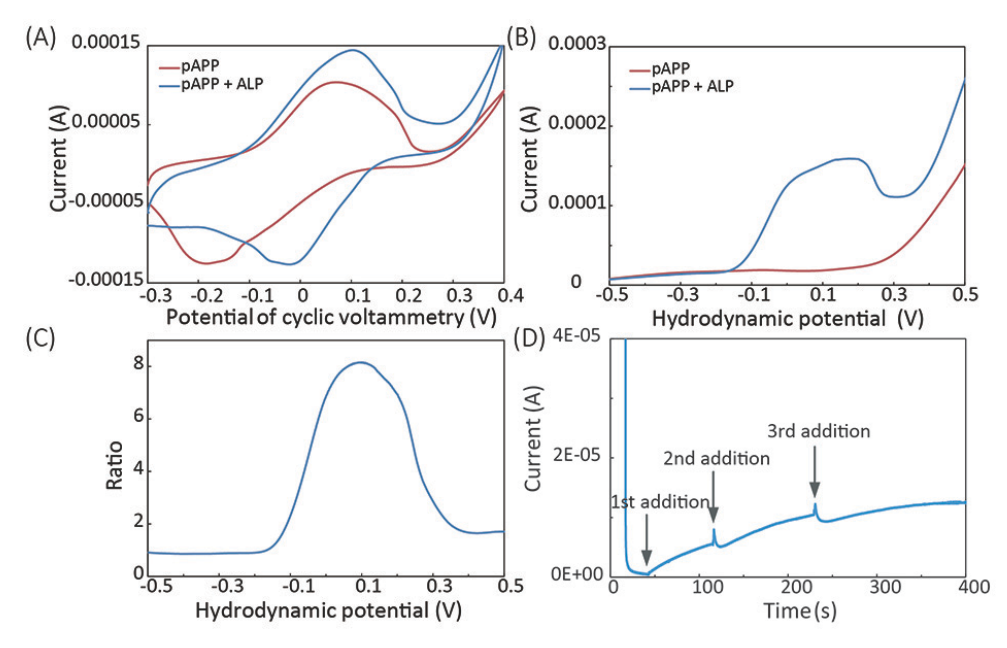


Figure 4-5. Electrochemical characterization of the reaction of pAPP and ALP-labelled antimouse IgG (ALP-antibody). (**A**) Cyclic voltammetry on solutions of pAPP plus ALP-antibody ("pAPP + ALP") and pAPP along ("pAPP"). (**B**) Results of hydrodynamic linear sweeping on the solutions of "pAPP + ALP" and "ALP". (**C**) The signal-to-background current ratio extracted from the hydrodynamic sweeping results. (**D**) Chronoamperometry measurement results on the solution of "pAPP" with ALP-antibody added subsequently. The CA potential of 0.12 V was used.

Figure 4-4 (B) shows the reaction mechanism of pAPP and the ALP-labelled anti-mouse IgG (ALP-antibody). pAPP was first catalyzed by ALP to p-aminophenol (pAP), and the generated pAP was then oxidized by an electrochemical potential applied between the WE and CE and produced two free electrons per molecule. The amperometric current was finally measured as the output signal of the indirect ELISA, which is proportional to the concentration of HIV or HCV antibody in the serum sample.

To characterize the electrochemical reaction of the pAPP and ALP, we firstly performed CV on immunosensors added with a mixture of 4 μl of 40 μg/ml ALP-antibody and 6 μL of 5 mg/ml pAPP ("pAPP + ALP" in **Figure 4-4 (A) and Figure 4-5 (A)**) or 6 μL of 5 mg/ml pAPP alone ("pAPP" in **Figure 4-5 (A)**). The CV measurements were performed in a voltage range of-0.3 V to 0.4 V with a scan rate of 100 mV/s. The cyclic voltammograms, as shown **Figure 4-4 (A) and Figure 4-5 (A)**, reveal that, compared to the solution of ALP-antibody plus pAPP, the solution of pAPP alone requires higher potential for oxidation and reduction and has a larger potential gap

between the oxidation and reduction peaks. Since pAPP can be oxidized by high potentials without ALP-antibody, we should choose a lower potential for assay signal readout.

We employed CA to trigger the oxidation of the pAP (catalyzed from pAPP), which has less interference with other species and thus offers higher accuracy and sensitivity than other electrochemical techniques. We optimized the CA step potential via hydrodynamic linear sweeping. With the solutions of "pAPP + ALP-antibody" and "pAPP" (with the same concentrations as the ones used in the CV measurement in **Figure 4-4 (A) and Figure 4-5 (A)**), we scanned their hydrodynamic potentials in the range of ± 0.5 V at a rate of 100 mV/s. As shown in **Figure 4-5 (B)**, the resultant current measured during the hydrodynamic potential scanning on the solution of "ALP + pAPP" presents an oxidation peak at ~0.1V, while the current measured from the solution of "pAPP" has no obvious oxidation peak.

Defining the ratio of the currents measured from the solutions of "ALP+pAPP" and "pAPP" as the signal-to-background-noise ratio, and one can find that the potential of 0.12 V yields the highest signal-to-background-noise ratio (**Figure 4-5** (**C**)). Thus, the potential of 0.12 V was selected for CV measurements of the final assays. At the potential of 0.12 V, we also performed CA measurement on the solution of 6 µL of 5 mg/ml pAPP, and added 4 µL of 40 µg/ml ALP-antibody consecutively while the current signal was recorded. As shown in **Figure 4-5** (**D**), the solution of pAPP gave a very low current before the first addition of ALP-antibody; the addition of ALP-antibody caused an instant current increase, and the current then reached to a steady state before the next addition.

4.3 Results

4.3.1 Electrochemical Characterization of the E-µPIA

We characterized the electrochemical performance of the E-µPIA (after the APDES and GA treatment) via CV in the solution of 10 mM potassium ferricyanide (K₃[Fe(CN)₆]) and 1 M potassium chloride (KCl). We scanned 5 immunosensors within the range of 0-0.6 V at a rate of 10-50 mV/s. **Figure 4-6 (A)** shows typical cyclic voltammograms measured at different scan rates, and the magnitudes of anode peak currents (Ipa) and cathode peak current (Ipc) are approximately identical. The results of the current peak magnitude as a function of the square root of the scan rate also show a typical linear relationship (**Figure 4-6 (B)**). These results reveal that each immunosensor is a reversible electrochemical system.

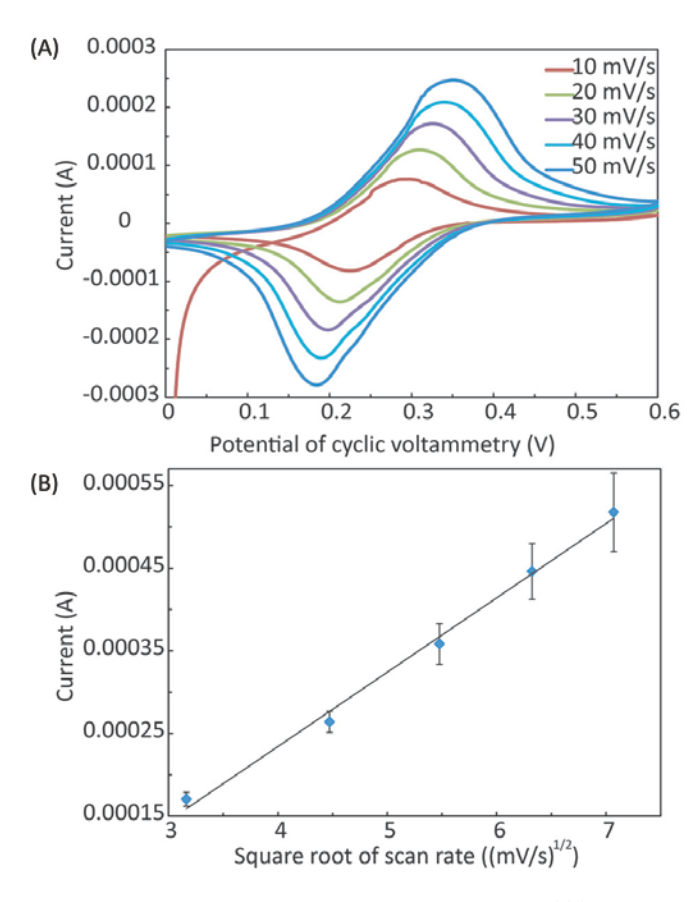


Figure 4-6. Electrochemical characterization of the E- μ PIA. (A) Cyclic voltammetry (CV) of individual immunosensors at the scanning rate from 10 mV/s to 50 mV/s. (B) Calibration results of the peak current magnitude vs. the square root of the scan rate (n = 5).

4.3.2 Detection of HIV/HCV Antibodies in Serum

Using spiked mouse serum, we calibrated the E-µPIA and obtained typical S-shaped calibration curves for both HIV and HCV antibodies (**Figure 4-7 (A)** and **Figure 4-7 (B)**). The LODs for detecting HIV and HCV antibodies were determined to be 300 pg/ml and 750 pg/ml, respectively, which are calculated by three times the standard deviation of output signals measured from blank samples. These LODs are lower than that of existing tests for HIV antibody (1 ng/ml; [26]) and HCV core antibody (5 ng/mL; [27]).

We also investigated the potential cross-reactivity of HIV and HCV antibody detections in the same sample by adding high-concentration interference analyte to serum samples with low-concentration target analyte. We added 10 µg/ml HCV antibody (interference analyte) to serum samples spiked with 10 ng/ml HIV antibody (target analyte) and vice versa, and compared the current outputs from serum samples with and without interference antibodies. **Figure 4-7 (C)**

and **Figure 4-7** (**D**) show the current outputs of assays performed on: (i) serum samples with only target antibody ("HIV 10 ng/ml" in **Figure 4-7** (**C**), and "HCV 10 ng/ml" in **Figure 4-7** (**D**)); and (ii) serum samples with both target antibody and interference antibody ("HIV 10 ng/ml + HCV 10 μg/ml" in **Figure 4-7** (**C**), and "HCV 10 ng/ml + HIV 10 μg/ml" in **Figure 4-7** (**D**)). The current outputs from both types of serum samples have similar values, and not significant difference was found between data groups in **Figure 4-7** (**C**) and **Figure 4-7** (**D**). The current differences between comparisons are 6.8% and 7.1% for HIV and HCV interference tests, respectively. These results prove that the interference between HIV and HCV antibody detections is negligible, and that our diagnostic platform has a great potential for practical diagnosis of HIV/HCV co-infection.

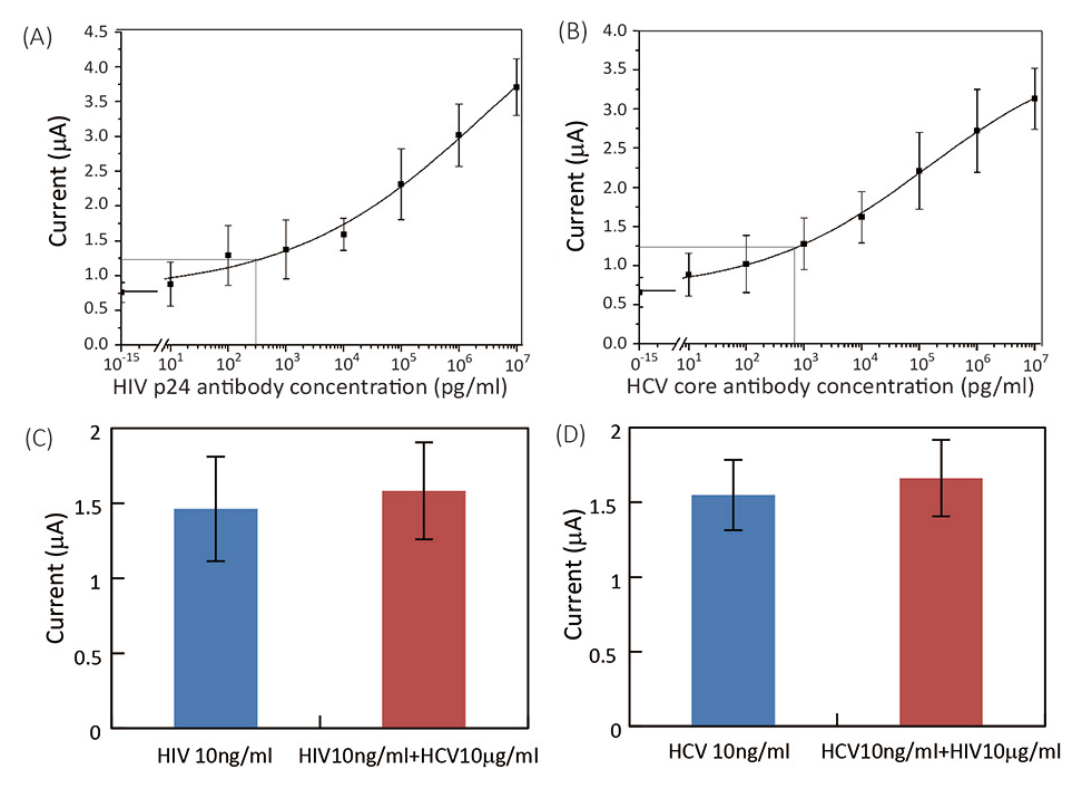


Figure 4-7. Experimental results of device calibration and cross-reactivity testing for HIV/HCV antibody detections. (**A**)(**B**) Calibration curves of (**A**) HIV and (**B**) HCV antibody detections (n = 8). (**C**) Output signals (n = 5) of HIV detection on serum samples with 10 ng/ml HIV antibody only ("HIV 10 ng/ml") and with 10 ng/ml HIV antibody and 10 μ g/ml interference HCV antibody ("HIV 10 ng/ml + HCV 10 μ g/ml"). (**D**) Output signals (n = 5) of HCV detection on serum samples with 10 ng/ml HCV antibody only ("HCV 10 ng/ml") and with 10 ng/ml HCV antibody and 10 μ g/ml interference HIV antibody ("HCV 10 ng/ml + HIV 10 μ g/ml").

4.4 Discussion

ELISA tests for HIV and HCV have been widely used in medical practices, which helps more and more people identify their HIV/HCV status, monitor their disease trends, and improve clinical outcomes. Nevertheless, low-cost, rapid POC tests for diagnosis of HIV/HCV coinfection are highly demanded for use in the developing countries, where the most basic health care facilities are still not readily accessible. The diagnostic platform presented in this work is the first integrated, paper-based electrochemical platform for low-cost diagnosis of the HIV/HCV co-infection. The developed E-μPIA includes eight electrochemical immunosensors capable of carrying out ELISAs in parallel and testing multiple serum samples for both HIV and HCV antibody markers. The electrochemical ELISA is highly accurate and sensitive, and provides lower LODs to existing HIV and HCV antibody tests. The platform allows a user to perform ELISA tests of eight serum samples within 20 minutes. The handheld multiplexing potentiostat makes the entire platform portable and therefore significantly improves its adaptability to POC uses. Given the wide applicability of electrochemical detection to many types of molecules, this platform can be readily extended to the detection of other protein disease markers, metabolites, ions, and nucleic acids.

This work was focused on the design and demonstration of the developed diagnostic platform for diagnosis of HIV/HCV co-infection. To make the platform ready for practical uses, we still need to investigate the stability of the E-µPIA over long-term storage. There have been many studies in the literature on improving the antigen/antibody storage stability on paper substrates [28-30]. Based on the previous results, we plan to improve the device stability by controlling the storage environment humidity and adding protein stabilizers to the E-µPIA. We will also work on the clinical testing of this platform using patient samples, and the further extension of the platform's diagnostic functionalities by targeting other protein markers.

4.5 Conclusions

We have successfully developed an integrated, paper-based diagnostic platform, with multiplexing and telemedicine capabilities, for detection of HIV/HCV co-infection. Indirect ELISAs of antibodies to HIV p24 and HCV core antigens was realized on an electrochemical microfluidic paper-based immunosensor array (E-µPIA), and a handheld potentiostat with a Bluetooth module was developed for readout of output signals from the device. The

electrochemical characterization of individual immunesensor revealed reversible electrochemical behavior. Using this platform, we demonstrated the detection of HIV and HCV antibodies in mouse serum at LODs of 300 pg/ml and 750 pg/ml, respectively. We also investigated the cross-reactivity of the HIV and HCV detections in the same serum samples, and showed negligible interference effect between the HIV and HCV tests.

4.6 Acknowledgements

This work was supported by a Star in Global Health Award from Grand Challenge Canada (0046-01-04-01-01), Natural Sciences and Engineering Research Council of Canada – NSERC (RGPIN 418553-12), Canadian Foundation for Innovation (CFI-LOF 30316), and McGill University (232201). We also acknowledge the financial support from the Canada Research Chairs Program (to XL; 237293) and the NSERC CREATE Training Program in Integrated Sensor Systems (to CZ).

4.7 References

- [1] P. J. Rider and F. Liu, "Crosstalk between HIV and hepatitis C virus during co-infection," *BMC medicine*, vol. 10, no. 1, p. 32, 2012.
- [2] E. A. Operskalski and A. Kovacs, "HIV/HCV co-infection: pathogenesis, clinical complications, treatment, and new therapeutic technologies," *Current HIV/AIDS Reports*, vol. 8, no. 1, pp. 12-22, 2011.
- [3] N. Alatrakchi and M. J. Koziel, "A tale of two viruses: hepatitis C in the age of HAART," *The Lancet*, vol. 362, no. 9397, pp. 1687-1688, 2003.
- [4] S. L. Chen and T. R. Morgan, "The natural history of hepatitis C virus (HCV) infection," *International journal of medical sciences*, vol. 3, no. 2, p. 47, 2006.
- [5] Y. Rotman and T. J. Liang, "Coinfection with hepatitis C virus and human immunodeficiency virus: virological, immunological, and clinical outcomes," *Journal of virology*, vol. 83, no. 15, pp. 7366-7374, 2009.
- [6] D. L. Thomas *et al.*, "The natural history of hepatitis C virus infection: host, viral, and environmental factors," *Jama*, vol. 284, no. 4, pp. 450-456, 2000.
- [7] A. W. Martinez, S. T. Phillips, G. M. Whitesides, and E. Carrilho, "Diagnostics for the developing world: microfluidic paper-based analytical devices," *Analytical chemistry*, vol. 82, no. 1, pp. 3-10, 2009.
- [8] A. K. Yetisen, M. S. Akram, and C. R. Lowe, "Paper-based microfluidic point-of-care diagnostic devices," *Lab on a Chip*, vol. 13, no. 12, pp. 2210-2251, 2013.
- [9] E. J. Maxwell, A. D. Mazzeo, and G. M. Whitesides, "Paper-based electroanalytical devices for accessible diagnostic testing," *MRS bulletin*, vol. 38, no. 04, pp. 309-314, 2013.
- [10] S. Ge, L. Ge, M. Yan, X. Song, J. Yu, and J. Huang, "A disposable paper-based electrochemical sensor with an addressable electrode array for cancer screening," *Chemical Communications*, 10.1039/C2CC34887J vol. 48, no. 75, pp. 9397-9399, 2012.

- [11] W. Dungchai, O. Chailapakul, and C. S. Henry, "Electrochemical detection for paper-based microfluidics," *Analytical chemistry*, vol. 81, no. 14, pp. 5821-5826, 2009.
- [12] Z. Nie *et al.*, "Electrochemical sensing in paper-based microfluidic devices," *Lab on a Chip*, vol. 10, no. 4, pp. 477-483, 2010.
- [13] A. Nemiroski *et al.*, "Universal mobile electrochemical detector designed for use in resource-limited applications," *Proceedings of the National Academy of Sciences*, vol. 111, no. 33, pp. 11984-11989, 2014.
- [14] Z. Nie, F. Deiss, X. Liu, O. Akbulut, and G. M. Whitesides, "Integration of paper-based microfluidic devices with commercial electrochemical readers," *Lab on a Chip*, vol. 10, no. 22, pp. 3163-3169, 2010.
- [15] C. Zhao, M. M. Thuo, and X. Liu, "A microfluidic paper-based electrochemical biosensor array for multiplexed detection of metabolic biomarkers," *Science and Technology of Advanced Materials*, vol. 14, no. 5, p. 054402, 2013.
- [16] D. Zang, L. Ge, M. Yan, X. Song, and J. Yu, "Electrochemical immunoassay on a 3D microfluidic paper-based device," *Chemical Communications*, vol. 48, no. 39, pp. 4683-4685, 2012.
- [17] Y. Wu, P. Xue, K. M. Hui, and Y. Kang, "Electrochemical and Fluorescent Mediated Signal Amplifications for Rapid Detection of Low Abundance Circulating Tumor Cells on a Paper Based Microfluidic Immunodevice," *ChemElectroChem*, vol. 1, no. 4, pp. 722-727, 2014.
- [18] X. Li, C. Zhao, and X. Liu, "A paper-based microfluidic biosensor integrating zinc oxide nanowires for electrochemical glucose detection," *Microsystems & Nanoengineering*, vol. 1, 2015.
- [19] J. A. Adkins and C. S. Henry, "Electrochemical detection in paper-based analytical devices using microwire electrodes," *Analytica chimica acta*, vol. 891, pp. 247-254, 2015.
- [20] N. Dossi, R. Toniolo, F. Terzi, F. Impellizzieri, and G. Bontempelli, "Pencil leads doped with electrochemically deposited Ag and AgCl for drawing reference electrodes on paper-based electrochemical devices," *Electrochimica Acta*, vol. 146, pp. 518-524, 2014.
- [21] K. Oldham, "The effect of uncompensated resistance on the potential-step method of investigating electrochemical kinetics," *Journal of Electroanalytical Chemistry* (1959), vol. 11, no. 3, pp. 171-187, 1966.
- [22] M. Hellerstein *et al.*, "Directly measured kinetics of circulating T lymphocytes in normal and HIV-1-infected humans," *Nature medicine*, vol. 5, no. 1, pp. 83-89, 1999.
- [23] M. W. Pandori *et al.*, "Assessment of the ability of a fourth-generation immunoassay for human immunodeficiency virus (HIV) antibody and p24 antigen to detect both acute and recent HIV infections in a high-risk setting," *Journal of clinical microbiology*, vol. 47, no. 8, pp. 2639-2642, 2009.
- [24] M. J. Alter, W. L. Kuhnert, and L. Finelli, *Guidelines for laboratory testing and result reporting of antibody to hepatitis C virus*. Massachusetts Medical Society, 2003.
- [25] W. Li *et al.*, "Multiplex electrochemical origami immunodevice based on cuboid silver-paper electrode and metal ions tagged nanoporous silver-chitosan," *Biosensors and Bioelectronics*, vol. 56, pp. 167-173, 2014.
- [26] A. Bhimji, A. A. Zaragoza, L. S. Live, and S. O. Kelley, "Electrochemical enzyme-linked immunosorbent assay featuring proximal reagent generation: detection of human

- immunodeficiency virus antibodies in clinical samples," *Analytical chemistry*, vol. 85, no. 14, pp. 6813-6819, 2013.
- [27] D. Moradpour, T. Wakita, K. Tokushige, R. I. Carlson, K. Krawczynski, and J. R. Wands, "Characterization of three novel monoclonal antibodies against hepatitis C virus core protein," *Journal of medical virology*, vol. 48, no. 3, pp. 234-241, 1996.
- [28] G. Wu, J. Srivastava, and M. H. Zaman, "Stability measurements of antibodies stored on paper," *Analytical biochemistry*, vol. 449, pp. 147-154, 2014.
- [29] J. Wang, B. Yiu, J. Obermeyer, C. D. Filipe, J. D. Brennan, and R. Pelton, "Effects of temperature and relative humidity on the stability of paper-immobilized antibodies," *Biomacromolecules*, vol. 13, no. 2, pp. 559-564, 2012.
- [30] A. S. Ferraz *et al.*, "Storage and stability of IgG and IgM monoclonal antibodies dried on filter paper and utility in Neisseria meningitidis serotyping by Dot-blot ELISA," *BMC infectious diseases*, vol. 8, no. 1, p. 30, 2008.

Link between Chapter 4 and Chapter 5

In the previous chapter, we developed the electrochemical microfluidic paper-based immunosensor platform with high resolution, and realized the immunoassay detection of human immune deficiency virus and hepatitis C virus co-infection. As another aspect of personal healthcare, wearable biosensors for physiological condition monitoring are critical and urge extensive development regarding biochemical variables in body fluid. To this end, a noninvasive thread-based wearable nanobiosensor is developed for continuous monitoring of lactate and sodium concentrations in sweat during perspiration. In virtue of this platform, Chapter 5 introduces the fabrication of a thread-based wearable sensing patch with zinc-oxide-nanowire (ZnO-NW) decorated electrode. Lactate sensing membrane and sodium sensing membrane are coated on the ZnO-NW electrode to enable the sensitive and selective measurements of lactate and sodium, respectively. This wearable nanobiosensor integrates an electronic smart headband capable of performing measurements, collecting results, and transmitting data. With this platform, multiplexed detection of lactate and sodium in human sweat is demonstrated with dynamic ranges of 0-25 mM and 0.1-100 mM, and LODs of 3.61 mM and 0.16 mM, respectively, both covering the clinical sweat levels. Accurate measurements on real sweat samples from a healthy donor are conducted, and the results (13.16 \pm 0.83 mM for lactate and 92.9 \pm 5mM for sodium) are in good agreement with standard test results.

Chapter 5 A thread-based wearable nanobiosensor

Chapter 5: A thread-based wearable nanobiosensor

Chen Zhao¹, Xiao Li^{1,2}, Ted Li¹, Qiyang Wu¹, and Xinyu Liu¹*

¹ Department of Mechanical Engineering, McGill University, 817 Sherbrooke Street West, Montreal, QC H3A 0C3, Canada.

²Department of Chemistry, Stanford University, 333 Campus Drive, Stanford, CA 94305, USA.

*Corresponding author: <u>xinyu.liu@mcgill.ca</u>.

To be submitted to Biosensors and Bioelectronics.

Non-invasive wearable biosensors provide an efficient way of continuously quantifying a person's biochemical variables, and are highly valuable for predicting human physiological conditions, and flagging risks and illness. Commercial wearable physical sensors are available for tracking a user's physical activities, but incapable of monitoring health-related bimolecular signals. E-textile-based biosensors enable new applications in this scenario because of its high flexibility/wearability, low cost, high level of electronic integration, and unobtrusiveness. However, challenges in developing E-textile sweat biosensors remain in the production of highconductivity textile materials, the designs of biosensor-skin interfaces, and the development of flexible/wearable embedded data acquisition/transmission electronics. Here, we propose a new thread-based wearable biosensor with zinc-oxide-nanowire-decorated electrodes, and apply it to lactate and sodium detection in sweat during physical exercise. Different from other E-textile sensors, our device is fully integrated and wireless, and is capable of accurate on-body sweat testing and real-time data transmission. We achieve the detection of lactate and sodium with dynamic ranges of 0-25 mM and 0.1-100 mM and limits of detection of 3.61 mM and 0.16 mM, respectively, providing analytical performance comparable to clinical tests. We also demonstrate accurate sweat measurements from a healthy donor, and achieve testing results in good agreement with those from gold-standard tests.

Keywords: wearable biosensor, nanobiosensor, sweat test, lactate, sodium, zinc oxide nanowire

5.1 Introduction

Non-invasive wearable sensors provide an efficient way of continuously quantifying information on the person's physical [1], chemical [2] and biological [3] variables, and is highly valuable for predicting people's physiological status and flagging risks and illness [4, 5]. Commercially available wearable physical sensors are capable of tracking an individual's certain physiological parameters like heart rate, blood pressure, electrocardiogram and skin temperature, but fail to provide insight over the user's health status at the biomolecular level [3]. Biosensors established on textiles embedded with electronic components (i.e., e-textile-based biosensors) have emerged as an attractive type of wearable devices for healthcare applications. It possesses valuable merits such as ease of fabrication, low cost, high level of electronic integration, and low level of obtrusiveness. It also offers an intimate but comfortable contact to skin with potential integration in real garments, and draws considerable attentions for direct sweat monitoring during daily routine within wearers' natural environment.

Recent efforts have been paid into the development of wearable biosensors focusing the monitoring of chemical and biomarkers such as metabolites [3, 6, 7], electrolytes [3, 8] and pH [9], in body fluids including saliva [6], sweat [3, 10], and tear [7, 11]. Considering its noninvasiveness of acquisition, easy accessibility, and abundant amount, sweat has become a popular body fluid for non-invasive diagnosis and health monitoring to retrieve multiple data and harvest further information on metabolites, electrolytes, and body temperature. Lactate and sodium, as the most common detected markers in sweat, play a meaningful role in the control of fitness, electrolyte imbalance, physical well-being, and personal healthcare. Lactate is a biochemical indicator of anaerobic metabolism in patients with circulatory failure, reflecting glycolytic ATP production supporting sweat formation and secretion in eccrine glands [12, 13]. Lactate has a clinically relevant range of 9-23 mM in sweat, and its concentration increases in sweat during physical exercise, making it a useful parameter to monitor wellness, physical fitness and the effect of exercise [13, 14]. The concentration of sodium in sweat varies widely but with a common range 15-65 mmol/L [15]. It is an excellent marker for electrolyte imbalance and provides valuable information regarding an individual's physical and mental well-being [8]. Considering the deleterious physiological risks due to sodium lost, its replenishment is essential for regulating water balance, pH, and osmotic pressure [8]. Thus, continuous sweat monitoring

of lactate and sodium concentrations are essential to athletics and people in exercise, as it helps alert the electrolyte loss and the concomitant need for electrolyte replenishment.

Early studies in e-textile sensors integrated with traditional conductive wires were demonstrated for monitoring of heart rate, ECG, blood pressure, oxygen blood saturation, and skin temperature [16]. Regarding e-textile sweat biosensors, pioneering work was demonstrated by the Diamond's group in the 2000s, measuring sweat pH using pH-sensitive dye and paired emitter-detector LEDs [17]. They also proposed an elasticated belt with electrochemical detection of sweat sodium on a polyvinyl chloride tubed ion selective electrode (ISE) in 2010, and the readout signal was measured by a commercial digital multi-meter [18]. In 2016, the group of Andrade reported a preliminary study on developing an ion-selective potentiometric sensor made from carbon nanotube and cotton yarn, for the detection of potassium, ammonium and pH [19]. Despite these recent advances, challenges in e-textile sweat wearable biosensors remain in the production of higher conductivity textile materials, sensor-skin interfacing design, and embedded electronics integration for data readout and wireless transmission [16, 19].

The integration of nanomaterials into wearable biosensors has the potential to significantly improve the device performance. In particular, zinc oxide nanowire (ZnO NW) is regarded as a versatile nanomaterial for biosensing on flexible substrates because of their superior properties such as nontoxicity, biocompatibility, high electron-transfer rate, and facile growth through hydrothermal processes [20]. Herein, we propose the design and integration of a new wearable thread-based biosensor integrating ZnO NWs and its electronic sweat headband, for real-time monitoring of lactate and sodium in sweat.

The wearable thread-based ZnO-NW biosensor provides a non-invasive way of gathering real-time lactate and sodium concentrations during perspiration. Thread-based carbon electrodes are decorated with ZnO NWs through a low-temperature hydrothermal process, and then coated with specific biosensing membranes for lactate and sodium detection. Using the ZnO-NW electrodes, two thread electrochemical cells are constructed on the same biosensor for contact with human skin, collection of sweat during user exercise, reaction with the sweat lactate and sodium, and generation of electrochemical readout signals. Based on this platform, multiplexed detection of lactate and sodium in human sweat is demonstrated with dynamic ranges of 0-25 mM and 0.1-100 mM, and limits of detection (LODs) of 3.61 mM and 0.16 mM, respectively, both meeting the clinical requirements for sweat testing. As a demonstration, a real sweat sample,

collected from a healthy donor after 30 minutes of exercise, is tested. The results are found to be 13.16 ± 0.83 mM for lactate and 92.9 ± 5 mM for sodium, both in good agreement with the standard test results. This wearable non-invasive biosensor holds a significant potential for monitoring of fitness conditions, electrolyte imbalance, physical well-being, and personal healthcare.

5.2 Experimental methods

5.2.1 Materials and reagents

Zinc acetate dehydrate, sodium hydroxide, ethanol, zinc nitrate hexahydrate, hexamethylenetetramine, tetrathiafulvalene (TTF), nafion (2%), chitosan, L-lactate oxidase (LOx) (33 U/mg), glutaraldehyde solution (70%), sodium chloride, selectophore™ grade sodium ionophore X, bis(2-ethylhexyl) sebacate (DOS), sodium tetrakis[3,5-bis(trifluoromethyl)phenyl] borate (Na-TFPB), polyvinyl chloride (PVC), polyvinyl butyral resin BUTVARs B-98 (PVB), tetrahydrofuran (THF), ammonium hydroxide solution (28%), acetic acid solution (49%-51%), lactic acid solution (85%) were purchased from *Sigma-Aldrich*, Canada, and used without further purification. Polydimethylsiloxane (PDMS) (mixing ratio of 10:1) were purchased from *VWR*, Canada. Carbon ink (E3456), silver (Ag) ink (E1660) and silver/silver chloride (Ag/AgCl) ink (E2411) were purchased from *Ercon Inc*, Wareham, USA.

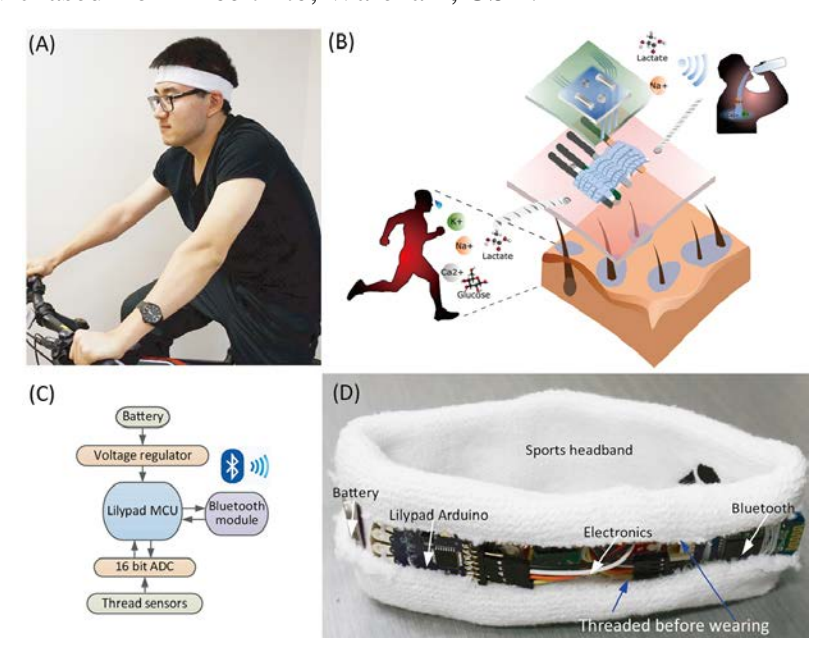


Figure 5-1. **(A)** A volunteer wearing smart headband. **(B)** Design configuration on the wearable device. **(C)** Electronic design principle. **(D)** Wireless smart headband.

The Arduino microcontroller (LilyPad, *Arduino*), 3 V lithium batteries (CR2032, *Energizer*), and a Bluetooth module (HC06, *iTead Studio*) were purchased from Robotshop, Canada. The voltage regulator (TPS 61097, *Texas Instruments*) and the analog-to-digital converter (ADS1115, *Texas Instruments*) were purchased from *Digikey*, Canada. The sweat headband was purchased from *Sports Experts*, Montreal, Canada. The cotton thread (size 10, *Aunt Lydia*) and the medical tape (3M Paper First Aid Tape, *Nexcare*) were purchased from *Walmart*, Canada. The transparency frame (Inkjet printer transparency film, *Staples*) was purchased from *Staples*, Canada.

5.2.2 System design

Figure 5-1 (A) shows a user wearing the electronic headband with a ZnO-NW biosensor attached to the head skin inside. Figure 5-1 (B) illustrates the concept of monitoring sweat lactate and sodium using the wearable biosensor during exercise. The wearable biosensor employs an enzymatic lactate sensing electrode and a sodium ion selective electrode, for measuring concentrations of the lactate and sodium ion in sweat, respectively. For either lactate or sodium detection, an electromotive force (EMF) potential can be measured between the sensing electrode and the reference/counter electrode as the readout signal, which is caused by the reaction of lactate and lactate oxidase inside the lactate enzymatic membrane or the accumulation of sodium ions in the sodium selective membrane.

To quantify the EMF potentials from the biosensor, we constructed a wearable electronic circuit as schematically shown in **Figure 5-1** (**C**). The circuit comprises a miniature microcontroller (LilyPad Arduino), a high-precision 16-bit analog-to-digital converter (ADC; ADS1115), two 3V lithium batteries (CR2032), a voltage regulator for 3.3V regulation (TPS 61097), and a low-power Bluetooth module (HC06) for wireless data transmission. **Figure 5-1** (**D**) shows the circuit arranged inside a sweat headband, before the opening of the headband is closed through threading. Before the integration into the headband, the circuit is wrapped with plastic membrane for electrical insulation.

5.2.3 Design and fabrication of the biosensor patch

The thread-based biosensor was constructed from four cotton-thread electrodes integrated on an adhesive patch. As shown in **Figure 5-2** (**A**), the four electrodes include a lactate sensing working electrode (LS-WE), a sodium sensing working electrode (SS-WE), a reference electrode

(RE), and a trigger electrode (TE). The RE is arranged between the two WEs to serve as a shared electrode, and the TE, designed to monitor the saturation of sweat collection by the wrapping bare threads, is placed on the left side of the LS-WE. The conducting parts were then connected with the wires out from the detection circuit. As shown in Figure 5-2Error! Reference source not found. (B), the four electrodes were first sewed onto a transparency frame through its openings (pre-cut by the laser cutter), by using bare cotton threads. The transparency frame provides mechanical support of the electrodes in the final integrated adhesive patch. Then, the transparency frame with the four electrodes was stacked onto a patterned single-sided adhesive tape (Nexcare Paper First Aid Tape), with the four electrodes in contact with the non-adhesive side of the tape and the wrapping bare threads exposed in the patterned window of the tape. Two strips of tape were used to securely fix the electrodes and the transparency frame onto the patch tape, which completed the fabrication process of the biosensor patch. When such a patch was attached to the human skin (Figure 5-2 (B)), only the bare threads exposed in the patterned window of the tape would be in contact with the skin, thus collect sweat through soaking, and transport the collected sweat onto the electrodes wrapped inside. For isolation purpose, a second layer of single-sided adhesive tape was applied atop the biosensor pad after attaching it to the skin with the conductive ends of the electrodes exposed for electrical connection.

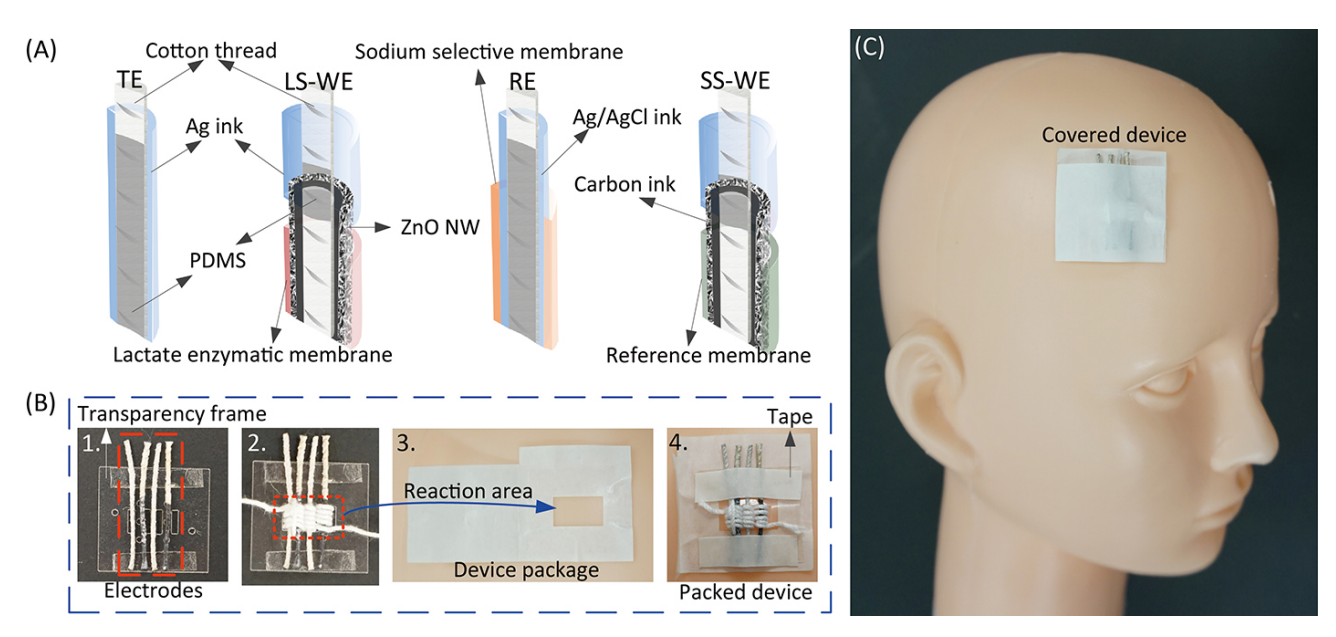


Figure 5-2. **(A)** Cross-section view of electrodes, and wearable device fabrication. **(B)** Packed wearable devices on the wearer's head.

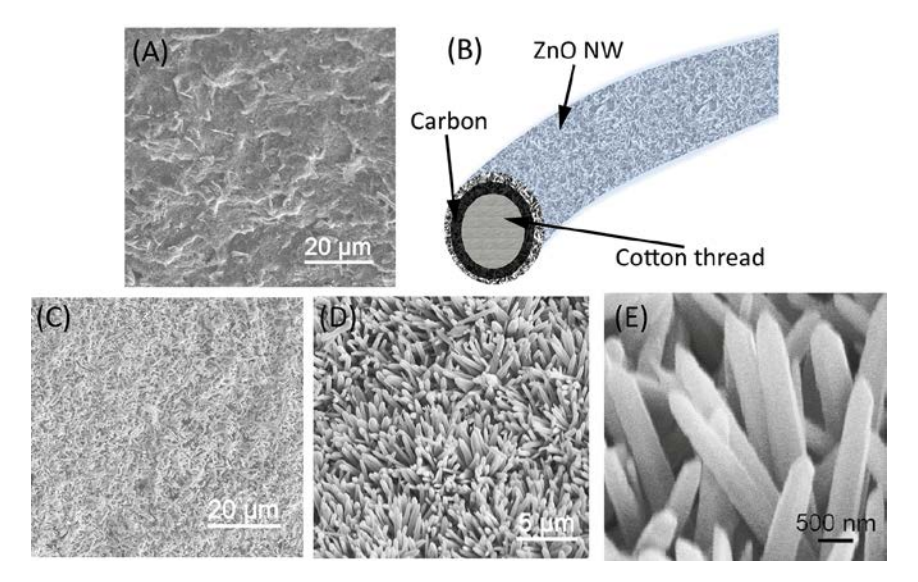


Figure 5-3. **(A)** Bare carbon electrode surface. **(B)** ZnO-NW electrode surface. **(C)(D)(E)** SEM photographs of ZnO-NW electrode at varied magnifications.

To fabricate the biosensor, patterns of the transparency frame and the adhesive patch were designed in AutoCAD (Autodesk, San Rafael, CA) and output to a laser cutter (VersaLASER VLS2.30, *Universal Laser System*) for material cutting. The fabrication and preparation of the electrodes will be introduced in **Section 5.2.4**. The sewing of electrodes with the transparency frame and the assembly of the transparency frame and single-sided adhesive tape were performed manually.

5.2.4 Electrode fabrication

The two working electrodes for lactate and sodium sensing (LS-WE and SS-WE) were fabricated from cotton threads (Aunt Lydia, size 10) sequentially coated with carbon ink, ZnO NWs, and lactate/sodium sensing membranes. The RE and TE were fabricated from cotton threads sequentially coated with PDMS and Ag/AgCl ink. The Ag/AgCl RE was also coated with a reference membrane to prevent potential changes over a large concentration range. To fabricate a bare carbon electrode, a 4 cm cotton thread was brush-coated with uncured PDMS (mixing ratio: 10:1) and baked at 90 °C for 6 hours, forming a 0.5 cm-long hydrophobic barrier inside the thread (as the PDMS wicked into the thread before baking). This barrier restrains sweat in the sensing segment of the sensing electrodes. Then the thread was coated by carbon ink though rolling-printing to cover 1 cm bare thread next to the PDMS-coated segment, and hung over a 75 °C hotplate for drying. This rolling-printing process was repeated twice to secure

adequate carbon coating with even and consistent thickness. The electrodes were washed in deionized (DI) water twice and dried in air before ZnO NW growth. **Figure 5-3 (A)** shows a scanning electron microscopy (SEM) photograph of the carbon surface of a dried electrode.

ZnO NWs were grown on the bare carbon electrode through a hydrothermal process modified from a previous protocol [21]. Firstly, ZnO nanoparticles (ZnO NPs) were synthesized in ethanol and applied to the thread electrode as seeds for hydrothermal growth of ZnO NWs. 17.6 mg of zinc acetate dihydrate (ZAD) and 5 mg of NaOH were dissolved into two flasks of 20 mL pure ethanol and incubated at 70 °C with heavy stirring for 20 min. 20 mL pure ethanol was then added to the ZAD solution for 1:2 dilution, and incubated at 70 °C for 30 min. After the ZAD and the NaOH solutions cooled down to room temperature, the NaOH solution was slowly added into the ZAD solution with constant stirring. The mixture was placed in a convection oven at 60 °C for 2 h to crystallize the ZnO NPs and form a colloidal seeding solution. For each batch of ZnO-NP seeding, the carbon-coated areas of ten bare carbon electrodes were immersed in the seeding solution for 3 min and dried at 86 °C for 3 min. The PDMS barrier stops the seeding solution from wicking to the non-immerged portion of the thread, and thus allows selective ZnO-NP seeding only on the carbon surface. This seeding process was repeated for three times to form a continuous and uniform seeding layer.

An aqueous solution of zinc nitrate hexahydrate (ZNH) and hexamethyl-enetetramine (HMTA) was made to grow ZnO NWs on the seeded electrodes. 2.98 g of ZNH and 0.7 g of HMTA were completely dissolved into two flasks with 190 mL DI water each, and then mixed together to form a solution of 50 mM ZNH and 25 mM HMTA. 10 mL of aqueous solution of pure ammonium hydroxide was then added to the mixture solution, which facilitates the hydrothermal growth by suppressing the homogeneous nucleation of ZnO NWs [21]. The final mixture was preheated in the oven to the hydrothermal growth temperature of 86 °C, and ten ZnO-NP seeded electrodes were then placed into the growth solution for 8 h at 86 °C. After the growth was completed, the ZnO-NW/carbon electrodes were washed in DI water and dried under ambient environment. **Figure 5-3 (B)** illustrates the cross-sectional structure of the final ZnO-NW/carbon electrode, and **Figure 5-3 (C)-(E)** are SEM photographs showing the arrangement and morphology of the ZnO NWs on the carbon electrode at different magnifications. One can see that the carbon electrode surface is uniformly covered by vertically arranged ZnO NWs, whose average width and density are 392 ± 51nm and 2.8 ± 0.21/μm² (n = 5), respectively. One

end of the ZnO-NW/carbon electrode was further coated with Ag ink to form an electrical contact with a 0.2 cm wide overlap with the ZnO-NW layer. Such a ZnO-NW/carbon electrode with Ag contact is ready for coating of lactate/sodium sensing membranes.

To prepare the LS-WE, the ZnO-NW/carbon electrode was functionalized with the enzymatic lactate sensing membrane. Firstly, a paired TTF-nafion reactive membrane was formed on the ZnO-NW surface by sequentially pipetting 3 μ L of 0.5 % (v/v) nafion aqueous solution and 5 μ L of 0.1M TTF ethanol/acetone (v/v ratio: 9:1) solution to the ZnO-NW-coated surface of the electrode. The TTF coating was repeated once more to achieve adequate and even coating. 3 μ L of LOx aqueous solution (200 unit/mL) was then pipetted to the ZnO-NW area and dried under ambient condition, and this surface was further coated with 3 μ L of a 1 % (w/w) chitosan solution prepared in 1% (w/w) acetic acid (heavily stirred for 24 hours). The ZnO-NW surface of the electrode was finally cross-linked through chemical vapor deposition of 15% (v/w) glutaraldehyde (GA) solution in a vacuum chamber at 4 °C for 4 h.

To prepare the SS-WE, a sodium selective membrane was coated onto the ZnO-NW coated surface of the electrode, through pipetting 5 μL of the sodium selective membrane cocktail twice. After each coating, the electrode was dried for 10 min under ambient condition. This membrane cocktail consisted of 1mg sodium ionophore X, 0.55 mg Na-TFPB, 33 mg PVC, and 65.45 mg DOS, all dissolved in 660 mL of nitrogen-purged THF with thorough mixing [8].

As both the lactate and sodium sensing cells have the two-electrode configuration, the RE in each cell also acts as a counter electrode to ensure a complete path of electron transfer through the EMF cell. To fabricate the reference/counter electrode, a 4 cm cotton thread was completely wicked with uncured PDMS (mixing ratio: 10:1) to prevent any potential change caused by liquid wicking inside the thread. Then, Ag/AgCl ink was roll-printed to the PDMS-coated thread and dried at 75 °C for 5 h. A reference membrane cocktail was prepared by dissolving 78.1 mg PVB and 50 mg NaCl in 1mL pure methanol, according to a previous recipe [8]. It contains electrolytes, forms a nanoporous structure on the electrode, and thus allows the free exchange of electrolytes with the solution. Therefore, the membrane-coated RE provides a stable potential and is insensitive to changes in the ion concentration over a large concentration range [8]. 5 μ L of the reference membrane cocktail was pipetted to the Ag/AgCl electrode twice to form the ultimate RE. After each coating, the electrode is dried under ambient condition for 10 min. A TE was included in the biosensor patch to indicate the saturation of sweat collection in the bare

threads wrapping the LS-WE and SS-WE. Its fabrication is the same as the RE without coating the reference membrane.

5.2.5 Preparation of artificial sweat

We used spiked artificial sweat for biosensor calibration. The artificial sweat was prepared following the ISO 3160-2 Standard, which is composed of with 20 g/L NaCl, 17.5 g/L NH₄Cl, 5g/L acetic acid and 15 g/L lactic acid with the pH adjusted to 7 by NH₄OH. For calibration of the lactate and sodium sensing EMF cells, the artificial sweat recipe was slightly adjusted by removing the compositions of lactic acid and NaCl, respectively. Specifically, the lactate-free artificial sweat contains 20g/L NaCl, 17.5 g/L NH₄Cl, 5g/L acetic acid (with the pH adjusted by NH₄OH), and the sodium-free artificial sweat contains 35.8 g/L NH₄Cl (concentration increased to maintain the same level of Cl⁻), 5g/L acetic acid, and 15 g/L lactic acid (with the pH adjusted by NH₄OH).

5.3 Results and Discussion

5.3.1 Pre-conditioning of the LS-WE

Before device calibration, the LS-WE coated with Nafion/TTF/LOx/chitosan/GA was preconditioned through twice of CV scanning from -0.25 V to 0.45 V to form TTF⁺ on the electrode surface, which serves as the mediator in lactate enzymatic reaction [22, 23]. The LS-WE was coupled with the thread RE through wrapping by a bare cotton thread, and placed in a tube with 1.5 mL *phosphate-buffered* saline (PBS) for CV scanning. **Figure 5-4** (**A**) illustrates the electrochemical behavior of TTF under two CV scans at a rate of 20 mV/s. TTF undergoes two one-electron oxidation processes in aqueous solution, resulting in the formation of TTF⁺ and TTF²⁺. In the absence of lactate, the enzyme does not contribute to the redox of TTF, and TTF in the Nafion polymer yields one-electron reversible cyclic voltammograms. In the scan range of 0.45 V and -0.25 V, the Nafion-TTF pair undergoes a redox reaction described in **Equation 5-1**. TTF was oxidized to TTF⁺ when the scanning waveform reaches a potential of ~0.25 V, and in the meanwhile, Na⁺ ions in the sulphonate group of Nafion were substituted with TFF⁺ and entered the phosphate buffer [23]. As shown in **Error! Reference source not found.Figure 5-4** (**A**), the two cyclic voltammograms overlaps with each other and have a 450 mV separation

between the anodic and cathodic potential peaks. This result demonstrates the high repeatability and reversibility of the TTF pairs on the electrode surface.

$$TTF + SO_3/Na^+ \rightarrow SO_3/TTF^+ + Na^+ + e^-$$
 (5-1)

5.3.2 Device calibration

Using spiked artificial sweat, we calibrated the EMF cells for lactate and sodium sensing. 50 mL of artificial sweat spiked with either lactate or sodium was pipetted onto the corresponding sweat collecting thread of a biosensor patch so that the entire sensing area of the electrode was immersed in the sample solution for reaction. At the same time, the signal readout circuit in the headband was triggered to read the EMF potential. Figure 5-4 (A) and (B) show the calibration data (n = 5) of the lactate-sensing EMF cell, which covers a linear range of 0-25 mM. As shown in Figure 5-4 (A), the EMF potential increases once the sample is applied and reaches equilibrium after 20 s. Thus, the EMF potential at 20 s after sample addition was used as the readout signal. During the reaction, lactate diffused from the solution to the lactate sensing membrane and got oxidized by the lactate oxidase; and simultaneously, TTF+ was reduced to TTF. This reaction mechanism can be described by **Equation 5-2**. The reaction causes a change in the concentration ratio of TTF⁺ to TTF in the membrane, which can be quantified by the EMF potential. The difference of EMF potential with and without lactate indicates that the TTF in the Nafion polymer could act as an electron-transfer relay system between the lactate oxidase and the ZnO-NW/carbon electrode. The LOD, defined as the lactate concentration of the sample that induces an EMF potential three times the standard deviation of output signals measured from blank samples, was determined to be 3.61 mM.

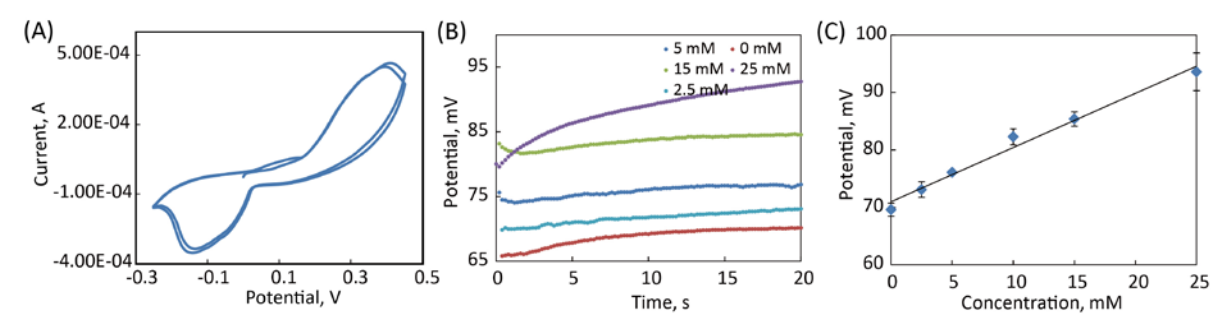


Figure 5-4. (**A**) Cyclic voltammograms of the LS-WE. (**B**) Typical EMF potential curves measured on artificial sweat spiked with lactate at different concentrations. (**C**) Calibration plot of the lactate sensing EMF cell (n=5), which covers a linear range of 0-25 mM with the regression equation: y = 0.94x + 71.

Lactate +
$$2TTF^+ \rightarrow pyruvate + 2TTF + 2H^+$$
 (5-2)

The sodium ion selective membrane contains sodium ionophore X, DOS, PVC, and Na-TFPB. DOS serves as the plasticizer to provides a homogeneous organic phase, and can reduce the viscosity and maintain a relatively high mobility of the membrane constituents [24]. It can also influence the ion-exchanging characteristics of the membrane and ensures the ion selectivity through its polarity and dielectric properties [24]. The polymeric matrix of PVC renders the membrane mechanically stable, and its inert characteristic prevents other chemical interaction with the sodium ions. Na-TFPB acts as a lipophilic cation exchanger to ensure the cation selectivity of the membrane. The sodium ionophore X serves an ion carrier and forms relatively strong, selective and reversible complexes with the target sodium ions, and thus prevents ion exchange by other interfering ions. This chemical composition of the sodium ion selective membrane provides superior selectivity for the potentiometric sodium detection.

Different from the enzymatic lactate detection, no redox process occurs in sodium detection and no electrochemical pre-conditioning of the sensing electrode is needed. Instead, the sodium ions directly partitions into the sodium selective membrane with the assistance of ionophore. With the continuous ion-exchange process, the equilibrium can be established at the solution-membrane interface, and the charge separation at the interface leads to a phase-boundary potential across the membrane and thus an EMF potential difference between the WE and RE. **Figure 5-5** (**A**) shows typical curves of the EMF data measured at different sodium concentrations. One can see that the EMF potential reaches its equilibrium 20 s after sample addition; thus the EMF potential signal at that time point was used as the sensor readout. **Figure 5-5** (**B**) shows the calibration plot of the sodium sensing cell, which covers a linear range of 0.1-100 mM with the regression equation: $y=42.9\log_{10} x+59.2$. The LOD for sodium detection was determined to be 0.16 mM. The measurement ranges of our biosensor match the clinical ranges of lactate and sodium in human sweat, and the corresponding LODs are comparable to those of the existing sweat tests [3].

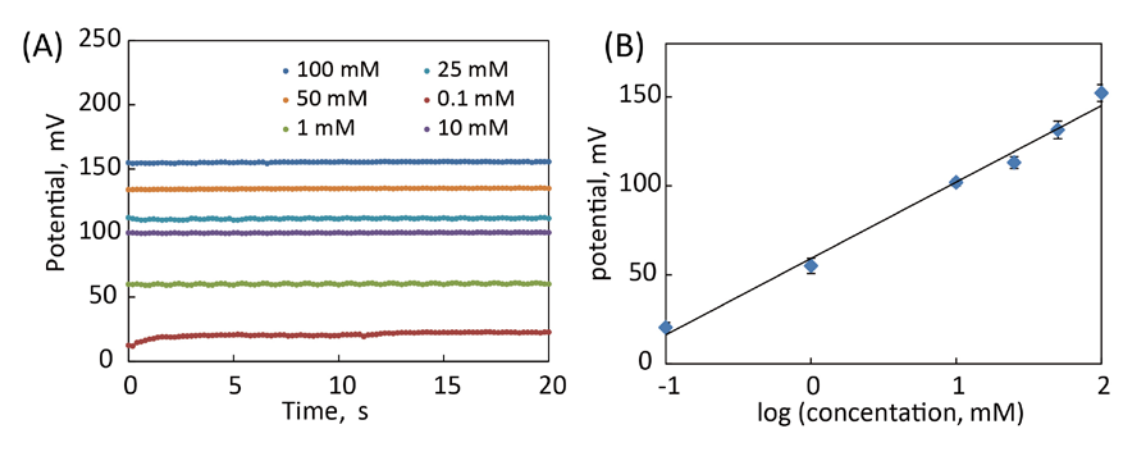


Figure 5-5. (A) and (B): calibration results of the biosensor for sodium sensing (n=5). The calibration curve covers 0.1-100 mM with a linear relationship of y=42.9x+59.2.

5.3.3 Off-body testing of real human sweat

As a practical demonstration, a real sweat sample, collected from a healthy donor after 30 minutes of exercise, was tested using our biosensor and standard lactate/sodium tests. As shown in **Figure 5-6**, the results from our biosensors were 13.16 ± 0.83 mM (n = 5) for lactate and 92.9 \pm 5 mM (n = 5) for sodium, both in good agreement with the standard test results of 13.26 ± 0.57 mM (n = 5), and 89.9 ± 2.42 mM (n = 5), respectively. This demonstrates the effectiveness of our biosensor for real sweat testing. In the near future, we will use the developed biosensor for on-body sweat testing for users in exercise.

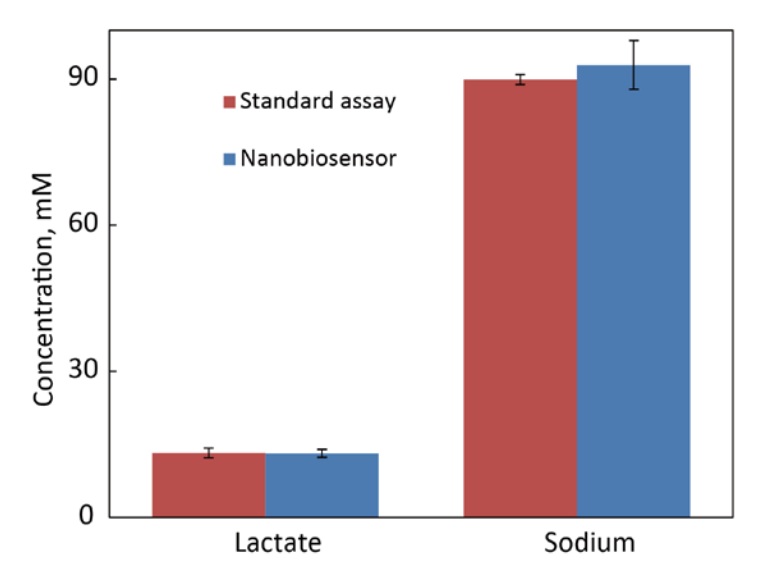


Figure 5-6. Testing results of real human sweat and their comparison with those from standard tests.

5.4 Conclusion

We developed a new wearable sweat testing platform based on a thread-based biosensor integrating ZnO-NW-decorated sensing electrodes, for accurate lactate and sodium detection in human perspiration during exercise. ZnO-NW LS-WE and SS-WE were fabricated for enzymatic lactate detection and ion-selective sodium detection, respectively. A biosensor patch was designed to integrate the LS-WE and SS-WE, a common RE and a TE (for monitoring sweat collection), forming two electrochemical cells for lactate and sodium measurements. A fully integrated electronic headband was constructed for signal readout from the biosensor patch and wireless data transmission (to a laptop and a smart phone). Using spiked artificial sweat, we calibrated the lactate and sodium sensing cells and achieved analytical performance meeting the clinical requirements. A real human sweat sample was also tested using our biosensor, providing testing results in good agreement with those from standard tests. This wearable biosensing platform holds great promise for practical sweat testing for monitoring conditions of user fitness, electrolyte imbalance, and physical well-being.

5.5 Reference

- [1] Y.-D. Lee and W.-Y. Chung, "Wireless sensor network based wearable smart shirt for ubiquitous health and activity monitoring," *Sensors and Actuators B: Chemical*, vol. 140, no. 2, pp. 390-395, 2009.
- [2] K. Mitsubayashi *et al.*, "Wearable and flexible oxygen sensor for transcutaneous oxygen monitoring," *Sensors and Actuators B: Chemical*, vol. 95, no. 1, pp. 373-377, 2003.
- [3] W. Gao *et al.*, "Fully integrated wearable sensor arrays for multiplexed in situ perspiration analysis," *Nature*, vol. 529, no. 7587, pp. 509-514, 2016.
- [4] A. Pantelopoulos and N. G. Bourbakis, "A survey on wearable sensor-based systems for health monitoring and prognosis," *IEEE Transactions on Systems, Man, and Cybernetics, Part C (Applications and Reviews)*, vol. 40, no. 1, pp. 1-12, 2010.
- [5] J. R. Windmiller and J. Wang, "Wearable electrochemical sensors and biosensors: a review," *Electroanalysis*, vol. 25, no. 1, pp. 29-46, 2013.
- [6] J. Kim *et al.*, "Wearable salivary uric acid mouthguard biosensor with integrated wireless electronics," *Biosensors and Bioelectronics*, vol. 74, pp. 1061-1068, 2015.
- [7] H. Yao *et al.*, "A contact lens with integrated telecommunication circuit and sensors for wireless and continuous tear glucose monitoring," *Journal of Micromechanics and Microengineering*, vol. 22, no. 7, p. 075007, 2012.
- [8] A. J. Bandodkar *et al.*, "Epidermal tattoo potentiometric sodium sensors with wireless signal transduction for continuous non-invasive sweat monitoring," *Biosensors and bioelectronics*, vol. 54, pp. 603-609, 2014.
- [9] V. F. Curto *et al.*, "Real-time sweat pH monitoring based on a wearable chemical barcode micro-fluidic platform incorporating ionic liquids," *Sensors and Actuators B: Chemical*, vol. 171, pp. 1327-1334, 2012.

- [10] M. Gamella *et al.*, "A novel non-invasive electrochemical biosensing device for in situ determination of the alcohol content in blood by monitoring ethanol in sweat," *Analytica chimica acta*, vol. 806, pp. 1-7, 2014.
- [11] S. Iguchi *et al.*, "A flexible and wearable biosensor for tear glucose measurement," *Biomedical microdevices*, vol. 9, no. 4, pp. 603-609, 2007.
- [12] S. Wolfe, G. Cage, M. Epstein, L. Tice, H. Miller, and R. Gordon Jr, "Metabolic studies of isolated human eccrine sweat glands," *Journal of Clinical Investigation*, vol. 49, no. 10, p. 1880, 1970.
- [13] M. J. Buono, N. V. Lee, and P. W. Miller, "The relationship between exercise intensity and the sweat lactate excretion rate," *The Journal of Physiological Sciences*, vol. 60, no. 2, pp. 103-107, 2010.
- [14] D. Khodagholy *et al.*, "Organic electrochemical transistor incorporating an ionogel as a solid state electrolyte for lactate sensing," *Journal of Materials Chemistry*, vol. 22, no. 10, pp. 4440-4443, 2012.
- [15] M. H. Rosner and J. Kirven, "Exercise-associated hyponatremia," *Clinical Journal of the American Society of Nephrology*, vol. 2, no. 1, pp. 151-161, 2007.
- [16] A. Lmberis and A. Dittmar, "Advanced wearable health systems and applications-Research and development efforts in the European Union," *IEEE Engineering in Medicine and Biology Magazine*, vol. 26, no. 3, pp. 29-33, 2007.
- [17] D. Morris, S. Coyle, Y. Wu, K. T. Lau, G. Wallace, and D. Diamond, "Bio-sensing textile based patch with integrated optical detection system for sweat monitoring," *Sensors and Actuators B: Chemical*, vol. 139, no. 1, pp. 231-236, 2009.
- [18] B. Schazmann *et al.*, "A wearable electrochemical sensor for the real-time measurement of sweat sodium concentration," *Analytical Methods*, vol. 2, no. 4, pp. 342-348, 2010.
- [19] T. Guinovart, M. Parrilla, G. A. Crespo, F. X. Rius, and F. J. Andrade, "Potentiometric sensors using cotton yarns, carbon nanotubes and polymeric membranes," *Analyst*, vol. 138, no. 18, pp. 5208-5215, 2013.
- [20] Y. Zhang, M. K. Ram, E. K. Stefanakos, and D. Y. Goswami, "Synthesis, characterization, and applications of ZnO nanowires," *Journal of Nanomaterials*, vol. 2012, p. 20, 2012.
- [21] X. Li, C. Zhao, and X. Liu, "A paper-based microfluidic biosensor integrating zinc oxide nanowires for electrochemical glucose detection," *Microsystems & Nanoengineering*, vol. 1, 2015.
- [22] G. Palleschi and A. P. Turner, "Amperometric tetrathiafulvalene-mediated lactate electrode using lactate oxidase absorbed on carbon foil," *Analytica Chimica Acta*, vol. 234, pp. 459-463, 1990.
- [23] H. Liu and J. Deng, "An amperometric lactate sensor employing tetrathiafulvalene in nafion film as electron shuttle," *Electrochimica acta*, vol. 40, no. 12, pp. 1845-1849, 1995.
- [24] C. Mihali and N. Vaum, "Use of plasticizers for electrochemical sensors," *Recent Advances in Plasticizers*, p. 125, 2012.

Link between Chapter 5 and Chapter 6

In the previous chapters, the healthcare related applications of disease diagnostic and physiological monitoring were covered. For the second branch of portable analytical platform, Chapter 6 and Chapter 7 explore on-site water quality monitoring of two major pollutants of heavy metal ions (aluminum and lead) and nutrients (total nitrogen). In particular, Chapter 6 investigates the colorimetric detection of metal ions in water through gold nanoparticle based colorimetric assays and a custom-made optical reader. Heavy metal ions released into various water systems have severe impact on the environment, and excess exposure to toxic metal ions through drinking water pose high risks to human health and cause life-threatening diseases. To meet the urgent needs of on-site heavy metal ion detection, a portable analytical platform is developed for rapid and sensitive detection of aluminum (Al³⁺) and lead (Pb²⁺) ions in water. Using this platform, the LODs of 30 ppb for Pb²⁺ and 89 ppb for Al³⁺ are achieved, with comparable performance to that of a bench-top analytical spectrometer.

Chapter 6

A portable lab-on-a-chip system for gold-nanoparticle-based colorimetric detection of metal ions in water

Chapter 6: A portable lab-on-a-chip system for gold-nanoparticlebased colorimetric detection of metal ions in water

Chen Zhao¹, Guowei Zhong², Da-Eun Kim¹, Jinxia Liu², and Xinyu Liu¹*

¹ Department of Mechanical Engineering, McGill University, 817 Sherbrooke Street West, Montreal, OC H3A 0C3, Canada.

² Department of Civil Engineering and Applied Mechanics, 817 Sherbrooke Street West, Montreal, QC H3A 0C3, Canada.

*Corresponding author: xinyu.liu@mcgill.ca.

Biomicrofluidics 8, 052107 (2014).

doi: http://dx.doi.org/10.1063/1.4894244.

Reproduced and adapted with permission from *Biomicrofluidics*.

Heavy metal ions released into various water systems have severe impact on the environment and human beings, and excess exposure to toxic metal ions through drinking water pose high risks to human health and cause life-threatening diseases. Thus, it is highly demanded to develop a rapid, low-cost and sensitive method for detection of metal ions in water. We present a portable analytical system for colorimetric detection of lead (Pb²⁺) and aluminum (Al³⁺) ions in water based on gold nanoparticle probes and lab-on-a-chip instrumentation. The colorimetric detection of metal ions is conducted via single-step assays with low limits of detection (LOD) and high selectivity. We design a custom-made microwell plate and a handheld colorimetric reader for implementing the assays and quantifying the signal readout. The calibration experiments demonstrate that this portable system provides LODs of 30 ppb for Pb²⁺ and 89 ppb for Al³⁺, both comparable to bench-top analytical spectrometers. It promises an effective platform for metal ion analysis in a more economical and convenient way, particularly for use in water quality monitoring in field and resource-poor settings.

Keywords: environmental monitoring; metal ion detection; gold nanoparticle; colorimetric detection; portable colorimetric reader

6.1 Introduction

Various metal ions are released into our aqueous environments from natural and anthropogenic sources, and some of these ions are toxic at excessive or even trace levels and could thus induce major threats to human health [1]. For instance, lead ions (Pb²⁺) cause hepatic toxicity associated with perturbations in multiple metabolic pathways (e.g., heme synthesis, cholesterol, and drug metabolisms), and long-term exposure to Pb²⁺ will cause chronic kidney and liver diseases [2]. Aluminum ions (Al³⁺), existing at high concentrations in more acidic or organics-rich water, are a risk factor that may cause or accelerate the onset of Alzheimer disease in humans [3]. The accurate detection and quantification of toxic metal ions in water are thus necessary and crucial in many applications such as environmental monitoring, water quality control, and waste water treatment [4-6]. In some application scenarios (e.g., on-site assays with limited resources), high portability, fast assay speed and ease of operations are desired features of the assays for detection of metal ions.

Conventional analytical techniques for detection of metal ions include inductively coupled plasma mass spectrometry [7, 8], atomic absorption spectrophotometry [9], X-ray fluorescence spectrometry [10, 11], and electrochemical analysis [12, 13], all of which provide accurate and sensitive quantifications of metal ions in aqueous solutions. However, these techniques usually rely on sophisticated and bulky instruments, and are highly skill dependent and time consuming; thus, they are difficult to implement outside laboratory environments, and cannot meet various needs of on-site metal ion assays. Different from these instrument-dependent analytical approaches, simple colorimetric assays represent another highly attractive route to detection of metal ions, which are easy to implement, moderately sensitive, highly specific, and less instrument-dependent. A common paradigm of colorimetric detection of metal ions employs the size-dependent optical properties of gold nanoparticles (AuNPs) for signal production and amplification. AuNPs, with properly tuned surface chemistry, could coordinate with metal ions and form aggregates, thus changing the surface plasmon resonance (SPR) absorbance of the assay solution. A variety of AuNP-based colorimetric assays have been developed for detection of metal ions [14-19], and these advances make it possible to develop portable platforms for onsite environmental monitoring.

The objective of this research is to create a portable analytical system for detection of metal ions in water by combining the powerful AuNP-based colorimetric methods with lab-on-a-chip

instrumentation. We utilize two AuNP-based, single-step assays for colorimetric detection of Pb^{2+} and Al^{3+} in water with high selectivity and low limits of detection (LOD). We develop a custom-made microwell plate for implementing the assays and a handheld colorimetric reader for signal quantification. We demonstrate that this portable system provides LODs of 30 ppb for Pb^{2+} (slightly higher than the requirement of ≤ 10 ppb from World Health Organization[20] or WHO) and 89 ppb for Al^{3+} (which meets the WHO requirement of ≤ 200 ppb). These results promise the practical application of our system after further protocol optimization of the Pb^{2+} assay. The portable system permits detection of metal ions in a more economical and convenient way, and is particularly useful for water quality monitoring in the field and resource-poor settings.

6.2 Experimental methods

6.2.1 Colorimetric detection of Pb²⁺ and Al³⁺

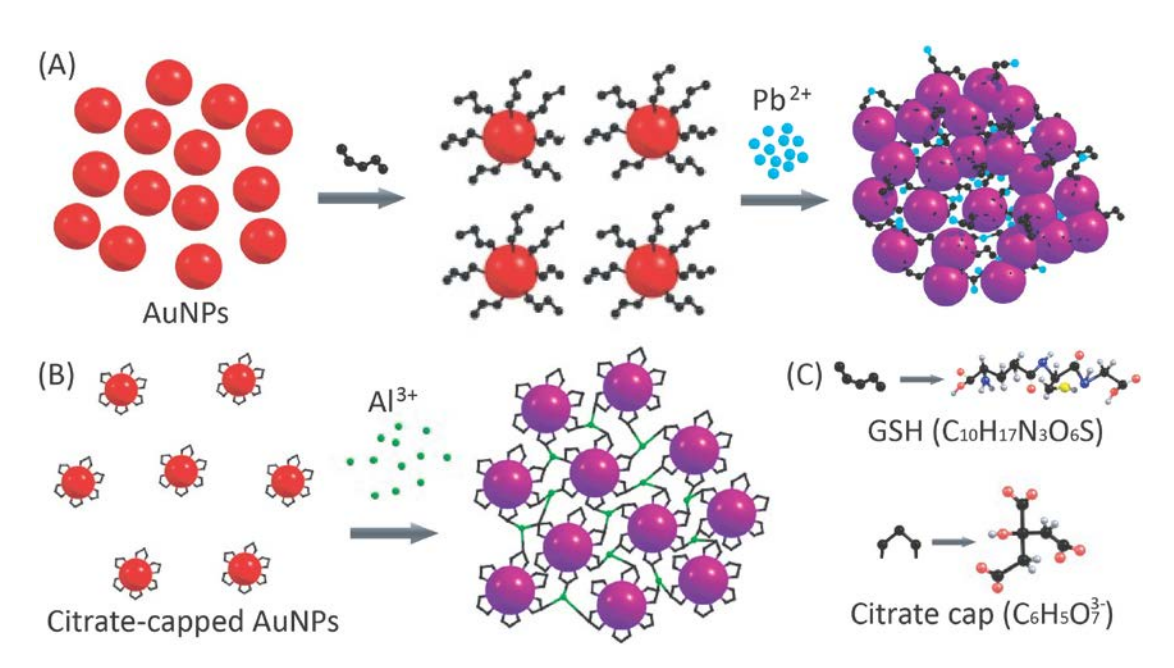


Figure 6-1. Schematic mechanisms of Pb²⁺ and Al³⁺ detection using AuNPs: (**A**) A glutathione (GSH) molecule binds with a label-free AuNP at its thiol group and simultaneously coordinates with Pb²⁺ at its carboxylic groups, leading to aggregation of AuNPs and shift of absorbance spectrum of the AuNP solution. (**B**) Citrate-capped AuNPs aggregate in the presence of Al³⁺, inducing shift of absorbance spectrum of the AuNP solution. (**C**) Molecular structures of the GSH and citrate cap.

Colloidal gold nanoparticles (AuNPs) have been one of the most popular nanomaterials for analytical applications [21-23]. AuNP is particularly suitable for use in optical sensing because its optical and chemical properties are readily tunable through adjusting its size, shape, concentration in solution, surface chemistry, and aggregation state [24]. A common paradigm of using AuNPs for detection of metal ions is based on the metal-ion-induced aggregation of AuNPs in solution and the resultant change in the solution's absorbance spectrum [15-17]. In this research, we employed two highly sensitive and specific assays for colorimetric detection of Pb²⁺ and Al³⁺. Both assays involve single-step mixing of the reagent and the water sample, and are particularly suitable for implementation on our portable system.

For Pb²⁺, we have developed a label-free colorimetric detection method based on peptide-facilitated gold nanoparticle aggregation [25]. This assay relies on *in-situ* conjugation of label-free AuNPs, a common peptide glutathione (GSH - C₁₀H₁₇N₃O₆S), and the Pb²⁺, and does not require tedious pre-labelling of the AuNPs. As the major reagent, label-free AuNPs are more stable in solutions than the labelled ones (we achieved three-month storage at room conditions without aggregation). Using a bench-top ultraviolet-visible (UV-Vis) spectrometer, we have experimentally demonstrated a limit of detection (LOD) of 6.0 ppb and high selectivity of Pb²⁺ detection over other 14 metal ions (including Al³⁺) [25]. In this work, we adapt this approach on our handheld analytical device for portable Pb²⁺ detection. As shown in **Figure 6-1** (**A**), the assay for Pb²⁺ detection involves the GSH to simultaneously functionalize AuNPs *in situ* (during the assay) and coordinate Pb²⁺, which induces AuNP aggregation. A GSH molecule contains one thiol group and two carboxyl groups (**Figure 6-1** (**C**)); the thiol group specifically recognizes AuNP with high affinity, and the carboxylic group binds with Pb²⁺ strongly due to chelating ligands. GSH itself can bind with AuNPs and cause weak aggregation; with the presence of Pb²⁺, the aggregation will be significantly magnified.

For detecting Al³⁺, we adopted a previously reported approach that involves citrate-capped AuNPs [21] for Al³⁺ induced aggregation. Compared with other ions, Al³⁺ has a much higher stable constant for citrate binding.[26] The reaction mechanism of Al³⁺ detection is illustrated in **Figure 6-1 (B)**. With the addition of Al³⁺ into a citrated-capped AuNP solution, the aggregation state of the AuNPs changes from mono-dispersion to emulsion, and its absorbance above 610 nm shifts according to the concentration of Al³⁺. Consequently, the solution changes its color from rich red to bluish purple.

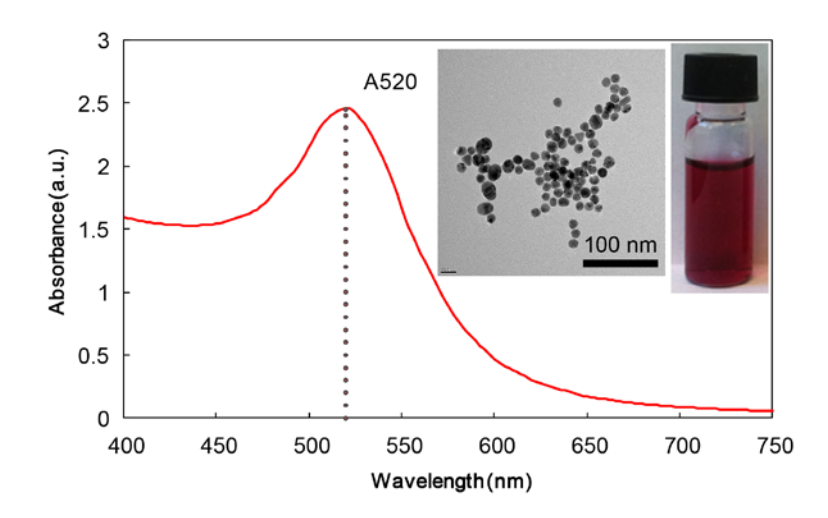


Figure 6-2. The absorbance curve of AuNP solution with a peak at 520 nm. The insets include a transmission electron microscopy (TEM) image of the gold nanoparticles and a photograph of the AuNP aqueous solution.

The AuNPs used in this work have a narrow size distribution of 15.2±3.6 nm, which corresponds to a characteristic absorbance peak of 520 nm (**Figure 6-2**). In both assays, the absorbance of AuNP solutions decreases at 520 nm and significantly increases at 610 nm. Although it is a common practice to measure the absorbance ratio at 610 nm and 520 nm, we opted to only quantify the absorbance at 610 nm as the readout because the absorbance shifts at 520 nm were too subtle to be accurately measured by our portable spectrometer. Our calibration experiments, presented in **Section 6.3**, demonstrate the absorbance measurement at 610 nm was sensitive enough to yield satisfactory analytical performance.

6.2.2 Synthesis of colloidal AuNPs

We synthesized citrate-capped AuNPs by using the traditional Turkevich-Frens method with minor modifications [25, 27, 28]. We first heated 100 mL of 1 mM HAuCl₄ to boiling in a flask with a condenser, then added 10 mL of 38.8 mM sodium citrate to the flask. After the solution turned from pale yellow into ruby red, we kept the mixture boiling for an additional 30 min to complete the reaction. We finally cooled down the AuNP solution with stirring and stored at room temperature prior to the assay. The concentration of the AuNPs was 13 nM. The citrate-capped AuNPs solution we synthesized had a shelf life of three months.

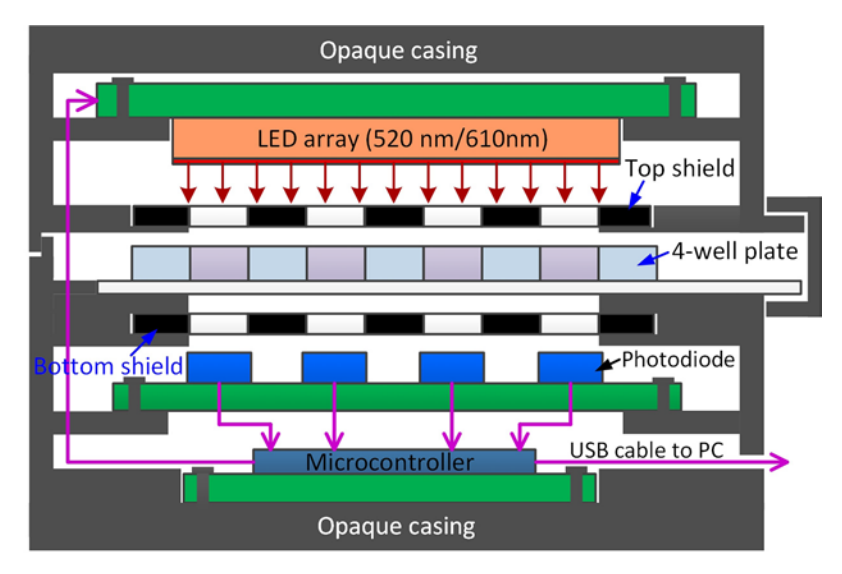


Figure 6-3. Schematic cross-section diagram of the portable analytical system which consists of a four-microwell plate and a handheld colorimetric reader. The four-microwell plate is inserted in the colorimetric reader for absorbance measurement.

6.2.3 Design and fabrication of the portable system

To implement the Pb²⁺ and Al³⁺ detections in a portable format, we developed a lab-on-a-chip platform for performing the metal ion assays and absorbance measurements on site. The platform, as schematically illustrated in **Figure 6-3**, includes a custom-made microwell plate for holding the assay solutions, and a handheld colorimetric reader for accommodating the microwell plate and measuring the absorbance shift in the solutions after reaction. The microwell plate includes four microwells (depth: 3.5 mm; diameter: 6.0 mm; pitch: 10.0 mm) constructed in a piece of polydimethylsiloxane (PDMS) elastomer. We determined the microwell diameter to be 6 mm based on the size of the photodiodes (3.6 mm×4 mm) in the colorimetric reader so that each photodiode could be well aligned underneath a microwell (**Figure 6-3**).

For fabrication of the microwell plate, we created through holes on the PDMS piece using a 6-mm biopsy punch, and then permanently bonded the PDMS piece onto a glass slide (25 mm×75 mm×1 mm) via oxygen plasma treatment. **Figure 6-4 (A)** shows the photograph of a microwell plate filled with solutions after Al³⁺ detection. The microplate is disposable, and can also be reused after thorough cleaning. Although we just integrated four microwells at the prototyping stage, the system architecture allows easy scale-up of the reaction microwells. A larger plate with more microwells simply requires the colorimetric reader to be enlarged and the

number of photodiodes to be increased accordingly. We used PDMS and glass for construction of the microwell plate due to their high transparency and flexibility for prototyping. For mass production, injection molding of transparent plastics can be employed to provide a much lower cost structure of the microwell plate.

The colorimetric reader includes four main components (**Figure 6-3**): (i) a narrow-band light-emitting diode (LED) array (model # YSM-2088CR3G2C, Young Sun LED) with emission wavelengths of 512-518 nm (green) and 610-625 nm (red); (ii) four photodiodes (model # 595-OPT101PG4, Texas Instruments) mounted on a printed circuit board (PCB); (iii) a microcontroller (Arduino UNO board) with Universal Serial Bus (USB) communication for controlling the LED array, quantifying the voltage outputs of the photodiodes, and transmitting measurement data to a computer; and (iv) an opaque plastic casing for accommodating and optically shielding all the electronic components and the microwell plate. The microwell plate can be inserted into the reader, and guiding slots on the plastic casing guarantees fixed gaps between the microwell plate and the LED/photodiodes. Two black shield layers with four openings were placed on the top and bottom of the microwell plate to decrease optical crosstalks between adjacent microwells and therefore suppress background noises in measurement. The total material cost of the colorimetric reader was calculated to be 87 CAD based on commercial prices of the electronic components.

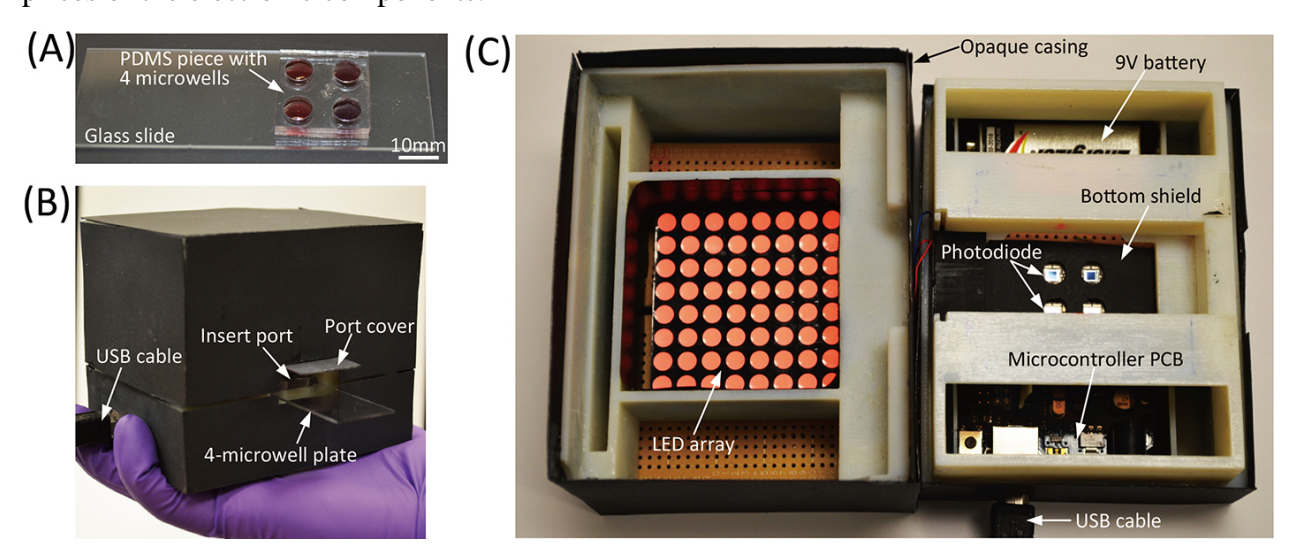


Figure 6-4. Photographs of the portable system. **(A)** A microwell plate filled with solutions of AuNP and Al³⁺. **(B)** The colorimetric reader held by a hand, with a microwell plate inserted. **(C)** Inside of the colorimetric reader with the LED array lighting up.

Figure 6-4 (B) shows the colorimetric reader held by a hand with a microwell plate inserted, and **Figure 6-4 (C)** shows the inside of the colorimetric reader. The LED array consists of 8 × 8 dual-color LED 'pixels', providing uniform illustration for absorbance measurement. The LED 'pixels' can emit light at wavelengths of 512-518 nm (green) and 610-625 nm (red), and the microprocessor controls the emission wavelength by altering the supply voltage to the LED array (4.4 V for green and 5.0 V for red). The emission range of 610-625 nm of the LED array was experimentally proved effective for the absorbance measurement at 610 nm. The photodiode chip integrates a signal conditioning circuit, and can be powered by a 9V battery (**Figure 6-4 (C)**). In our current prototype, voltage signals from the photodiodes are transmitted to a computer for data analysis via the USB cable. It is also feasible to integrate a liquid crystal display (LCD) for direct readout of assay results and a Bluetooth module for wireless data transmission from the reader to other devices such as smartphones, tablets, and computers for further analysis.

6.2.4 Assay protocols

For Pb^{2+} detection, we used the original AuNP solution, and prepared a GSH mixture by the following steps. We firstly made a solution of NaCl (1 M) as background electrolyte, a phosphate buffer solution (50 mM, pH 7), and a GSH solution (100 mM). Then, we prepared the GSH mixture by mixing 110 μ L of the NaCl solution, 620 μ L of the phosphate butter, and 480 μ L of the GSH solution, and 790 μ L of distilled water. Before each experiment, we prepared fresh deionized (DI) water samples spiked with Pb^{2+} at incremental concentrations of 0 ppb, 50 ppb, 100 ppb, 200 ppb, and 500 ppb. To perform an assay, we first filled 41.5 μ L of Pb^{2+} spiked water in a microwell, then added 12 μ L of GSH mixture and 34.6 μ L of AuNP solution, and mixed them by pipetting. After 10 minutes of incubation (determined experimentally; refer to Section 6.3), we slowly slid the microwell plate into the colorimetric for absorbance measurement.

For Al³⁺ detection, we directly used citrate-capped AuNPs that can be coordinated by Al³⁺ and form aggregates. We experimentally determined the optimal pH value of the AuNP solution to be 2.24, which yielded the best sensitivity at low concentrations of Al³⁺. Before experiments, we prepared fresh DI water samples spiked with Al³⁺ at incremental concentrations of 0 ppb, 100 ppb, 200 ppb, 300 ppb, and 400 ppb. For detections performed on the four-microwell plate, we

first filled 45 μ L of the Al³⁺ spiked water in each microwell and then added 45 μ L of AuNP to the microwell to initiate the reaction. After complete mixing via pipetting, we incubated the mixtures for 8 min (determined experimentally; refer to **Section 6.3**) and measured colorimetric signals from all the microwells using the colorimetric reader.

For performance comparison, we also implemented the same assays of Pb^{2+} and Al^{3+} in 96-well plates using UV-Vis spectrometry. For Pb^{2+} detection, we mixed 100 μ L of water sample, 50 μ L of GSH mixture, and 150 μ L of AuNP solution in each well, incubated the mixture for 10 min, and measured the absorbance at A_{610} . For Al^{3+} detection, we mixed 150 μ L of water sample and 150 μ L of AuNP solution, incubated the mixture for 8 min, and measured the absorbance at A_{610} . Note that we adopted a higher volume of the sample/reagent mixture for assays on UV-Vis spectrometry (300 μ L vs. ~90 μ L for assays on the portable system) to achieve an adequate length of light path through the solution for UV-Vis measurement.

6.3 Results and discussion

6.3.1 Analysis of AuNP aggregation kinetics via the handheld reader

To understand the kinetics of AuNP aggregation during Pb²⁺ and Al³⁺ assays, we quantified the changes in absorbance of the mixture of water sample and detection reagent at 610 nm using the portable system. The absorbance of the sample/reagent mixture was monitored within the first 11 minutes of the reaction. Figure 6-5 (A) and Figure 6-6 (A) show the reaction kinetics of Pb²⁺ and Al³⁺ assays in terms of light absorbance change. The output signal from the photodiode is in the form of voltage, while a higher voltage value linearly corresponds to a lower absorbance level at 610 nm. In the Pb²⁺ assays (**Figure 6-5 (A)**), the absorbance of light at 610 nm through the reaction solution became lower with time; at the same time point of reaction, higher concentrations of Pb2+ vielded higher absorbance levels (lower output voltages of the photodiode) in the measurement range of 0-500 ppb. The Al³⁺ assay followed the same trend of light absorbance in the measurement range of 0-400 ppb. Beyond these measurement ranges, the aggregated AuNPs were too large to remain colloidal in the solution, resulting in saturated or even lower light absorbance. Based on the data of reaction kinetics, we chose the time points for signal measurement in Pb²⁺ and Al³⁺ assays to be 10 min and 8 min after reaction starts. At 0 ppb of Pb²⁺, the absorbance level slightly increased (which corresponds to the 0 ppb data curve in Figure 6-5 (A)) because of the GSH-induced weak aggregation of AuNPs in the absence of Pb²⁺.

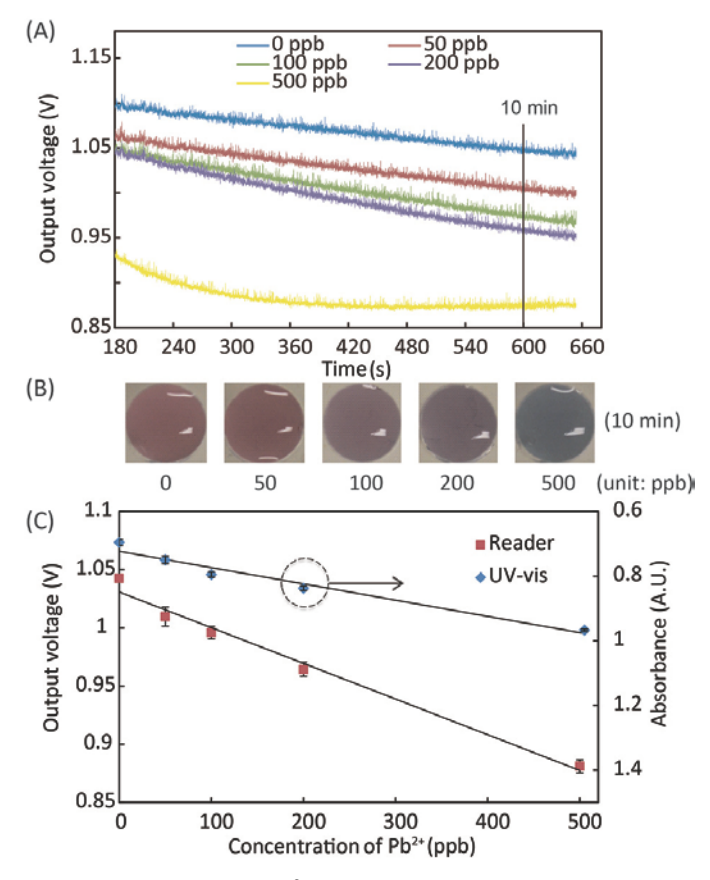


Figure 6-5. Experimental results of the Pb²⁺ assay. (**A**) The kinetic curve of AuNP aggregation in Pb²⁺ solutions in terms of light absorbance at 610 nm. (**B**) Photographs of assay solutions at different Pb²⁺ concentrations, which generated different levels of color change after 10-minute reaction. (**C**) Calibration curves of the Pb²⁺ assay, obtained using the portable reader and UV-vis spectrometer [25], with linear regression equations of y = -0.00031x + 1.0 and y = 0.00050x + 0.72, for data from the portable reader and UV-Vis spectrometer respectively.

6.3.2 Calibration results of Pb^{2+} and Al^{3+} assays

We performed calibration experiments of the Pb²⁺ and Al³⁺ assays using our portable system, and compared the results with the ones obtained using the conventional 96-well plate on a UV-Vis spectrometer. **Figure 6-5 (B)** and **Figure 6-6 (B)** show the color changes of assay solutions vs. Pb²⁺ and Al³⁺ concentrations, respectively. **Figure 6-5 (C)** and **Figure 6-6 (C)** illustrate calibration curves of the Pb²⁺ and Al³⁺ assays, collected using both the portable system and the UV-Vis spectrometer. The calibration curves from the portable system reveal very similar trends as the ones from the UV-Vis spectrometry, which validates the effectiveness of the colorimetric reader.

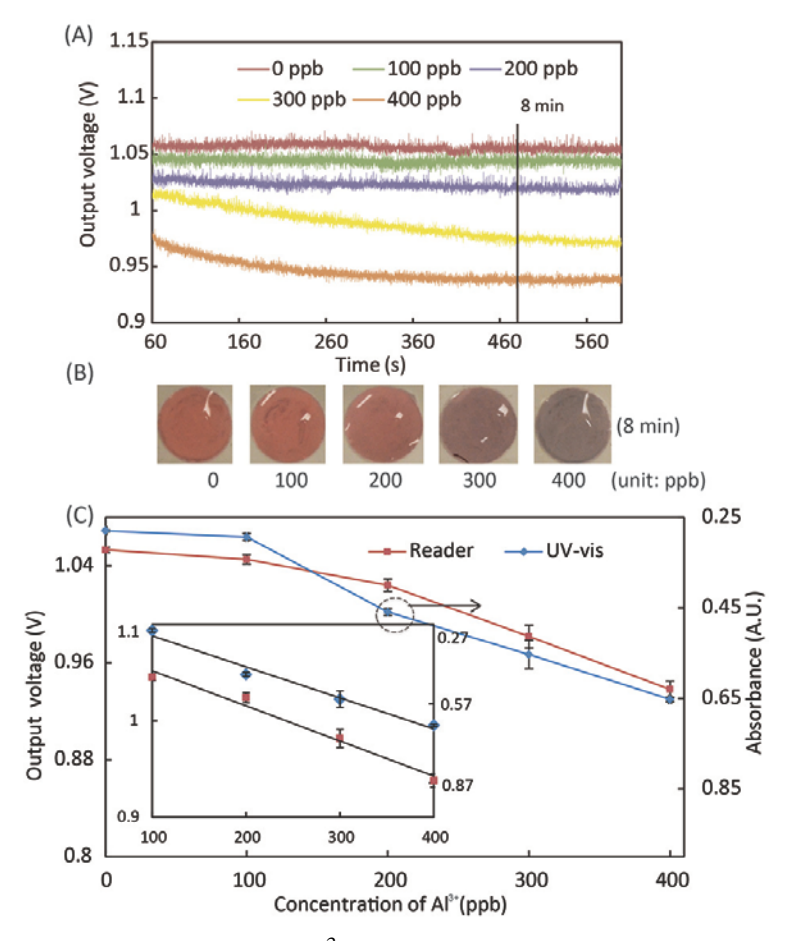


Figure 6-6. Experimental results of the Al^{3+} assay. (**A**) The kinetic curve of AuNP aggregation in Al^{3+} solutions in terms of light absorbance at 610 nm. (**B**) Photographs of assay solutions at different Al^{3+} concentrations, which generated different levels of color change after 8-minute reaction. (**C**) Calibration curves of the Al^{3+} assay, obtained using the portable reader and UV-Vis spectrometer. The inset includes linear regression curves of the calibration data in the range of 100-400 ppb, with equations of y = -0.00036x + 1.1 (for data from the portable reader) and y = 0.0012x + 0.20 (for data from the UV-Vis spectrometer).

We calculated the LOD of Pb²⁺ assay using the linear regression of the data in the whole measurement range of 0-500 ppb. Considering the nonlinear calibration data of Al³⁺ assay at low concentrations, we calculated the LOD of Al³⁺ assay using the linear regression of the data in the range of 0–100 ppb. LODs of 30 ppb for Pb²⁺ and 89 ppb for Al³⁺ were achieved by the portable system, which are comparable with the UV-Vis spectrometry (56 ppb for Pb²⁺ and 46 ppb for Al³⁺). Our measurement ranges for Pb²⁺ (0–500 ppb) and Al³⁺ (0–400 ppb) cover the requirement

for practical applications. The LOD of our Al^{3+} assay (89 ppb) meets the WHO standard (\leq 200 ppb), but our LOD for Pb²⁺ (30 ppb) is slightly higher than the WHO cutoff (\leq 10 ppb).

6.3.3 Assay selectivity

We [25] and others [21] have experimentally demonstrated that the selectivity of the Pb²⁺ and Al³⁺ assays is sufficient to eliminate the interference of other metal ions possibly existing in water. In a previous study [25], we evaluated the selectivity of the Pb²⁺ assay against 14 metal ions (Ca²⁺, As³⁺, Mg²⁺, Hg²⁺, Cu²⁺, Ni²⁺, Fe³⁺, Ba²⁺, Co²⁺, Ag⁺, Mn²⁺, Cd²⁺, Zn²⁺, Cr³⁺, Al³⁺) using UV-Vis spectrometry. Masking agents that have high formation constants with the interfering ions were added to the reagent solution for minimizing the ions' interference with the Pb²⁺ assay. The experimental results show that most of the metal ions had negligible impact on the Pb²⁺ assay [25]. Chen *et al.* [21] investigated the interference of 10 metal ions (Hg²⁺, Fe³⁺, Cd²⁺, Ag⁺, Pb²⁺, Cu²⁺, Ni²⁺, Zn²⁺, Mn²⁺, Co²⁺) with the Al³⁺ assay we used in this work, and demonstrated the high selectivity of the assay over these metal ions. These results show that the Pb²⁺ and Al³⁺ assays have great potential to selectively detect the target metal ions in real water samples. We are currently performing more experiments on detecting Pb²⁺ and Al³⁺ in tap water samples, and investigating chemical routes to minimize the effect of other potential interfering ions and compounds in the samples.

6.4 Conclusions

We have developed a portable and cost-effective lab-on-a-chip system and used it for colorimetric detection of Pb²⁺ and Al³⁺ in water. The Pb²⁺ and Al³⁺ assays were based on metal-ion-coordinated aggregation of AuNPs in solution, which produced changes in the light absorbance and therefore the color of the assay solution. We performed the reactions on a PDMS microwell plate, and employed a custom-made colorimetric reader for signal readout. The assay operations only included single-time mixing of the AuNP reagent solution and the water sample, timed incubation, and colorimetric signal measurement. We demonstrated that our portable system provided LODs of 30 ppb for Pb²⁺ and 89 ppb for Al³⁺, which are comparable with the values obtained via bench-top spectrometry. This portable system represents a promising solution to on-site analysis of metal ions in real water samples.

6.5 Acknowledgement

This research was supported by Natural Sciences and Engineering Research Council of Canada (NSERC), Canada Foundation for Innovation, and McGill University. The authors also acknowledge financial supports from the Canada Research Chairs Program and the McGill Chwang-Seto Faculty Scholarship Program (to Xinyu Liu), the McGill Summer Undergraduate Research in Engineering (SURE) Program (to Da-Eun Kim), and the NSERC-CREATE Training Program in Integrated Sensor Systems (to Chen Zhao).

6.6 Reference

- [1] L. Järup, "Hazards of heavy metal contamination," *British medical bulletin*, vol. 68, no. 1, pp. 167-182, 2003.
- [2] A. Mudipalli, "Lead hepatotoxicity & potential health effects," *Indian Journal of Medical Research*, vol. 126, no. 6, p. 518, 2007.
- [3] L. Tomljenovic, "Aluminum and Alzheimer's disease: after a century of controversy, is there a plausible link?," *Journal of Alzheimer's Disease*, vol. 23, no. 4, pp. 567-598, 2011.
- [4] F. Fu and Q. Wang, "Removal of heavy metal ions from wastewaters: A review," *Journal of Environmental Management*, vol. 92, no. 3, pp. 407-418, 2011.
- [5] G. Aragay, J. Pons, and A. Merkoçi, "Recent trends in macro-, micro-, and nanomaterial-based tools and strategies for heavy-metal detection," *Chemical reviews*, vol. 111, no. 5, pp. 3433-3458, 2011.
- [6] H. Li *et al.*, "Chrysanthemum-like α-FeOOH microspheres produced by a simple green method and their outstanding ability in heavy metal ion removal," *Journal of Materials Chemistry*, vol. 21, no. 22, pp. 7878-7881, 2011.
- [7] P. Liang, Y. Liu, L. Guo, J. Zeng, and H. Lu, "Multiwalled carbon nanotubes as solid-phase extraction adsorbent for the preconcentration of trace metal ions and their determination by inductively coupled plasma atomic emission spectrometry," *J. Anal. At. Spectrom.*, vol. 19, no. 11, pp. 1489-1492, 2004.
- [8] Y. Liu, P. Liang, and L. Guo, "Nanometer titanium dioxide immobilized on silica gel as sorbent for preconcentration of metal ions prior to their determination by inductively coupled plasma atomic emission spectrometry," *Talanta*, vol. 68, no. 1, pp. 25-30, 2005.
- [9] M. Frankowski *et al.*, "Determination of aluminium in groundwater samples by GF-AAS, ICP-AES, ICP-MS and modelling of inorganic aluminium complexes," *Environmental monitoring and assessment*, vol. 182, no. 1-4, pp. 71-84, 2011.
- [10] B. Hołyńska, B. Ostachowicz, and D. Węgrzynek, "Simple method of determination of copper, mercury and lead in potable water with preliminary pre-concentration by total reflection X-ray fluorescence spectrometry," *Spectrochimica Acta Part B: Atomic Spectroscopy*, vol. 51, no. 7, pp. 769-773, 1996.
- [11] H. Watanabe, S. Berman, and D. Russell, "Determination of trace metals in water using X-ray fluorescence spectrometry," *Talanta*, vol. 19, no. 11, pp. 1363-1375, 1972.
- [12] Z. Nie *et al.*, "Electrochemical sensing in paper-based microfluidic devices," *Lab on a Chip*, vol. 10, no. 4, pp. 477-483, 2010.

- [13] J. Shi, F. Tang, H. Xing, H. Zheng, B. Lianhua, and W. Wei, "Electrochemical detection of Pb and Cd in paper-based microfluidic devices," *Journal of the Brazilian Chemical Society*, vol. 23, no. 6, pp. 1124-1130, 2012.
- [14] Y. Guo, Z. Wang, W. Qu, H. Shao, and X. Jiang, "Colorimetric detection of mercury, lead and copper ions simultaneously using protein-functionalized gold nanoparticles," *Biosensors and Bioelectronics*, vol. 26, no. 10, pp. 4064-4069, 2011.
- [15] Y. Date *et al.*, "Microfluidic heavy metal immunoassay based on absorbance measurement," *Biosensors and Bioelectronics*, vol. 33, no. 1, pp. 106-112, 2012.
- [16] Y. Date *et al.*, "Trace-Level Mercury Ion (Hg2+) Analysis in Aqueous Sample Based on Solid-Phase Extraction Followed by Microfluidic Immunoassay," *Analytical Chemistry*, vol. 85, no. 1, pp. 434-440, 2012.
- [17] A. Gao *et al.*, "Digital Microfluidic Chip for Rapid Portable Detection of Mercury (II)," *Sensors Journal, IEEE*, vol. 11, no. 11, pp. 2820-2824, 2011.
- [18] C. Fan, S. He, G. Liu, L. Wang, and S. Song, "A Portable and Power-Free Microfluidic Device for Rapid and Sensitive Lead (Pb2+) Detection," *Sensors*, vol. 12, no. 7, pp. 9467-9475, 2012.
- [19] J. Sun, Y. Xianyu, and X. Jiang, "Point-of-care biochemical assays using gold nanoparticle-implemented microfluidics," *Chemical Society Reviews*, 2014.
- [20] W. H. Organization, Guidelines for Drinking-water Quality: First Addendum to Third Edition, Volume 1, Recommendations. World Health Organization, 2006.
- [21] S. Chen *et al.*, "Rapid visual detection of aluminium ion using citrate capped gold nanoparticles," *Analyst*, vol. 137, no. 9, pp. 2021-2023, 2012.
- [22] M. S. Khan, G. D. Vishakante, and H. Siddaramaiah, "Gold nanoparticles: A paradigm shift in biomedical applications," *Advances in colloid and interface science*, vol. 199, pp. 44-58, 2013.
- [23] X. Cao, Y. Ye, and S. Liu, "Gold nanoparticle-based signal amplification for biosensing," *Analytical biochemistry*, vol. 417, no. 1, pp. 1-16, 2011.
- [24] W. Haiss, N. T. Thanh, J. Aveyard, and D. G. Fernig, "Determination of size and concentration of gold nanoparticles from UV-vis spectra," *Analytical Chemistry*, vol. 79, no. 11, pp. 4215-4221, 2007.
- [25] G. Zhong, "Rapid Detection of Trace Metal Ions on Microfluidic Platforms using Gold Nanoparticle Sensors," *Master's thesis, McGill University*, July 2013.
- [26] R. B. Martin, "Citrate binding of Al3+ and Fe3+," *Journal of inorganic biochemistry*, vol. 28, no. 2-3, p. 181, 1986.
- [27] J. Turkevich, P. C. Stevenson, and J. Hillier, "A study of the nucleation and growth processes in the synthesis of colloidal gold," *Discussions of the Faraday Society*, vol. 11, pp. 55-75, 1951.
- [28] J. Liu and Y. Lu, "Preparation of aptamer-linked gold nanoparticle purple aggregates for colorimetric sensing of analytes," *Nature Protocols*, vol. 1, no. 1, pp. 246-252, 2006.

Link between Chapter 6 and Chapter 7

In the previous chapter, a portable lab-on-a-chip system was reported, for gold-nanoparticle-based colorimetric detection of metal ions in water. Another important type of pollutant in water systems we target here is total nitrogen (TN), a nutrient pollutant causes significant water quality and health issues at a global scale. The excess amount of TN present in water leads to algae bloom with a notable negative impact on the environment, the economy, and the human health. To face this situation, regular monitoring of TN levels in water systems is required, for which portable TN analyzers represent an attractive solution. In this chapter, a novel analytical system is developed comprising a portable ultraviolet C reaction chamber (for digesting organic nitrogen) and a colorimetric reader (for final detection of total nitrite). With this system, rapid digestion and colorimetric determination of total nitrogen are achieved in 36 minutes, with a limit of detection (LOD) of 1.20 mg/l, which is much lower than the required LOD of World Health Organization standard (10 mg/l).

Chapter 7

Rapid on-site determination of total nitrogen in water using a portable analytical system

Rapid on-site determination of total nitrogen in water using a portable analytical system

Chen Zhao^{#1}, Longyan Chen^{#1}, Guowei Zhong², Qiyang Wu¹, Jinxia Liu², and Xinyu Liu¹

*Corresponding author: <u>xinyu.liu@mcgill.ca</u>.

An excess amount of total nitrogen (TN) in water causes notable negative impact on the environment, human health, and economy at a global scale. Conventional analytical techniques for determining total nitrogen in water usually involve long and tedious processes requiring extensive sample preparation for digestion and titration. Emerging lab-on-a-chip platforms have enabled in-situ measurements of water pollutants such as nitrate, nitrite, and ammonium. However, the digestion of organic nitrogen compounds in aqueous environments still remains a challenge for portable analytical systems. In this paper, a portable analytical system is developed, which integrates an ultraviolet C (UVC)-assisted digestion chamber and a portable colorimetric reader, for on-site determination of TN in water samples. Extensive experiments are performed to explore the parameters of organic digestion/oxidation and colorimetric detection, including oxidation time, temperature and substrate, oxidizer concentrations, nitrate reduction time, nitrite colorimetric reaction time, and reagents stability over time. Our system can complete fast oxidation and colorimetric determination of TN within 36 minutes, with a measurement range of 1 μg/L to 10 g/L and a limit of detection of 1.2 mg/L (lower than the World Health Organization standard of 10 mg/L). We believe this portable system is a useful tool for on-site water TN testing with much shorter assay time and lower cost.

Keywords: Nutrient contaminant, total nitrogen, UVC digestion, portable analytical platform, colorimetric assay, water quality monitoring

¹ Department of Mechanical Engineering, McGill University, 817 Sherbrooke Street West, Montreal, QC H3A 0C3, Canada.

² Department of Civil Engineering and Applied Mechanics, 817 Sherbrooke Street West, Montreal, QC H3A 0C3, Canada.

[#] Authors with equal contributions.

7.1 Introduction

Total nitrogen (TN) in our water systems includes inorganic compounds of nitrate (NO₃⁻), nitrite (NO₂⁻), ammonia (NH₄⁺), and organic compounds of proteins, peptides, nucleic acids, urea, and numerous synthetic organic materials. It has sources from natural environments and human-related activities such as industrial waste waters, domestic sewage, and agricultural fertilization (from nitrogenous fertilizers and manures). Surplus nitrogen readily moves with water bodies, and causes significant water quality and health issues at a global scale. It could lead to algae bloom, a phenomenon that consumes a large amount of oxygen and deprives the living chances from fishes and aquatic organisms, resulting in a notable negative impact on our environment and economy [1]. In addition, excessive amounts of nitrate/nitrite nitrogen (>10 mg/L, World Health Organization (WHO) standard [2]) in drinking water can pose high carcinogenic risks to human [3, 4], cause growth inhibition [2], and contribute to the illness known as methemoglobinemia in infants [5, 6]. Therefore, quantitative determination of TN in water is of great importance.

Conventional laboratory analytical methods for TN quantification are primarily based on wet chemistry, and usually involve long and tedious sample digestion and titration processes ranging from one to six hours [7-9]. Commercialized TN analyzers are also available from vendors such as Shimadzu [10], Thermo Scientific [11], and Skalar [12]. The digestion of organic nitrogen compounds on these systems are all based on catalytic thermal decomposition at high temperature (e.g., 380 °C), which are not suitable for on-site TN measurements close to water systems. More research efforts have been shifted towards platform miniaturization and protocol development for in-situ TN detection. For instance, Beaton et al. developed a microfluidic device for colorimetric analysis of nitrate and nitrite. The device represented a new generation of miniaturized field analyzers based on microfluidic technology, and provided a field-deployable technology for automated nitrate analysis [13]. Fraser et al. invented an integrated centrifugal microfluidic system for on-site colorimetric analysis of nitrate [14]. Sun and his colleagues developed a portable soil nitrogen detector based on near-infrared spectroscopy [15]. Those technologies enable on-site measurements of inorganic nitrogen in water samples. However, none of them have covered the full range of TN (including both inorganic and organic nitrogen) in aqueous environments.

On-site measurement of TN on a portable device with short assay time is critical and urgently needed. In this paper, we aim to develop a portable analytical system for TN determination from water samples. The portable system consists of an ultraviolet C (UVC)-assisted oxidation chamber and a portable colorimetric reader. Both the digestion chamber and the colorimetric reader are designed to fit a standard 4-well strip. We implement the persulfate digestion method and United States Environmental Protection Agency (EPA) approved nitrite determination method on the portable system. Thorough investigations and experiments are conducted to optimize the assay protocol for on-site TN measurement with a short assay time and satisfactory analytical performance. The protocol parameters explored include the digestion time, temperature and substrate, oxidizer concentrations, nitrate reduction time, nitrite colorimetric reaction time, and reagents stability over time. We achieve fast oxidation and colorimetric determination (in 36 minutes) of TN in water in the range of 1 µg/L to 10 g/L with a limit of detection (LOD) of 1.2 mg/L, which is much lower than the WHO standard of 10 mg/L. Compared with conventional laboratory analytical systems, our system provides sufficient measurement range and LOD in a much shorter assay time [16, 17]. These superior performances and capabilities enable the digestion and measurement of TN in a portable and low-cost manner, proving this system suitable for on-site water quality monitoring.

7.2 Experiment design

7.2.1 Materials and reagents

Copper (II) sulfate (CuSO₄), zinc sulfate (ZnSO₄), potassium persulfate ($K_2S_2O_8$), sodium hydroxide (NaOH), hydrazine sulfate ($H_6N_2O_4S$), sulfanilamide ($C_6H_8N_2O_2S$), hydrogen chloride (HCl) solution, N-(1-Naphthyl) ethylenendiamine (NEDD), potassium nitrate (KNO₃), ammonium chloride (NH₄Cl), glycine ($C_2H_5NO_2$), urea (CH₄N₂O), tris ($C_4H_{11}NO_3$), and glutathione ($C_{10}H_{17}N_3O_6S$, GSH) were purchased from *Sigma-Aldrich*, Canada. All chemicals were used as received without further purification.

Arduino microcontroller (Uno, *Arduino*), low-voltage heating pad (RB-Spa-716, *Sparkfun Electronics*), temperature sensor (DHT22, *Aosong Electronics*), cooling fan (RB-All-77, *Roboticist's Choice*), Bluetooth (HC-06, *iTead Studio*), LCD screen (RB-See-86, *SeeedStudio*) were purchased from *Robotshop*, Canada. The UVC bulb (254 nm U-shape dual lamp, 50 mm × 8 mm × 50mm, *Rexim*) and its power converter (5V dual lamp DC Inverter, *Rexim*) were

purchased from *Rexim*, USA. 8-well strip (Costar Clear 1 × 8, *Corning Inc.*) was purchased from *VWR*, Canada, and spilt to two 4-well strips before use. The 3 mm round red LED (1497-1260-ND), green LED (1497-1258-ND), yellow LED (1497-1261-ND), blue LED (1497-1003-ND), and photodetector (MAX44008, *Maxim Integrated*) were purchased from *Digikey*, Canada.

7.2.2 Reaction system design

The principle of the TN measurement is to digest low valence state nitrogen (organic compound and ammonium) to nitrate, reduce the nitrate to nitrite, and eventually detect the nitrite using a colorimetric assay protocol. There are many ways of nitrogen digestion, including Kjeldahl method [18], microwave method [19, 20], UVC-thermal oxidation [21, 22], and high-temperature catalytic combustion [23, 24]. Among them, the UVC-thermal digestion is the most effective and eco-friendly (with less and mild chemicals) way to thoroughly oxidize the organic nitrogen [17, 25-27]. The portable analytical system is designed to integrate a reaction chamber for UVC-thermal digestion of organic nitrogen and a colorimetric reader for quantitative analysis of nitrite colorimetric assay.

Firstly, the cases, holders, and holding slots were designed by SolidWorks (*SolidWorks Corporation*), out-sourced by a 3D printer (I3, *Prusa*) and assembled with electronic components. The digestion chamber consists of a low-voltage UVC unit and a closed-loop automatic temperature controlling system. The UVC bulb (U-shape, dual lamps) has a peak radiation at 254 nm, and can act as an effective nitrogen digestion source in aqueous environment. A voltage power inverter was utilized to convert the supply voltage from 5 V to 675 V to ignite the mercury in the UVC bulb, which can illuminate ultraviolet at a peak wavelength of 254 nm. **Figure 7-1 (A)** shows the schematic of the digestion chamber design. Two sample holding slots were created to fit two 4-well strips and radially arrange them at a 1 cm distance to the UVC bulb center. The U-shaped dual lamp design of this UVC bulb ensures equal and sufficient digestion of organic nitrogen in each 4-well strip within a short reaction time.

The temperature controlling system was designed by integrating a low-voltage heating pad, a temperature sensor, and a ventilation fan. The heating pad $(5 \text{ cm} \times 10 \text{ cm})$ was wrapped around the 3D printed holder with a radius of 4 cm (**Figure 7-1** (**A**)), and the ventilation fan was placed at the end of the holder center (**Figure 7-2** (**A**)). **Figure 7-2** (**C**) shows the closed-loop control mechanism of this system. The temperature is precisely monitored by the Arduino

microcontroller and temperature sensor, with negative feedback regulation from heating (by heating pad) and cooling (by ventilation fan) at ± 3 °C precision. Such design considerations are made to maintain a uniform temperature environment to ensure reaction repeatability for the UVC-thermal method.

From the 4-well strip, three reservoirs were employed for the TN reaction, and one reservoir (nearest to the fan) was filled with water to maintain the humidity and reduce solution loss in high temperature and ventilation. The colorimetric reader was built of three sets of LEDs and photodetectors to accommodate three reaction reservoirs. Each LED-photodetector set consisted of four small LEDs and one integrated photodetector placed in the center of four LEDs (**Figure 7-1** (C)). The LEDs have four peak spectrums of wavelength at 470 nm (blue LED), 520 nm (green LED), 580 nm (yellow LED) and 630 nm (red LED). These spectrums cover absorbance peaks of typical colorimetrical assays [14, 28, 29]. The microcontroller was programmed to control the LEDs separately, and could help select the most sensitive wavelength for a particular colorimetric assay by reading and differentiating the signals from these LEDs. The photodetectors integrate RGB sensors covering the whole visible light spectrum, and are able to quantify light intensity through the solution, rapidly and simultaneously.

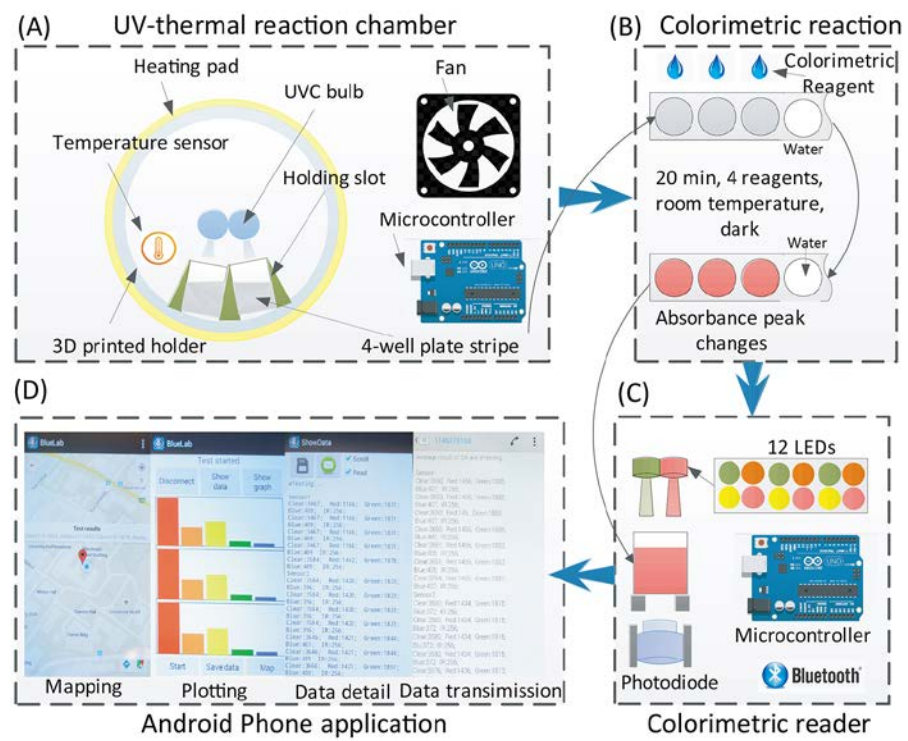


Figure 7-1. Platform design schematic. **(A)** UVC-thermal digestion chamber. **(B)** Colorimetric reaction step. **(C)** Colorimetric reader. **(D)** Interfaces of a smart phone application.

To better assist on-site TN measurements, a cellphone application (APP) is created for Bluetooth communication, data collection and analysis, and mapping of testing locations on Google map through the mobile network. This APP can also transmit testing data through text messaging, which ensures tele-transmission capabilities in rural areas and developing countries lacking communication facilities (Internet). **Figure 7-1** (**C**) shows different interfaces of the APP, including the mapping application program interface (API), result plots, data display, and Bluetooth transmission. The material cost of this system is CAD \$95.

To perform the digestion, the digestion chamber was firstly ignited on the UVC bulb, and pre-heated till the temperature was stabilized at a target value (*e.g.* 35 °C). Two 4-well strips filled with nitrogen samples and water were then slide into the holding slots, where the position of the slide was confined symmetrically aside the UVC bulb to ensure equal UVC illumination. After digestion (*e.g.* 20 min), TN had been converted to nitrate (NO₃), theoretically. The total nitrate, including original nitrate and oxidized nitrate from organic nitrogen and ammonium, was further reduced to nitrite NO₂, which was the final target molecule for the colorimetric detection of TN. The reduction process was conducted in the dark environment after the UVC lamp was off. In the end, the 4-well strip was slide into the colorimetric reader (**Figure 7-2 (B)**) for quantitative analysis. All the results were transmitted and analyzed by the phone APP.

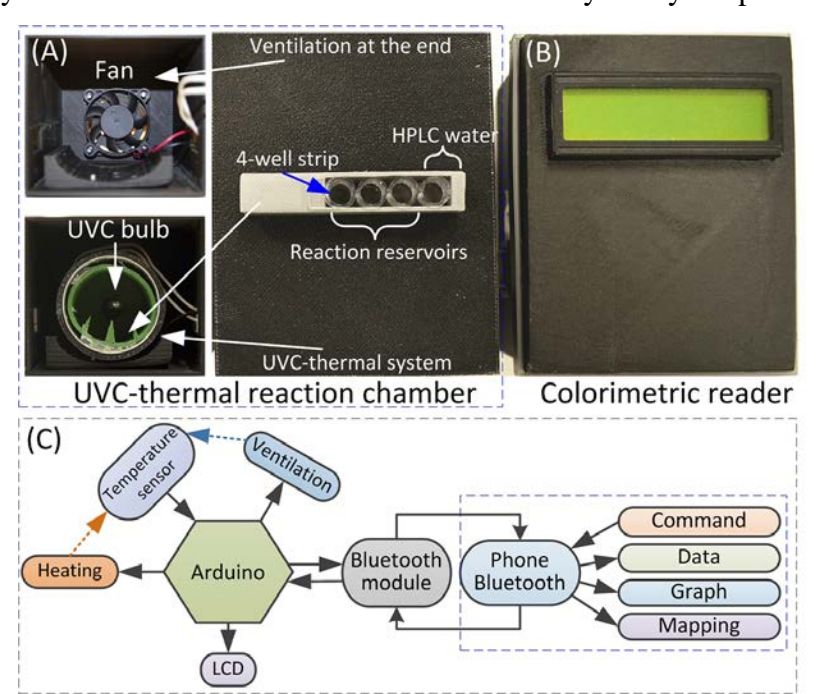


Figure 7-2. **(A)** UVC-thermal reaction chamber. **(B)** Colorimetric reader. **(C)** The controlling algorism of the application program.

7.2.3 Assay protocol

The principle of the TN detection is to first convert organic nitrogen and ammonium to nitrate, reduce the nitrate to nitrite, and finally perform colorimetric detection on the nitrite. Digestion of organic nitrogen was achieved via UVC-thermal oxidation. During the process, several redox reactions took place to generate the activated hydroxyl radical as an oxidizer for organic nitrogen and ammonium. After their conversion to nitrate, CuSO₄/ZnSO₄ was used to reduce the nitrate to nitrite. And then, the nitrite could be detected using a modified EPA colorimetric assay.

Nitrogen samples were oxidized by potassium persulfate under UVC irradiation. In a typical experiment, a solution was prepared in one reaction reservoir (3 reservoirs used in the 4-well strip) by adding 20 µL of nitrogen sample solution, 3 µL of potassium persulfate (175 mM), 3 µL of NaOH solution (100 mM) into high-performance liquid chromatography (HPLC) water to obtain a final volume of 120 µL. The well was then slid into the portable oxidation chamber, which could accommodate two 4-well strips each time. With the heating effect of UVC bulb, the temperature of the chamber was soon conditioned at 35 °C. An irradiation time of 20 min was used for nitrogen oxidation. **Equations 7-1** to **7-4** illustrate this mechanism. During the UVC illumination, persulfate was first decomposed to two sulfate ion radicals; and simultaneously, water molecular was decomposed to a hydroxyl radical. The sulfate ion radical was then converted to sulfate ion and a hydroxyl radical. Next, nitrogen at low covalence status would be oxidized to nitrate ions with the aid of abundant hydroxyl radicals.

$$S_2O_8 \xrightarrow{hv} 2SO_4^{-1} \tag{7-1}$$

$$H_2O \xrightarrow{hv} H^+ + OH^-$$
 (7-2)

$$SO_4^- + H_2O \longrightarrow SO_4^{2-} + OH + H^+$$
 (7-3)

$$OH \cdot + R_2 - N - R_1 \longrightarrow NO_3^- + \dots$$
 (7-4)

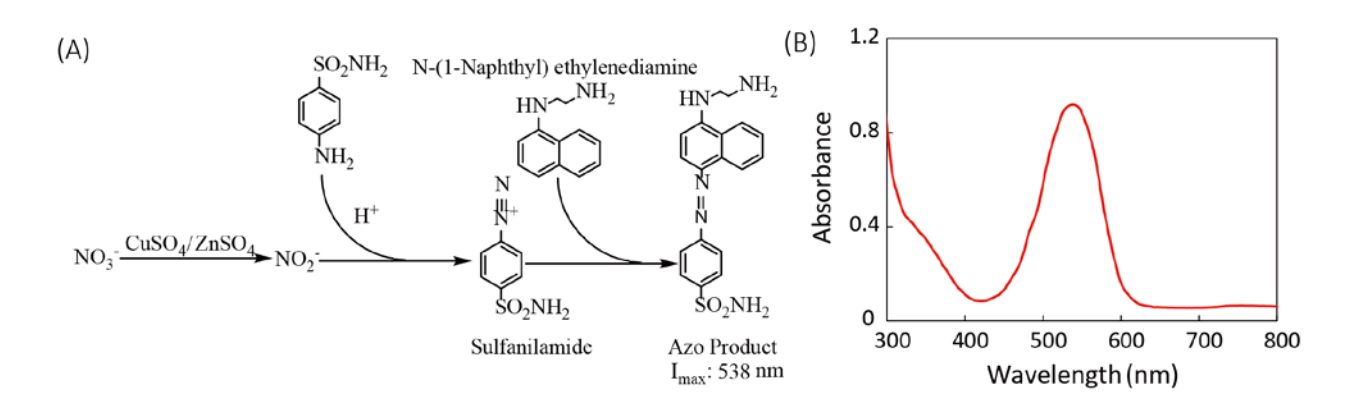


Figure 7-3. **(A)** Reaction mechanism of the colorimetric detection of nitrate detection. **(B)** Absorbance spectrum of Azo product from UV-vis, with a max light absorption at 538 nm.

After the digestion, total nitrogen and ammonium have all been turned to nitrate ions. Thus, the water sample remains nitrate and nitrite as the final forms of nitrogen. A modified EPA standard method was adopted for nitrate-nitrite determination. In brief, a reductant solution was prepared by mixing an equal volume of reagent A (0.14 mM of CuSO₄ and 5 mM of ZnSO₄), reagent B (1 M of NaOH) and reagent C (4 mM of hydrazine sulfate). This kind of mixing is to further reduce the assay time without sacrificing the reaction efficiency. 60 μ L of the reductant solution was added in each well and allowed for 5 min incubation. Afterwards, 75 μ L of sulfanilamide-HCl solution (10 g/L in 3.5 M HCl) was added to neutralize the reduction reaction, followed by adding 20 μ L of NEDD (1 g/L). The final solution was incubated in the dark environment for 5 min for color development (**Figure 7-1 (B)**). With the aid of NEDD, Azo product was generated, with a max light absorption at 538 nm (**Figure 7-3 (B)**). The absorbance rate for each reactive well was then collected by the optical reader.

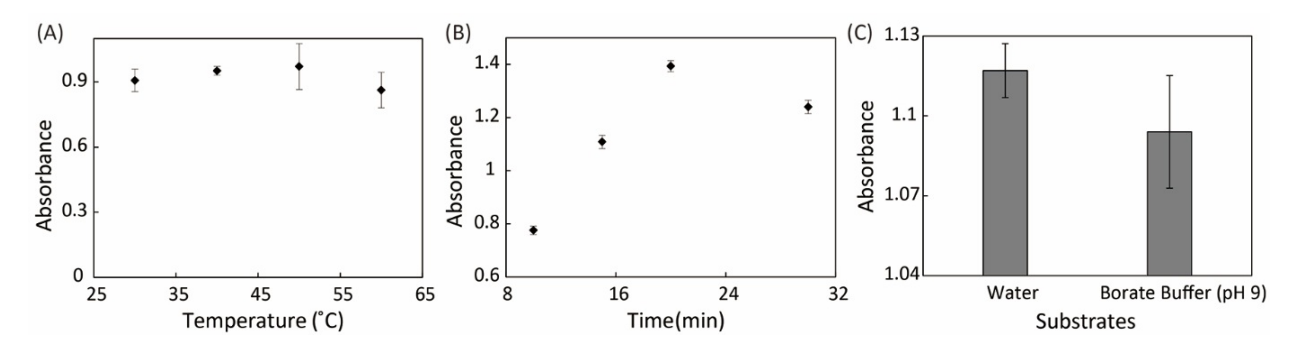


Figure 7-4. Optimization of oxidation parameters reflected by absorbance (n=6). **(A)** Heating temperature from 30 °C to 60 °C. **(B)** UV-thermal oxidation time from 10 min to 30 min. **(C)** Substrate effect between water and borate buffer (pH=9).

7.3 Results and Discussions

The determination of total nitrogen involves nitrogen oxidation, reduction, and colorimetric reaction. Protocol optimizations have been investigated to achieve better sensitivity and accuracy. Nitrogen standards were prepared from potassium nitrate (nitrate), ammonium chloride (ammonium), glycine (amino acid), urea (organic nitrogen), tris (organic nitrogen), and glutathione (organic nitrogen) for a final stock solution of 1000 mg/L nitrogen.

7.3.1 Oxidation optimization

The digestion efficiency is the key factor to accurately monitor the organic nitrogen among the total nitrogen. Thus, oxidation optimization conditions were explored including the oxidation time, reaction temperature, and substrate buffer. Firstly, we analyzed the oxidation effect using glycine (600 µM) solution as a model. From Figure 7-4 (A), the values of 30 °C, 35 °C, 40 °C, 50 °C and 60 °C were investigated to optimize the oxidation temperature. Within those temperatures, the corresponding absorbance was relatively constant around 0.92. No significant change was found on the oxidation effect with increasing incubation temperature. It was noted the natural chamber temperature was 35 °C after UVC illumination for 5 minutes. As this temperature provided the optimal condition, no further temperature control was needed in the digestion reaction here. Figure 7-4 (B) investigated the time-absorbance effect during the oxidation, and the optimal irradiation time was found to be 20 minutes, with the highest absorbance of 1.4. During longer oxidation time, the absorbance decreases to 1.25 at 32 minutes. This is probably because the sample solution evaporated largely after a long time exposure, and resulted less volume (less light absorption) during colorimetric reaction. We also investigated the substrate effect on the oxidation rate, reflected by the absorbance. Figure 7-4 (C) shows that, no significant difference was found between borate buffer and water. Borate buffer was preferred because it can eliminate the pH effect from analyzed samples, as pH will directly affect the reaction. Thus, with the above investigations, the parameters of temperature (35 °C), oxidation time (20 min), and substrate (borate buffer) were then adopted in the continuing experiments.

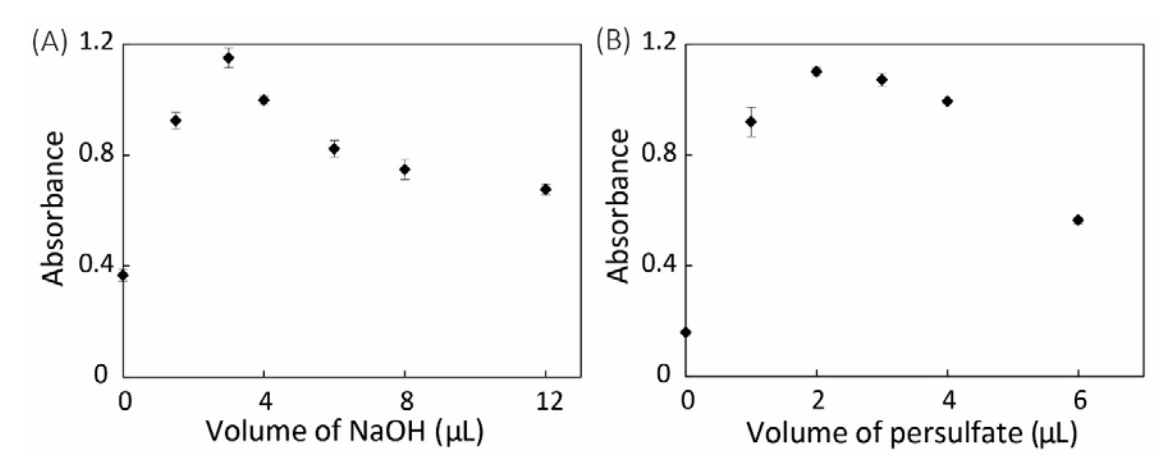


Figure 7-5. Oxidation assay protocol optimization (n=6): **(A)** The NaOH volume effect (pH) on the oxidation rate reflected by absorbance. **(B)** The potassium persulfate (oxidizer) volume effect on the oxidation rate reflected by absorbance.

Equations 7-1 and **7-2** show the first two oxidation procedures. The key factor in the oxidation protocol involves the hydroxyl radical (OH·) generation from molecules of water (H₂O) and persulfate (S₂O₈). Thus, it is crucial to monitor the pH and persulfate contents in this reaction to ensure adequate OH· for organic nitrogen digestion (**Equations 7-3** and **7-4**). The oxidation was carried in the basic solution of 600 μM glycine. To observe the pH effect, NaOH (100 mM) volume was tuned from 0 to 12 μL to find the optimal value. **Figure 7-5 (A)** shows that the absorbance reached highest as 1.1 at the volume of 3 μL, and decreased at lower or higher NaOH volume. 3 μL provided the optimal pH for highest oxidation rate, resulted to a final concentration of 2.5 nM NaOH. By fixing the NaOH concentration (2.5 nM), the optimal oxidizer concentration of persulfate was tested. **Figure 7-5 (B)** shows the oxidation effect from a series of potassium persulfate volume (175 mM, 0-6 μL), reflected by absorbance. The optimal volume was found to be 2 μL, resulting a final concentration of 3 nM in the reaction solution. It was noted that lower concentrated persulfate provided inadequate oxidizer while higher concentrated persulfate would suppress the reaction rate. Thus, the optimal conditions of NaOH (100 mM) and potassium persulfate (175 mM) were settled down with 3 μL and 2 μL, respectively.

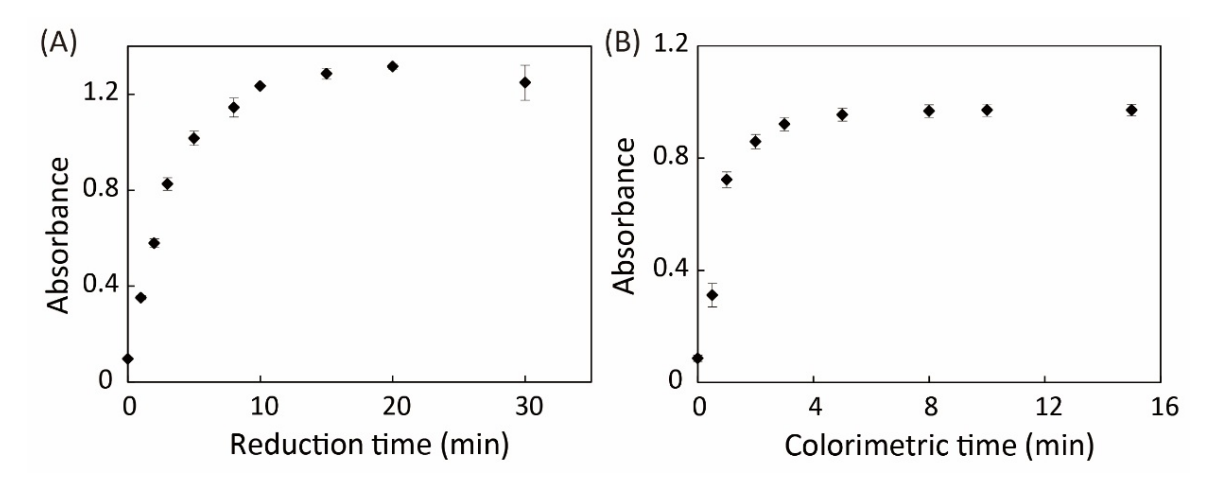


Figure 7-6. **(A)** Nitrate reduction efficiency over time, reflected by absorbance (n=6). **(B)** Colorimetric assay efficiency over time, reflected by absorbance (n=6).

7.3.2 Colorimetric assay optimization

With those oxidation optimizations, the protocol was set to be carried out by adding 3 μ L NaOH (100 mM) and 2 μ L potassium persulfate (175 mM) in substrate of borate buffer at 35 °C for 20 mins. Next, the nitrogen products were processed with standard nitrate/nitrite colorimetric reaction. Briefly, the oxidized solution (nitrate) will get reduced to nitrite firstly. With all the nitrite representing the TN, nitrite will be determined by colorimetric reaction as the last step.

The determination of the oxidized nitrogen would be the modified method for EPA nitrate-nitrite detection. To introduce, the nitrate would first get reduced with the reduction agent of CuSO₄/ZnSO₄; then, sulfanilamide-HCl solution would be added to neutralize the reduction reaction. With colorimetric reagent of NEDD, the sample reaction would turn to a final product of Azo, with a max light absorbance of 538 nm. The absorbance for each well was collected using the UV-vis spectrometer and our optical reader. As required by *in-situ* determination, it's necessary to investigate the time-absorbance relationship and get the fastest assay protocol with the highest absorbance. The reduction time and the colorimetric reaction time are critical, and pose un-negligible effect to the final sensitivity and limit of detection. The optimization experiments on these two factors were conducted from 0-30 min for reduction time and 0-16 min for colorimetric reaction time. During the colorimetric reaction, **Figure 7-6 (A)** shows that the reduction rate of nitrate to nitrite increased and reached to plateau after 15 min, reflected by absorbance. And at 5 min, it could achieve 80% of the maximum reduction efficiency. To facilitate the on-site detection, a 5-min reduction time was adopted to ensure short assay time. In

Figure 7-6 (B), the colorimetric reaction was fast and reached to plateau value within 5 min. The color was stable afterwards, even overnight. Thus, we adopted 5-min reduction time and 5-min colorimetric time as the final protocol.

Next, reagents stability was tested over time. **Figure 7-7** (**A**) illustrates the oxidizer stability (represented by absorbance) of persulfate/NaOH in the range of 0 to 24 hours. Although there were slight fluctuations, an acceptable absorbance level of 1.1 was achieved from 0.1h to 24h. **Figure 7-7** (**B**) shows the stability of reductant solution over 4 hours. Within 60 minutes, the absorbance gave fairly stable values over 1.1, and decreased significantly after 3 hours. Thus, it's suggested to freshly make the reductant solutions and use it within 1 hour. **Figure 7-7** (**C**) tested the reliability of the colorimetric reagents of sulfanilamide-HCl solution (10 g/L in 3.5 M HCl) and NEDD (1 g/L), and it shows that the reagent kept steady at 4°C up to one month.

As the compositions of total nitrogen are complex, the conversion rates of nitrogen digestion (organic nitrogen and ammonium) were tested. **Table 7-1** shows the determination results of the nitrogen concentration from various N-containing compounds of glycine, urea, tris, NH₄Cl, and GSH. Based on 8.4 mg N/L nitrogen concentration, the percentage of recovery rates are 99.0 \pm 1.53, 110.3 \pm 0.51, 82.1 \pm 1.73, 84.4 \pm 0.65, and 90.1 \pm 1.87, respectively. All the conversion rates reach a high percentage (>80%) and show a high digestion efficiency among those nitrogen compounds.

The calibration test was carried in nitrogen concentrations from 0.14 mg N/L to 17.5 mg N/L. Based on the parameters and protocols indicated above, linear relationships between nitrate concentration and absorbance were found in the ranges of 0.14 to 1.1 mg and 1.1 mg N/L to 17.5 mg N/L, as shown in **Figure 7-8**. As 10 mg N/L is the WHO standard for drinking water, the dynamic range from 1 mg N/L to 17.5 mg N/L is chosen for analysis. Within this range, the linear fitting euqations are y = 0.26x - 0.053 for our colorimetric reader, and y = 0.43x - 0.025 for the UV-vis reading. The LOD of colorimetric assay by using standard nitrate solutions was found to be 1.20 mg N/L from the colorimetric reader, and 1.07 mg N/L from UV-vis. The performance from our reader is comparable to that from UV-vis, and both lower than the standard nitrogen concentration (10 mg N/L) required by the WHO [2].

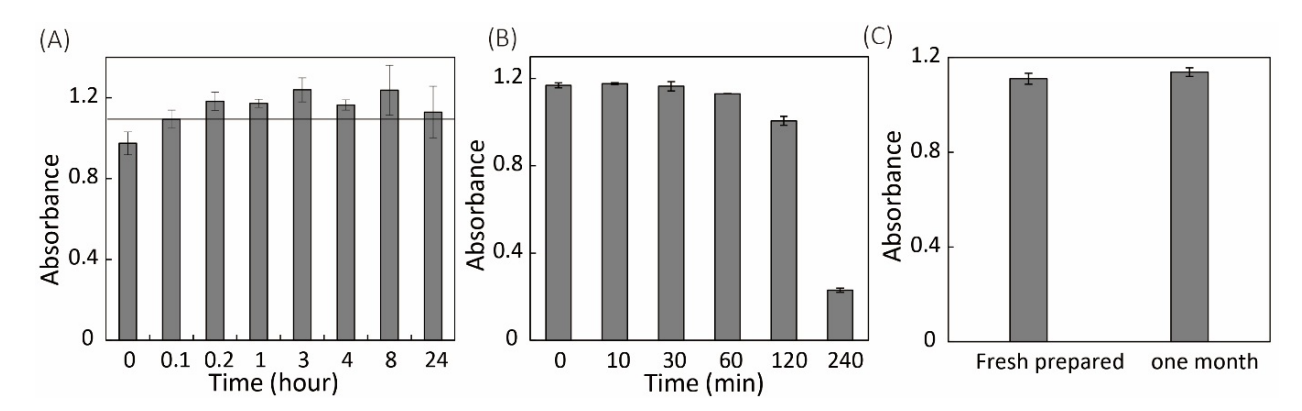


Figure 7-7. The testing results of reagents stability over time (n=6): (A) persulfate/NaOH regents (one day at 4° C). (B) Reductant solution. (C) Colorimetric reagents over time (at 4° C) under dark environment).

Table 7-1. The results of TN determination (mg N/L)

Compounds (8.4 mg N/L)	% Recovery
Glycine	99.0 ± 1.53
Urea	110.3 ± 0.51
Tris	82.1 ± 1.73
NH ₄ Cl	84.4 ± 0.65
GSH	90.1± 1.87

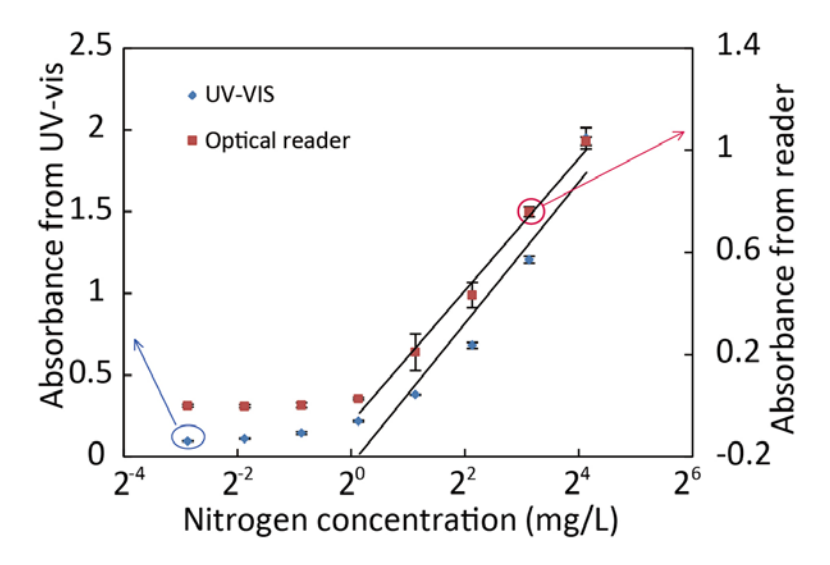


Figure 7-8. Detection of TN by the colorimetric assay (n=6). The linear fitting equations are: y = 0.2565x - 0.0533 for our colorimetric reader; y = 0.4283x - 0.025 for the UV-vis reading.

7.4 Conclusion

We successfully developed a portable analytical system for on-site TN determination in water samples. The system contains a UVC-thermal digestion chamber and a portable colorimetric reader, and has unique advantages such as low cost, rapid assay, high portability and satisfactory analytical performance. The UCV-thermal digestion method and the EPA-approved nitrate-nitrite determination method were implemented on our portable analytical system. We optimized the experimental parameters of the assay such as oxidation time, temperature, substrate, oxidizer concentrations, nitrate reduction time, nitrite colorimetric reaction time, and reagents stability. Fast oxidation and colorimetric determination of TN in water were achieved in the range from 0.14 mg N/L to 17.5 mg N/L at a limit of detection of 1.2 mg/L (lower than the 10 mg/L WHO standard) within 36 minutes in total. Compared with existing laboratory instruments, the system requires much shorter incubation time and enables the digestion and measurement of TN in a portable and low-cost manner. In the future, selectivity testing and real water monitoring will be performed regarding tap water, river, and industrial waste water.

7.5 References

- [1] B. De Borba, R. F. Jack, and J. Rohrer, "Determination of Total Nitrogen and Phosphorus in Wastewaters by Alkaline Persulfate Digestion Followed by IC."
- [2] W. H. Organization, *Guidelines for drinking-water quality: recommendations*. World Health Organization, 2004.
- [3] P. J. Weyer *et al.*, "Municipal drinking water nitrate level and cancer risk in older women: the Iowa Women's Health Study," *Epidemiology*, vol. 12, no. 3, pp. 327-338, 2001.
- [4] K. P. Cantor, "Drinking water and cancer," *Cancer Causes & Control*, vol. 8, no. 3, pp. 292-308, 1997.
- [5] L. Fewtrell, "Drinking-water nitrate, methemoglobinemia, and global burden of disease: a discussion," *Environmental health perspectives*, pp. 1371-1374, 2004.
- [6] G. Walton, "Survey of literature relating to infant methemoglobinemia due to nitrate-contaminated water," *American Journal of Public Health and the Nations Health*, vol. 41, no. 8_Pt_1, pp. 986-996, 1951.
- [7] M. Hosomi and R. Sudo, "Simultaneous determination of total nitrogen and total phosphorus in freshwater samples using persulfate digestion," *International Journal of Environmental Studies*, vol. 27, no. 3-4, pp. 267-275, 1986.
- [8] D. Cataldo, L. Schrader, and V. Youngs, "Analysis by digestion and colorimetric assay of total nitrogen in plant tissues high in nitrate," *Crop Science*, vol. 14, no. 6, pp. 854-856, 1974.

- [9] D. Nelson and L. Sommers, "A simple digestion procedure for estimation of total nitrogen in soils and sediments," *Journal of Environmental Quality*, vol. 1, no. 4, pp. 423-425, 1972.
- [10] SHIMADZU, "TN (Total Nitrogen) Unit."
- [11] T. Scientific, "TN 3000 Total Nitrogen Analyzer."
- [12] Formacs, "The FormacsSERIES Total Organic Carbon (TOC) / Total Nitrogen analyzers ".
- [13] A. D. Beaton *et al.*, "Lab-on-chip measurement of nitrate and nitrite for in situ analysis of natural waters," *Environmental science & technology*, vol. 46, no. 17, pp. 9548-9556, 2012
- [14] M. Czugala *et al.*, "CMAS: fully integrated portable centrifugal microfluidic analysis system for on-site colorimetric analysis," *RSC Advances*, vol. 3, no. 36, pp. 15928-15938, 2013.
- [15] X. An, M. Li, L. Zheng, Y. Liu, and H. Sun, "A portable soil nitrogen detector based on NIRS," *Precision agriculture*, vol. 15, no. 1, pp. 3-16, 2014.
- [16] J. Ebina, T. Tsutsui, and T. Shirai, "Simultaneous determination of total nitrogen and total phosphorus in water using peroxodisulfate oxidation," *Water research*, vol. 17, no. 12, pp. 1721-1726, 1983.
- [17] T. A. Frankovich and R. D. Jones, "A rapid, precise and sensitive method for the determination of total nitrogen in natural waters," *Marine Chemistry*, vol. 60, no. 3, pp. 227-234, 1998.
- [18] J. Bremner *et al.*, "Nitrogen-total," *Methods of soil analysis. Part 3-chemical methods.*, pp. 1085-1121, 1996.
- [19] P. Johnes and A. L. Heathwaite, "A procedure for the simultaneous determination of total nitrogen and total phosphorus in freshwater samples using persulphate microwave digestion," *Water Research*, vol. 26, no. 10, pp. 1281-1287, 1992.
- [20] M. Colina and P. Gardiner, "Simultaneous determination of total nitrogen, phosphorus and sulphur by means of microwave digestion and ion chromatography," *Journal of Chromatography A*, vol. 847, no. 1, pp. 285-290, 1999.
- [21] H. Kroon, "Determination of nitrogen in water: comparison of a continuous-flow method with on-line UV digestion with the original Kjeldahl method," *Analytica Chimica Acta*, vol. 276, no. 2, pp. 287-293, 1993.
- [22] W. Hong, "Determination of Total Nitrogen in Waste Water by Alkaline Potassium Persulfate Digestion-UV Spectrophotometric Method [J]," *MODERN SCIENTIFIC INSTRUMENTS*, vol. 5, p. 027, 1999.
- [23] P. Tingvall, "Determination of nitrogen with copper as catalyst for high-temperature digestion," *Analyst*, vol. 103, no. 1225, pp. 406-409, 1978.
- [24] T. W. Walsh, "Total dissolved nitrogen in seawater: a new-high-temperature combustion method and a comparison with photo-oxidation," *Marine Chemistry*, vol. 26, no. 4, pp. 295-311, 1989.
- [25] D. A. Bronk, M. W. Lomas, P. M. Glibert, K. J. Schukert, and M. P. Sanderson, "Total dissolved nitrogen analysis: comparisons between the persulfate, UV and high temperature oxidation methods," *Marine Chemistry*, vol. 69, no. 1, pp. 163-178, 2000.
- [26] O. Thomas, F. Théraulaz, V. Cerdà, D. Constant, and P. Quevauviller, "Wastewater quality monitoring," *TrAC Trends in Analytical Chemistry*, vol. 16, no. 7, pp. 419-424, 1997.

- [27] B. Roig, C. Gonzalez, and O. Thomas, "Measurement of dissolved total nitrogen in wastewater by UV photooxidation with peroxodisulphate," *Analytica chimica acta*, vol. 389, no. 1, pp. 267-274, 1999.
- [28] G.-H. Chen, W.-Y. Chen, Y.-C. Yen, C.-W. Wang, H.-T. Chang, and C.-F. Chen, "Detection of mercury (II) ions using colorimetric gold nanoparticles on paper-based analytical devices," *Analytical chemistry*, vol. 86, no. 14, pp. 6843-6849, 2014.
- [29] C. Zhao, G. Zhong, D.-E. Kim, J. Liu, and X. Liu, "A portable lab-on-a-chip system for gold-nanoparticle-based colorimetric detection of metal ions in water," *Biomicrofluidics*, vol. 8, no. 5, p. 052107, 2014.

Chapter 8

Conclusion

Chapter 8: Conclusion

8.1 Summary of accomplishments and contributions

New research recently emerged from the miniaturization of sensing techniques and materials, making possible the integration of multiple smart functions into a single portable analytical platform. This thesis contributes to the design methodologies of portable analytical systems for in-situ biomedical applications. The portable platforms developed in this research hold significant potential for on-site analysis of disease markers and water pollutants, which will enable effective identification and control of pathological, physiological, and environmental threats to human health and our environment. With the aid of those tools, this thesis devotes efforts to two important aspects: disease diagnostics and physiological healthcare monitoring, and water environmental monitoring. We first proposed a disease diagnostic platform based on an electrochemical microfluidic paper-based immunosensor array (E-µPIA) and a handheld electrochemical reader (potentiostat) for multiplexed detections of metabolites and protein markers. Next, we developed a wearable microfluidic thread-based zinc-oxide-nanowire (ZnO-NW) biosensor for continuous monitoring of lactate and sodium concentrations in sweat during perspiration. Then, a portable analytical platform was developed for rapid and sensitive detection of aluminum (Al³⁺) and lead (Pb²⁺) ions in water targeting on-site heavy metal ion detection. Last but not the least, a novel analytical system was developed comprising a portable ultraviolet C (UVC) reaction chamber (for digesting organic nitrogen) and a colorimetric reader (for final detection of total nitrite). Through these efforts, innovative platforms and approaches were developed, as summarized below.

1. A comprehensive review on portable analytical platforms introduces the design considerations, sensing techniques, and progresses regarding the on-site applications. The major sensing techniques and detection principles have been discovered under two main analytical aspects of optical methods and electrochemical methods. Research achievements were summarized towards disease diagnostics, physiological monitoring, water pollution, and food safety applications with focus on metabolites, immunoassays, electrolytes, metal ions, nutrients, and nucleic acids. In the end, future trends were proposed regarding the improvement of assay protocols, hybridization of miniaturized microfluidic devices, integrations of flexible electronics,

real sample trial, and smart healthcare, with challenges, critical considerations and possible approaches.

- 2. The development of a novel portable disease diagnostic platform using E-µPIAs and a handheld electrochemical potentiostat. The E-µPIA is capable of performing diagnostic tests of biochemical molecules in a multiplexing and high-throughput fashion. The potentiostat was designed to interface with the E-µPIA for electrochemical signal readout with telemedicine capabilities. This platform was demonstrated for multiplexed detection of metabolites (glucose, lactate, and uric acid) and protein biomarkers (HIV and HCV) with analytical performance sufficient for clinical assays. This system forms a portable, self-contained, easy-to-operate electrochemical biosensing platform, and is particularly useful for low-cost, point-of-care diagnostic applications.
- 3. The first thread-based wearable ZnO-NW nanobiosensor for continuous monitoring of lactate and sodium concentrations in sweat during perspiration. Multiplexed detection of lactate and sodium in human sweat was demonstrated with dynamic ranges of 0-25 mM and 0.1-100 mM, and LODs of 3.61 mM and 0.16 mM, respectively, both covering the clinical sweat levels. Off-body real sweat testing was conducted in good agreement with standard assays. This wearable non-invasive biosensor possesses a significant potential to the practical controlling of fitness, electrolyte imbalance, physical well-being, and personal healthcare.
- 4. A new portable and cost-effective lab-on-a-chip system for colorimetric detection of Pb²⁺ and Al³⁺ in water, based on metal-ion-coordinated aggregation of gold nanoparticles (AuNPs) in solution. The assay operations only include single-time mixing of the AuNP reagent solution and the water sample, timed incubation, and colorimetric signal measurement. This portable platform provided LODs of 30 ppb for Pb²⁺ and 89 ppb for Al³⁺, comparable with the values obtained via bench-top spectrometry. This system represents a promising solution to on-site analysis of metal ions in real water samples.
- 5. The first portable total nitrogen analytical system is developed, comprising a portable UVC reaction chamber for digesting organic nitrogen, and a colorimetric reader for final detection of total nitrite. Fast oxidation and colorimetric determination of total nitrogen in water were achieved in the range of 0.14 mg N/L to 17.5 mg N/L with a limit of detection of 1.2 mg/L (lower than the 10 mg/L WHO standard) within 36 minutes. Compared with bench-top

instruments, this system has unique advantages of low cost, rapid assay, high portability and satisfactory analytical performance.

8.2 Future work

The presented research focused on the development of four portable analytical platforms, and the involved biochemical molecules/ions have been detected and calibrated. Efforts are contributed to the advanced performance and portability of carrying laboratory analytical techniques to point of test. The proposed portable analytical systems are currently employed on specific markers. The wide applicability of electrochemical and colorimetric detection reveals the potential of extending the detections to many other types of targets, including but not limited to, protein disease markers, ions, nutrients, and nucleic acids.

These platforms show satisfactory performance on the proposed markers in pure samples. However, there are also limitations to be considered, such as cross-talk in real sample test (whole blood and polluted water), interferences and selectivity, long-term storage stability, device shelf-life, and platform reliability in the field. Based on the previous results, limitations, and potentials, we plan to further improve the performance of both the sensing techniques and the portable readers, expand these platforms to more molecules, validate the sensors' performance through long-time preservation, and push them forward to real sample trials.

- 1. For the E- μ PIA platform, there are several approaches to further improve the sensing performance. Gold nanoparticles will be introduced on the E- μ PIA to improve the sensitivity, and enhance the protein immobilization. The device stability and shelf life will need to be explored by controlling the storage environment humidity and adding protein stabilizers to the E- μ PIA. The clinical testing of this platform will be conducted using patient samples, and further extended to improve the diagnostic capabilities targeting other protein markers.
- 2. Regarding the thread-based wearable ZnO biosensor, the continuous monitoring on the ZnO thread biosensor will be examined to face the long-time exercising and wearing. A cellphone application will be created to interface with the smart headband for wireless data transmission and analysis. On-body sweat monitoring will be conducted on multiple volunteers in exercise. Clinical relevant data will be collected aiming at chronic healthcare monitoring and over-exercising alerting.

- 3. For nutrient pollutant monitor in water, the detection on total phosphorous will be investigated together with total nitrogen to form a systematic research for nutrient pollution in water. Then, real water test on heavy metal ions and nutrients will be performed in drinking water, river, and polluted industrial water. Database will be constructed based on the regular monitoring and analysis of heavy metal ions and nutrients according to various sites as prevention of severe water pollution.
- 4. The real sample trials on those platforms should be conducted within the normal ranges of the markers, and also abnormal concentrations. Database will be constructed for both healthcare and water environmental quality. Power consumption and supplementary will be solved for long-time on-site monitoring. Intelligent applications will be developed and optimized for wireless communication and automatic analysis. The prediction and alerting will be integrated into the algorithm based on the data analysis through regular measurements.

8.3 Publications

8.3.1 Refereed journal papers

- Chen Zhao and Xinyu Liu, "A portable paper-based microfluidic platform for multiplexed electrochemical detection of HIV and HCV antibodies in serum", *Biomicrofluidics*, Vol. 10, No. 2, 024119 (10pp), 2016. Highlighted as an Editor's Pick Article; Featured by >10 science news magazine/websites, such as: Pathologist Magazine; Science Daily; American Institute of Physics; the Electrochemical Society; Medical Design Technology; Phys.org
- 2. Xiao Li, **Chen Zhao**, and Xinyu Liu, "A paper-based microfluidic biosensor integrating zinc oxide nanowires for electrochemical glucose detection", *Microsystems and Nanoengineering* (Nature Publishing Group), Vol. 1, article #15014 (7pp), 2015.
- 3. Stephanie Oyola-Reynoso, Andrew P. Heim, **Chen Zhao**, Ian D. Tevis, Simge Çınar, Xinyu Liu, and Martin M. Thuo, "Draw your assay: fabrication of low-cost paper-based diagnostic and multi-well test zones by drawing on a paper", *Talanta*, Vol. 144, pp. 289-293, 2015.
- 4. **Chen Zhao**, Guowei Zhong, Da Eun Kim, Jinxia Liu, and Xinyu Liu, "A portable lab-on-achip system for gold-nanoparticle-based colorimetric detection of metal ions in water", *Biomicrofluidics*, Vol. 8, No. 5, 052107 (9pp), 2014. (**Best Paper Award Finalist**)
- 5. Xiao Li *, Yu-Hsuan Wang *, Chen Zhao, and Xinyu Liu, "Paper-based piezoelectric touch

pads with hydrothermally grown zinc oxide nanowires", *ACS Applied Materials and Interfaces*, Vol. 6, No. 24, pp. 22004–22012, 2014.

- 6. **Chen Zhao**, Martin M. Thuo, and Xinyu Liu, "A microfluidic paper-based electrochemical biosensor array for multiplexed detection of metabolic biomarkers", *Science and Technology of Advanced Materials*, Vol. 14, No. 5, 054402 (7pp), 2013.
- 7. Xiaohua Sun, **Chen Zhao**, "An Automatic Measuring Instrument of Static Magnetism Characteristics Based On Virtual Instrument", *J. Control and Instruments in Chemistry Industry*, No. 02, pp. 186-189, 2012.

8.3.2 Journal papers in preparation (manuscripts available upon request)

- 1. **Chen Zhao**, Xiao Li, Qiyang Wu, Ted Li, and Xinyu Liu, "Wearable microfluidic thread-based ZnO-NW electrochemical biosensor", to be submitted to *Biosensors and Bioelectronics*.
- 2. **Chen Zhao** *, Longyan Chen *, Guowei Zhong, Qiyang Wu, Jinxia Liu, and Xinyu Liu, "Rapid on-site determination of total nitrogen in water using a portable analytical system", to be submitted to *Analytical Chemistry*.
 - [#] Authors with equal contributions.
- 3. **Chen Zhao**, and Xinyu Liu, "Adaptive reuse of commercial dropper bottles for microliter volume metering and pipetting in low-cost, point-of-care diagnostics", to be submitted to *Biomicrofluidics*.
- 4. **Chen Zhao**, and Xinyu liu, "Electroanalytical sensing in paper-based microfluidics: technologies and applications", to be submitted to *Biosensors and Bioelectronics*.
- 5. **Chen Zhao**, and Xinyu Liu, "Cell-phone-based biosensing: a critical review", to be submitted to *Critical Reviews in Biotechnology*.
- 6. Pengfei Song, **Chen Zhao**, Vicky Wang, and Xinyu Liu, "A paper-based electronic force sensor for undergraduate lab", to be submitted to *IEEE Transactions on Education*.
- 7. Hao Fu, Qiyang Wu, **Chen Zhao**, Xiao Li, Nicole Li-Jessen, and Xinyu Liu, "An Integrated Paper-based Microfluidic Platform for Autonomous, Point-of-care ELISA", to be submitted

[#] Authors with equal contributions.

to Lab on a Chip.

8.3.3 Conference papers (full paper)

- 1. Chen Zhao, Xiao Li, Ted Li, and Xinyu Liu, "A Thead-based Wearable Nanobiosensor", The 21st International Conference on Miniaturized Systems for Chemistry and Life Sciences (MicroTAS 2017), Savannah, Georgia, USA, October 22-26, 2017 (Oral presentation, selection rate: 9%).
- 2. Qiyang Wu, Tomas Diaz Jimenez, Juntian Qu, **Chen Zhao**, and Xinyu Liu, "Regulating Surface Traction of a Soft Robot Through Electrostatic Adhesion Control", IEEE/RSJ International Conference on Intelligent Robots and Systems (IROS 2017), Vancouver, Canada, September 24–28, 2017.
- 3. **Chen Zhao** *, Qiyang Wu *, Tyler Clancy *, and Xinyu Liu, "A 3D-printed portable microindenter for mechanical characterization of soft materials", IEEE International Conference on Automation Science and Engineering (CASE), Fort Worth, Texas, USA, August 21-24, 2016.
 - [#] Authors with equal contributions.
- Chen Zhao, and Xinyu Liu, "A portable, paper-based multiplexing immunosensor for detection of HIV and HCV markers in serum", International Conference on Solid-State Sensors, Actuators and Microsystems, Transducer 2015, Alaska, America, June 21-25, 2015.
- Xiao Li, Chen Zhao, and Xinyu Liu, "An electrochemical microfluidic paper-based glucose sensor integrating zinc oxide nanowires", IEEE International Conference on Micro Electro Mechanical Systems (MEMS'15), Estoril, Portugal, January 18–22, 2015.
- 6. **Chen Zhao**, Guowei Zhong, Da Eun Kim, Jinxia Liu, and Xinyu Liu, "A portable sensing system for gold-nanoparticle-based colorimetric detection of metal ions in water", ASME 2014 International Mechanical Engineering Congress & Exposition (IMECE'14), Montreal, Canada, November 14–20, 2014.
- 7. Yu-Hsuan Wang *, Xiao Li *, **Chen Zhao**, and Xinyu Liu. "Paper-Based Piezoelectric Touch Pads Integrating Zinc Oxide Nanowires", IEEE International Conference on Micro Electro Mechanical Systems (MEMS'14), San Francisco, California, Jan 26-30, 2014.

- [#] Authors with equal contributions.
- 8. **Chen Zhao**, Martin M. Thuo, and Xinyu Liu, "A paper-based microfluidic device for multiplexed electrochemical detection of biomarkers", IEEE International Conference on Manipulation, Manufacturing, and Measurement on the Nanoscale (3M-NANO), Suzhou, China, August 26-30, 2013 (**Best Application Paper Award Finalist**).

8.3.4 Book chapter

Chen Zhao, Martin M Thuo, and Xinyu Liu, "Microfluidic Paper-Based Multiplexing
Biosensors for Electrochemical Detection of Metabolic Biomarkers", Microfluidic Methods
for Molecular Biology, eds. Chang Lu, Scott S. Verbridge, Springer International Publishing,
pp. 205-218, 2016.

8.3.5 Patent

1. Xinyu Liu, Xiao Li, and **Chen Zhao**, "Paper-based nano biosensor device and method", US patent, filed on Oct. 24, 2016 (No. 15/332,657).